

FIELD AND LABORATORY STUDIES
OF THE
MECHANICS OF FAULTING

by

LUCILE MERRILL JONES
A.B., Brown University
(1976)

SUBMITTED IN PARTIAL FULFILLMENT
OF THE REQUIREMENTS FOR THE
DEGREE OF

DOCTOR OF PHILOSOPHY

at the

MASSACHUSETTS INSTITUTE OF TECHNOLOGY

June 1981

© Massachusetts Institute of Technology 1981

Signature of Author _____

Department of Earth and Planetary Sciences
May 15, 1981

Certified by _____

Peter Molnar
Thesis Supervisor

W.F. Brace
Thesis Supervisor

Accepted by _____

Theodore Madden
Chairman, Department Committee

WITHDRAWN
MASSACHUSETTS INSTITUTE
OF TECHNOLOGY
MIT LIBRARIES
LIBRARIES

FIELD AND LABORATORY STUDIES
OF THE MECHANICS OF FAULTING

by

LUCILE MERRILL JONES

Submitted to the Department of Earth and Planetary Sciences
on May 15, 1981, in partial fulfillment of the
requirement for the degree of Doctor of Philosophy

ABSTRACT

The development of instabilities in geologic materials has been studied using the techniques of both seismology and rock mechanics. In the field the deformation that occurs prior to an earthquake was studied through the analysis of foreshocks. Foreshocks occur before a large fraction of the world's major ($M \geq 7.0$) earthquakes. Teleseismically located events before major earthquakes from 1914 to 1973 were considered together to examine possible average temporal and spatial patterns of foreshock occurrence. Several days before the main shocks and apparently near the epicenters of them ($\Delta \lesssim 30$ km) the activity begins to increase, culminating in a final rapid acceleration of activity in the last day. The acceleration continues up to the time of the main shocks, except for a possible temporary decrease about 6 hours before them. The seismicity increases approximately as the inverse of time before main shock. This relationship is essentially unrelated to the magnitude of the main shock. The magnitude of the largest foreshock is also unrelated to the magnitude of the main shock. In addition, pairs of major events are common. Ten percent of the world's major events are preceded by other major events within 100 km and 3 months.

For foreshocks within each of three sequences studied, the ratio of the amplitudes of the P and S waves were approximately the same, suggesting that the faulting mechanisms are the same for events in each sequence. By assuming an inhomogeneous fault plane on which asperities fail by static fatigue, we derived an equation for accelerating premonitory slip as a function of time, which agrees with the observed time dependence of the foreshocks.

To see more details of a foreshock sequence than that available from teleseismic data, the locations and radiation patterns of one foreshock sequence, that of the 4 February, 1975, Haicheng earthquake ($M = 7.3$) were examined. Using arrival times from six local seismic stations, the foreshocks and mainshock were located relative to a master event. The foreshocks occurred

in a tight cluster that elongated with time. Before the largest foreshock, the activity was located within a small, equidimensional volume with a diameter of about two kilometers. After the largest foreshock, the activity spread northwest and southeast forming a six kilometer long, northwest trending zone. First motions and ratios of -P to S amplitudes indicate that two different faulting mechanisms occurred during the foreshock sequence. The two radiation patterns can tentatively be correlated with different parts of the zone. The hypocenter of the mainshock was not located on the same fault as that defined by the foreshock's hypocenters but rather was located six kilometers south of and several kilometers shallower than the foreshock cluster. This large separation between foreshocks and mainshock in a direction perpendicular both to the plane of rupture of the mainshock and to the trend of the foreshocks might be the result of an en echelon step in the fault that slipped during the mainshock. An analysis of the change in stress due to slip on the possible foreshock faults shows that the increase in shear stress on the mainshock fault caused by the foreshocks can be no more than 4% of the stress drop associated with the foreshocks.

In the laboratory, the development of instabilities was examined by a study of the mechanics of simulated fault gouge. Deformation of Kayenta Sandstone (24% initial porosity) was observed in triaxial stress tests through several stress cycles. Between 50- and 300-MPa effective pressure the specimens deformed stably without stress drops and with deformation occurring throughout the sample. At 400-MPa effective pressure the specimens underwent strain-softening with the deformation occurring along one plane. However, the difference in behavior seems to be due to the density variation at different pressures rather than to the difference in pressure. After peak stress was reached in each cycle, the samples dilated such that the volumetric strain and the linear strain maintained a constant ratio (approximately 0.1) at all pressures. The behavior was independent of the number of stress cycles to linear strains up to 90% and was in general agreement with laws of soil behavior derived from experiments conducted at low pressure (below 5 MPa).

To clarify the nature of the dependence of the behavior on porosity seen in the Kayenta sandstone, the mechanical behavior of a material whose initial porosity could be varied, crushed Westerly granite, was also observed in triaxial stress tests. Samples consisting solely of crushed granite with an initial median grain size of 100 μm and different initial porosities (ranging from 10% to 22%) were repeatedly cycled past peak stress at an effective pressure of 190 MPa. Both peak stress and the rate of strain-softening after peak stress were found to increase with decreasing porosity. The axial and volumetric strains at peak stress, however, do not depend upon porosity, but rather are proportional to each other and seem to depend upon the strain history of the material.

The permeability of the crushed Westerly granite decreases dramatically with strain, so that after 30-50% linear strain microdarcy permeabilities are common. The permeability decreases even when the porosity is increasing. This is attributed to the increased surface area of the particles in contact with the fluid, caused by the crushing of grains during deformation. In fact, direct surface measurements of the material showed that the specific surface area increased by more than ten times over two to three cycles of stress and that the permeability, k , is related to the specific surface area, S , by $k \propto 1/S^2$. This means that the permeability of highly-strained granular fault gouge can be as low as that of clay gouge. Moreover, larger amounts of energy (at least 4% of the total energy) are being consumed by surface area production than had previously been supposed.

Thesis supervisors: Peter Molnar
Associate Professor of Geophysics

W.F. Brace
Professor of Geology

LIST OF CONTENTS

	Page
Abstract	ii
Acknowledgments	vii
Preface	1
CHAPTER I:	
Some characteristics of foreshocks and their possible relationship to earthquake prediction and premonitory slip on faults	6
Abstract	7
Introduction	7
Data	7
Temporal and spatial distribution of foreshocks	8
Possible phases of foreshock activity	9
Background seismicity	9
Effects of tectonic and regional setting	10
Dependence on magnitude of the main shock	11
Summary of time dependences of foreshock activity and frequency of occurrence of foreshocks	11
Relative magnitudes of foreshocks and main shocks ...	12
Amplitude ratios of P and S waves from foreshocks ...	14
Discussion	15
Conclusions	18
References	19
CHAPTER II:	
The foreshock sequence of the 4 February 1975 Haicheng earthquake (M = 7.3)	20
Introduction	21
Data	22
Technique	24
Results	27
Ratios of the P and S Wave amplitudes	29
Discussion	33
Summary	40
References	47
CHAPTER III:	
Cyclic loading of simulated fault gouge to large strains	63
Introduction	64
Experimental methods	64
Experimental results	66
Discussion	66
Dilatancy	66
Comparison with typical soil behavior	67

CHAPTER III (contd.):	Page
Shear strength	68
Relevance to earthquakes	68
Role of clay	68
Strain rate and temperature	69
Conclusions	69
References	69
CHAPTER IV:	
The effect of porosity and grain-crushing on the deformational behavior and permeability of crushed Westerly granite	71
Introduction	72
Experimental methods	75
Experimental results	78
Stress-strain behavior	78
Permeability	80
Permeability and surface area	81
Discussion	83
Physical mechanisms of deformation	83
Implications for earthquakes	84
Conclusions	87
References	91
Biographical note	106

Acknowledgments

First and foremost in this list must be my thanks to Peter Molnar and William Brace. They have both acted as my advisor for this thesis and have always been available with help, suggestions, encouragement, and criticism when needed. They have also been understanding about the difficulties of serving two masters.

There are many others I wish to thank who have also helped me in the execution of this work. Herbert Einstein, especially, has been of great assistance to me in planning my laboratory experiments and understanding their results. Tom Fitch was always ready to instruct and help me in running the computer programs for the earthquake locations. The laboratory work would have been impossible without Derek Hirst's help in keeping the machines running. David Pollard lent me his computer programs and gave useful suggestions for some of this work. I have also had many helpful discussions with Teng-fong Wong, Brian Evans, and Joseph Walsh. Madge Slavin and Jean Titilah have typed the manuscript.

Part of the work for this thesis was done in the People's Republic of China. There are many people and groups who have helped me in going to China and making it easy to work once I was there, to whom I am very grateful. The Committee on Scholarly Communication with the People's Republic of China (USA), the Ministry of Education (PRC), and the State Seismological Bureau (PRC) made the trips to China possible and assisted me

while I was there. I benefited greatly from the help of many Chinese scientists while I was there, most especially Wang Biqian and Xu Shaoxie of the Institute of Geophysics and Deng Qidong and Jiang Pu of the Institute of Geology.

In addition, Ma Xingyuan, the deputy director of the State Seismology Bureau, took special interest in my work. To inspire me to continue my work in earthquake prediction and finishing my thesis, he presented me with a fan on which was written a poem for children about earthquake prediction. In appreciation of Director Ma's concern, I present this poem so that we may all share in the inspiration. The poem was quite freely translated by my father, D.L. Jones, to preserve the flavor of the original.

Earthquakes are feared
When the animals are weird
The fauna act queer
When an earthquake is near.
When the fish leave the lake,
Then the grounds going to shake
When the cats run from home,
Then the ground's going to moan.
When the snakes wake their sleep,
Then the mountain will creep.
When the birds start to chatter,
Then the fault's going to shatter.
When the mice have no fear,
Then a tremor is near.
When the dogs are all barking,
Then the earth will start rocking.
When the cow kicks its stall in,
Then the rock's going to fall in.
So stay wide awake
And predict the next quake!

Preface

In the past fifteen years, earthquake prediction has ceased to be solely the province of seers and mystics and has become the research project of countless scientists. Much effort has been spent to give the prediction of earthquakes a scientific basis, but the science is still very immature. Three large earthquakes have been predicted in China, but at the expense of numerous false alarms. The largest earthquake yet predicted in the United States was assigned a magnitude of 4 and many more larger ones have occurred unannounced.

One of the central problems impeding the successful prediction of earthquakes is that it is not yet known exactly how earthquakes occur. Since Reid presented his elastic rebound theory in 1906, geophysicists have realized that earthquakes are the sudden release through slip on a fault of strain energy that has slowly accumulated in the crust. However, the exact physical process by which the transition from slow accumulation of strain to unstable release occurs is still undetermined. The research presented in this thesis has been conducted to investigate some aspects of this problem by two different methods.

Both seismology and rock mechanics can be used to study the problem of earthquake mechanics, each with different advantages and problems. Using seismology, one knows that actual earthquakes are indeed being studied, but the

conditions under which they occur - the state of stress, pore pressure, permeability of the rock, rock type, condition of the rock (degree of fracturing, rehealing, etc.), temperature - are all unknown. Using rock mechanics, these conditions are determined, but how an instability in a sample five centimeters long relates to an earthquake on a fault four hundred kilometers long is very unclear. In spite of the problems, however, each technique is valuable in that it allows different aspects of the problem to be studied. Both have been used in the research presented here to study the generation of instabilities.

The seismological research has examined the occurrence of foreshocks. The basis of much earthquake prediction research is the idea that the transition from slow accumulation of energy to dynamic release by slip on the fault does not occur instantaneously but rather may be preceded by a period of accelerating deformation of the crust. Foreshocks, when they occur, are the most obvious sign of this deformation and, as such, can shed light on the processes leading to the instability. However, it is difficult to study foreshocks because of the paucity of well-recorded sequences. Therefore, in Chapter I, the study was begun by considering an average foreshock sequence that was created by combining all of the foreshocks recorded in the teleseismic catalogue to all earthquakes with $M \geq 7$ from 1950 to 1973. The temporal, spatial and magnitude relationships of the foreshocks to the mainshocks were considered to estimate the extent in time and space of the precursory deformation. The results

were then compared to those expected from a model of time-dependent rupture of asperities on a fault.

While this method supplies enough data for a statistical analysis, the noise in teleseismic data can obscure patterns (and perhaps create artificial ones, as well). Case studies of individual sequences are also needed to see details of the foreshock process. Thus Chapter II presents an analysis of the spatial distribution and radiation patterns of the 500 foreshocks of the 4 February 1975 Haicheng, China, earthquake. These data were then used to calculate an approximation of the stresses that triggered the main shock.

To investigate the occurrence of instabilities in the laboratory, the research focused on the behavior of fault gouge. Many mature fault zones have extensive regions of fault gouge which consists of both crushed rock and clay. (To avoid the complications of clay, only crushed rock was used here.) While the resolution of earthquake locations is insufficient to determine exactly where within the fault the earthquakes occur, it is generally assumed that the presence of gouge with different mechanical properties than the surrounding rock will greatly affect the response of the rock gouge system to loading stresses. Many models have been developed to calculate the interaction of the country rock and the gouge that have assumed the mechanical behavior of the gouge in isolation. The experiments presented in Chapters III and IV were conducted to determine if this assumed behavior was feasible under conditions thought to apply to

fault zones. The pressure, strain history, porosity and grain size dependencies of the mechanical behavior were examined.

In Chapter IV, changes in permeability and grain crushing during deformation were also examined. These are important for other aspects of the earthquake problem. The permeability controls the pore pressure in, and thus the effective stress acting on, the fault gouge, which is one of the least well determined parameters in natural fault zone. If large strains change the permeability significantly, as was investigated here, the permeability in mature fault zones could be much different than supposed. The amount of grain crushing during deformation is important to know for determining how much of the energy put into a fault zone is used to produce new surface and is thus not available for seismic energy release or frictional heating.

Included in this volume are two papers with more than one author. Since these works are being submitted as a Ph.D. thesis, it is necessary to give some account of how much of the work was done by the candidate. In the following, the relative contributions of the authors are discussed.

Chapter I: The basic idea of how to conduct this research was P. Molnar's. He also suggested creating several of the figures and added changes to drafts of the manuscript. The derivation of the model was done by both P. Molnar and L. Jones. L. Jones did the rest.

Chapter II: The arrival times were read by L. Jones and B. Wang. The computation of S/P ratios was done by

B. Wang and S. Xu. T. Fitch developed the programs used to determine relative locations of the events and helped with the computation. L. Jones did the rest.

CHAPTER I :

SOME CHARACTERISTICS OF FORESHOCKS
AND THEIR POSSIBLE RELATIONSHIP TO
EARTHQUAKE PREDICTION AND PREMONITORY SLIP ON FAULTS

SOME CHARACTERISTICS OF FORESHOCKS AND THEIR POSSIBLE RELATIONSHIP TO
EARTHQUAKE PREDICTION AND PREMONITORY SLIP ON FAULTS

Lucile M. Jones and Peter Molnar

Department of Earth and Planetary Sciences, Massachusetts Institute of Technology,
Cambridge, Massachusetts 02139

Abstract. Foreshocks occur before a large fraction of the world's major ($M \geq 7.0$) earthquakes. Teleseismically located events before major earthquakes from 1914 to 1973 were considered together to examine possible average temporal and spatial patterns of foreshock occurrence. Several days before the main shocks and apparently near the epicenters of them ($\Delta \approx 30$ km) the activity begins to increase, culminating in a final rapid acceleration of activity in the last day. The acceleration continues up to the time of the main shocks, except for a possible temporary decrease about 6 hours before them. The seismicity increases approximately as the inverse of time before main shock. This relationship is essentially unrelated to the magnitude of the main shock. The magnitude of the largest foreshock is also unrelated to the magnitude of the main shock. In addition, pairs of major events are common. Ten percent of the world's major events are preceded by other major events within 100 km and 3 months. For foreshocks within each of three sequences studied, the ratio of the amplitudes of the P and S waves were approximately the same, suggesting that the faulting mechanisms are the same for events in each sequence. By assuming an inhomogeneous fault plane on which asperities fail by static fatigue, we derived an equation for accelerating premonitory slip as a function of time, which agrees with the observed time dependence of foreshocks.

Introduction

When present, foreshocks are the most obvious premonitory phenomenon preceding major earthquakes. If they could be recognized as such before a main event, they would be a very useful tool in earthquake prediction because they accurately pinpoint the time and location of the forthcoming earthquake. This was demonstrated by the successful prediction of the February 4, 1975, Haicheng earthquake, wherein foreshocks played a crucial role [Raleigh et al., 1977; Wu et al., 1976; Zhu, 1976]. But even beyond their use in earthquake prediction, foreshocks are the most convincing evidence that we have of deformation of the earth before major earthquakes. Therefore an improved understanding of foreshocks may provide important information about precursory deformation. Motivated both by the possibility of using foreshocks as a short-term predictor and by the need to better understand the mechanical behavior of the nearby rocks

immediately preceding major earthquakes, we studied some characteristics of foreshocks that occur in the few hours, days, and weeks before large events.

In presenting the results we first discuss the temporal and spatial distribution of seismicity prior to main shocks to define temporal patterns of short-term foreshock activity and to determine how common foreshocks are. As part of this analysis we consider the possible effects of various characteristics of the main shocks (magnitude, tectonic setting, geographical position, etc.) on these patterns. We then examine the relative magnitudes of foreshocks and main shocks and the radiation patterns of three foreshock sequences for possibly recognizable characteristics. Finally, we compare the data with a simple mathematical expression derived for accelerating premonitory fault slip.

Data

We considered foreshocks before three groups of main shocks. The first is all major ($M \geq 7.0$) shallow (depth < 100 km) earthquakes in the world from 1914 to 1949 (511 events), listed by Duda [1965]. We searched for foreshocks in the Bulletins of the International Seismological Summary (ISS). The second group is all major shallow earthquakes in the world from 1950 to 1964 [Duda, 1965] and from 1965 to 1973 (250 events) [U.S. Government Printing Office, 1965-1973]. For this group, earthquakes were taken from the catalogue of world events prepared by the National Oceanic and Atmospheric Administration (NOAA) and Bulletins of the International Seismological Center (ISC). All of the locations had been computed from teleseismic data. Because of the location capability of worldwide networks, the magnitudes of essentially all of these earthquakes are greater than 4 and usually greater than $4 \frac{1}{2}$ [Evernden, 1970, 1971]. The appendix table lists the main shocks and foreshocks from these two data sets used in the following analysis.¹

We also searched the literature for field reports of foreshock activity before individual main shocks. Such foreshocks are also listed in the appendix, but were not used in most of

¹Appendix table is available with entire article on microfiche. Order from American Geophysical Union, 1909 K Street, N.W., Washington, DC 20006. Document J79-005; \$1.00 Payment must accompany order.

the analysis. For some of the analysis, however, we did use a third group of main shocks, earthquakes occurring near Greece, with $M \geq 5.6$ for events between 1911 and 1965 and $M \geq 5.1$ between 1966 and 1973. Many of these events were preceded by foreshock sequences, which are listed by Papazachos et al. [1967; Papazachos, 1975a].

In some situations, two or more major earthquakes occurred very close to each other in time and space. In such cases it did not seem reasonable to call these events separate main shocks. When the events occurred within 3 months and 100 km of each other (within the most extreme limit of foreshock activity discussed below), we considered the series of events to be only one sequence. These multiple major events occurred quite frequently. Of 939 major sequences recorded since 1897, 92 included two or more events with magnitudes greater than 7.0 and occurring within 3 months of each other. Of these 92 sequences, 67 were not clear main shock-aftershock sequences in the sense that the first event was either smaller than, or no more than 0.4 units of magnitude greater than, a later event.

If the first of the large events had the largest magnitude, its origin time was naturally used as that of the main shock. If the magnitude of the first event was no more than 0.2 units of magnitude less than the later events, the series was considered to be a double event, and again the origin time of the first event was used. Only if the second event had a magnitude more than 0.2 units greater than the magnitude of the first event was the first event considered to be a foreshock. In general, the smaller events occurring between the two large events were not considered to be foreshocks, because they appeared to be aftershocks of the large foreshock. Only when we could distinguish which of the events occurring between the two large earthquakes were the aftershocks of the large foreshock and which were foreshocks of the second event were the latter used. For instance, an event with $M \sim 6.0$ occurred on March 7, 1966, 15 days before the March 22, 1966, Hsing-tai earthquake. In the day following the first earthquake there were six events listed in the NOAA catalogue, which we assume were aftershocks. Then two events occurred on March 11, one on March 19, and two more on March 22. Among these we assumed that only the main event of March 7 and those on March 19 and March 22 were foreshocks.

None of the sequences that included main events with $M \geq 7.0$ resembled swarms, as defined by Mogi [1963] and Sykes [1970]. In general, two, or at most three, events clearly were the largest, and the first of these was never preceded by the gradual increase in either frequency of occurrence or magnitude of earthquakes that characterizes swarms. Therefore of the three types of sequences described by Mogi [1963] - main shocks with foreshocks, main shocks without foreshocks, and swarms - only the first two categories seem to be represented by major earthquakes. Swarms appear to be a property only of earthquakes with magnitudes smaller than 7.

Temporal and Spatial Distribution

of Foreshocks

In studying the temporal variation in foreshock occurrence a definition of foreshocks that distinguishes them from background seismicity is necessary. To obtain a crude impression of the frequency of occurrence, we first considered any earthquake a foreshock if its computed location was within 100 km and it occurred within 40 days of the main event [see Jones and Molnar, 1976]. This definition is only a starting point for the discussion, and criteria for distinguishing foreshocks from background seismicity are discussed below. One hundred kilometers was chosen because it allows inclusion of essentially all events that occurred within the rupture area of main shocks with $M \sim 7$, given the errors in the locations. All locations were taken from the sources cited above. Forty days was arbitrarily chosen because it seemed to correspond to the common usage of the term foreshock in the literature. By these criteria the percentage of main shocks preceded by foreshocks increases steadily until the present (Figure 1). This observation is almost surely a result of poorer recording capability earlier in the century. Notice also that the percentage of earthquakes with such foreshocks reported becomes nearly constant in 1950. For that reason we rely primarily on the second data set to draw inferences about foreshock activity.

In search of temporal patterns of foreshock activity, we examined the seismicity for a year before each of the main shocks that occurred after 1950 with more than two aftershocks listed in the NOAA catalogue. We assumed that if only two aftershocks were located by teleseismic data, the location capability of the network was poor. Indeed, the number of major events with only two or fewer aftershocks located teleseismically and preceded by foreshocks (as defined above) was considerably less than those with three or more aftershocks (Fig. 1). Because of the poor location capability of the network before 1950, we did not examine the entire year before the main shocks during this interval. Nor did we use the events near Greece for this analysis, because Papazachos [1975a] did not list locations of events and did not describe the seismicity for the entire year before these main shocks. Examining 1 year is obviously insufficient to determine long-term trends in seismicity, but our purpose here is to analyze only the activity a few weeks before the main shocks, not years. For this situation a year of data is enough to define a background level and to allow recognition of short-term changes in earthquake occurrence.

The events occurring during the year before the main shocks were separated into three groups by the distance between their computed locations and those of the main shocks, 30, 60, and 100 km. Since no individual sequence contained enough recorded events to define temporal and spatial patterns of occurrence, all of the sequences were combined into a

single sequence. This was done by putting all of the sequences onto the same axis where the origin is the time of occurrence of each main shock. A histogram was made by plotting the total number of foreshocks occurring in each 24-hour period before the mainshocks (Figure 2).

Possible Phases of Foreshock Activity

There is a suggestion of three changes in level of seismic activity preceding major earthquakes. Close to the epicenters of the main shocks, there are a very large number of events that occur in the day immediately preceding the mainshocks. This large number of events appears to be the culmination of an increasing frequency of occurrence near the main shocks beginning several days earlier. Farther from the main shocks, there is also a suggestion of an increase in activity that starts about 3 months before the main shocks.

It is necessary to determine how representative these patterns are of all foreshock sequences. Below we consider a number of possible factors that could affect the temporal pattern of foreshock activity in Figure 2. Among these factors are various ways that background seismicity could distort the patterns and dependencies of foreshock activity on magnitudes of main shocks and on their tectonic or regional setting. We find that only the two increases in activity close to the main shocks in time and space seem to be representative of premonitory seismic activity.

Background Seismicity

Mislocation of earthquakes could contaminate the data by introducing background seismicity into the plot in Figure 2. A systematic relocation of seismicity will probably sharpen the temporal and spatial relationships to main shocks (and is in progress). A crude test of whether mislocations are introducing

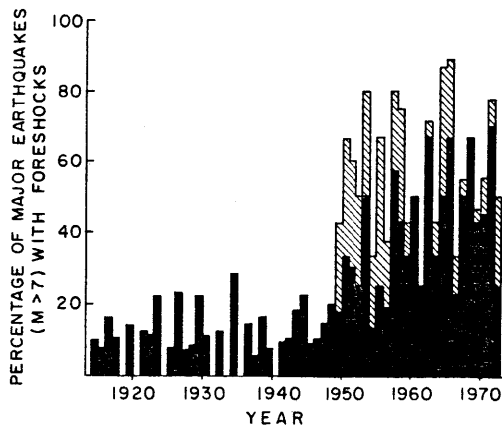


Fig. 1. Percentage of major earthquakes ($M \geq 7$) in each year from 1914 to 1973 that were preceded by recorded foreshocks. For 1950 to 1973 the hatched area is the percentage of earthquakes that had at least two aftershocks recorded by NOAA and that were preceded by foreshocks.

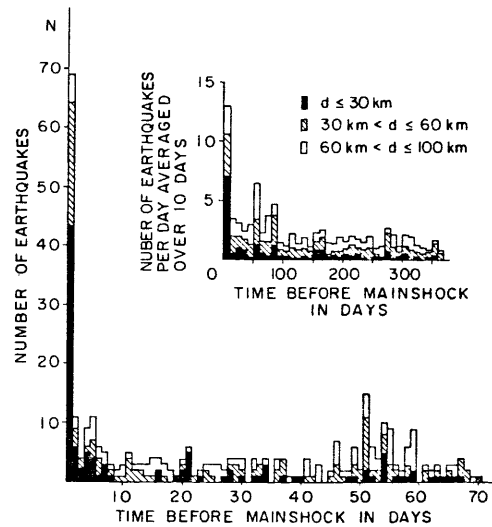


Fig. 2. Foreshock activity as a function of time before main shocks occurring between 1950 and 1973. The number of foreshocks are given separately for three different ranges of distance between the computed foreshock and main shock epicenters. Inset shows the number of foreshocks averaged over 10-day periods for a 1-year period preceding the main shocks.

spurious temporal patterns can be made by plotting a subset of the data, those earthquakes occurring after 1964, which are the more reliably located (Figure 3). The similarity between Figures 2 and 3 suggests that either poor locations do not contaminate the data or that a careful relocation of hypocenters is required to reveal a contaminating effect.

A large number of foreshocks from a few main shocks could be dominating the plots in Figures 2 and 3 so that they are not representative of average foreshock sequences. To test for this possibility, separate histograms were made for main shocks from the second data set with only one, two or three, four or five, and more than five events within 40 days of the mainshocks (Figure 4). The peak on the last day exists for all cases and clearly does not depend upon how many foreshocks occurred before any event. Although the increase in activity a few days before the main shocks is less well-defined (perhaps due in part to the smaller data base involved), it does occur before main shocks with more than one foreshock. Therefore we conclude that neither the increase in activity beginning a few days before the main shocks nor the peak in activity on the last day is due to abundant seismicity before a small number of main shocks.

The increase in activity beginning about 90 days before the main shocks, however, does seem to be due to events preceding a few main shocks. Almost half of the events occurring in the 50 to 90 day period occurred before three main shocks, two in the New Hebrides (January 23, 1972 and November 2, 1972) and one in the Aleutians (May 2, 1971). To illustrate this, Figure 5 separates the data in Figure 2 into plots of seismicity preceding main shocks in the New Hebrides and the Solomon Islands alone

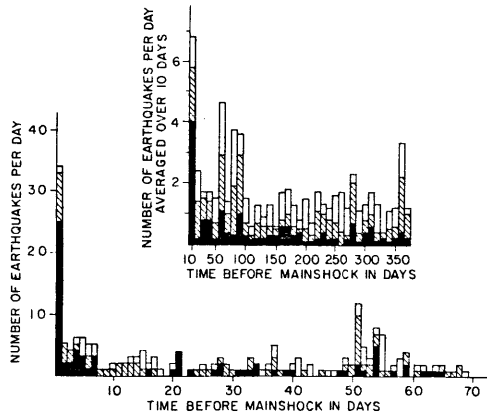


Fig. 3. Foreshock activity as a function of time before main shocks between 1964 and 1973 (procedure as in Figure 2).

and of seismicity from the rest of the world exclusive of these regions. Notice that the increase beginning about 90 days before the main shocks in Figures 2 and 3 is barely discernible when data from the New Hebrides and the Solomon Islands are excluded. Thus we conclude that the apparent increase 90 days before the main shocks is probably not a common feature of foreshock sequences.

The absence of any pronounced foreshock activity in the last few days before main shocks in the Solomon Islands (Figure 5) suggests that inclusion of the seismicity preceding these events in Figures 2 and 3 merely increases the background level of activity without clarifying the relationships between main shocks and the seismicity that precedes them. To investigate the background seismicity further, we determined how many events were preceded by earthquakes in three arbitrary 10 and 40 day periods well before the times of the main shocks (Table 1). For this we used the 161 major earthquakes occurring between 1950 and 1973 with more than two reported aftershocks. Seismicity occurred within 100 km of about 25% of the main shocks in the 40-day intervals, but it occurred within 30 km of only about 6% of them. For 10-day periods the percentages were closer to 2%. Therefore the increase in activity in the several days before the main shocks is clearly not strongly influenced by background activity.

Perhaps more important for this analysis was the recognition that the background seismicity was much higher in active subduction zones than elsewhere (Table 1). To illustrate this, Figure 6 shows a plot like those in Figures 2 and 3 but for earthquakes in nonsubduction zones. Of the 41 events in nonsubduction zones, 21 were preceded by seismicity in the 40 days preceding them, and 20 were preceded by foreshocks within 30 km of the mainshocks in the last 10 days. (These numbers, but not the data in Figure 6, include foreshocks reported in the literature but not located teleseismically.) Note that the background activity preceding mainshocks in nonsubduction zone regions is low and the increase in activity within 30 km of the main shocks begins several days before them.

This approximately 10 day initiation of foreshock activity may also occur for subduction zones, despite the contamination by background seismicity. As described above, the activity in the New Hebrides seemed to contribute to a spurious apparent increase about 90 days before the main shock. The plot of all the data, except for events from the New Hebrides and from the Solomon Islands, for which there does not seem to have been foreshock activity (Figure 5c), reveals an increase in activity relatively close to them (computed location, less than 30 km), beginning about 10 days before the main shock. For this distance range the activity in the last 10 days is clearly more pronounced than that in preceding periods of the same duration. Better locations can probably enhance this pattern.

Effects of Tectonic and Regional Setting

We were unable to detect any clear dependence of the temporal pattern of foreshock activity on the tectonic setting of the main shocks. At the same time our limited data set might be inadequate to reveal such a dependence. The greater percentage of events in nonsubduction zones with seismicity 10 days before them than for those in subduction zones may indicate that the occurrence of foreshock activity is dependent upon the tectonic setting. The data at present, however, are probably insufficient to explore this possibility further.

Similarly, the data are probably inadequate to reveal a regional difference in the temporal patterns of foreshock activity. Although the increase beginning several days before main shocks is absent in the New Hebrides and the sharp increase on the last day is absent in the Solomon Islands (Figure 5), we do not think that these data are sufficient to show that

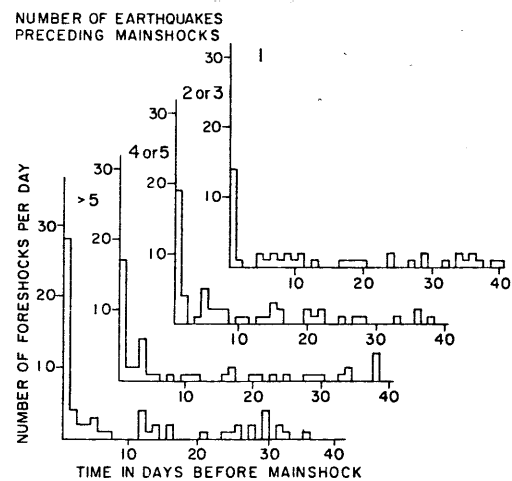


Fig. 4. Number of foreshocks per day as a function of number of the foreshocks recorded for different earthquakes. Separate plots are shown for foreshock sequences consisting of only 1 event, 2 or 3, 3 or 4, or greater than 5 events. Note that the increase about 5 days before the main shocks and the peak on the last day do not depend upon how many foreshocks preceded each event.

regional differences in the temporal patterns exist. There may be regional differences in the frequency of occurrence of foreshocks. The apparent absence of foreshocks in the Solomon Islands may be one example. Moreover, foreshocks seem to be common in several regions and not in others [see Jones and Molnar, 1976, Figure 2], but once again we do not think that these data are sufficient to demonstrate regional variations in the frequency of occurrence.

Dependence on Magnitude of the Main Shock

A dependence of foreshock activity on magnitude also might affect the reliability of the patterns in Figure 2. To examine this possibility, sequences were plotted separately for main shocks with $M < 7.0$ (Greek events only), $7.0 \leq M < 7.8$, and $M \geq 7.8$ (Figures 7a-7c). The time dependences of these three sequences are very similar to each other and also to that of the combined sequence (Figure 7d). All of the sequences show the same pattern of seismicity - an increase in activity a few days before the main events, culminating in a prominent maximum on the day before the main shocks.

The data in Figure 7 were fitted to both exponential and power law functions by linear regression. Unlike the data of Pho et al. [1976], exponential functions fit poorly and are probably not a good representation of the physical processes involved. The data fit much better to power law equations. The combined data showed that foreshock activity is proportional to time raised to the minus one power, which agrees with the findings of Kagan and Knopoff [1978] and Papazachos [1974a,b, 1975b]. Although the calculated exponent is more negative for main shocks with larger magnitudes, the difference is slight and probably negligible.

In reference to very short term premonitory seismicity a plot by hour of foreshock activity in the last few days shows that the frequency of occurrence continues to increase toward the time of the mainshocks (Figure 8). This average pattern continues except for a lull in activity 5-8 hours before the main shocks. This peak is defined by foreshocks before 18 events, not by just a few main shocks. This peak followed by a lull is of interest because Chinese seismologists reported a drop in foreshock activity 4-8 hours before both the 1973 Haicheng and the 1966 Hsing-tai earthquakes [Wu et al., 1976].

Summary of Time Dependences of Foreshock Activity and Frequency of Occurrence of Foreshocks

The data presented in Figures 2-8 suggest several different possible definitions of foreshocks. The data in Figure 2 suggest three possible phases in activity beginning about 90 days, a few days (5-10), and on the last day before the main shocks. Although many main shocks are preceded by seismicity 90 days or less before them (Table 2), the apparent abrupt increase at that time appears

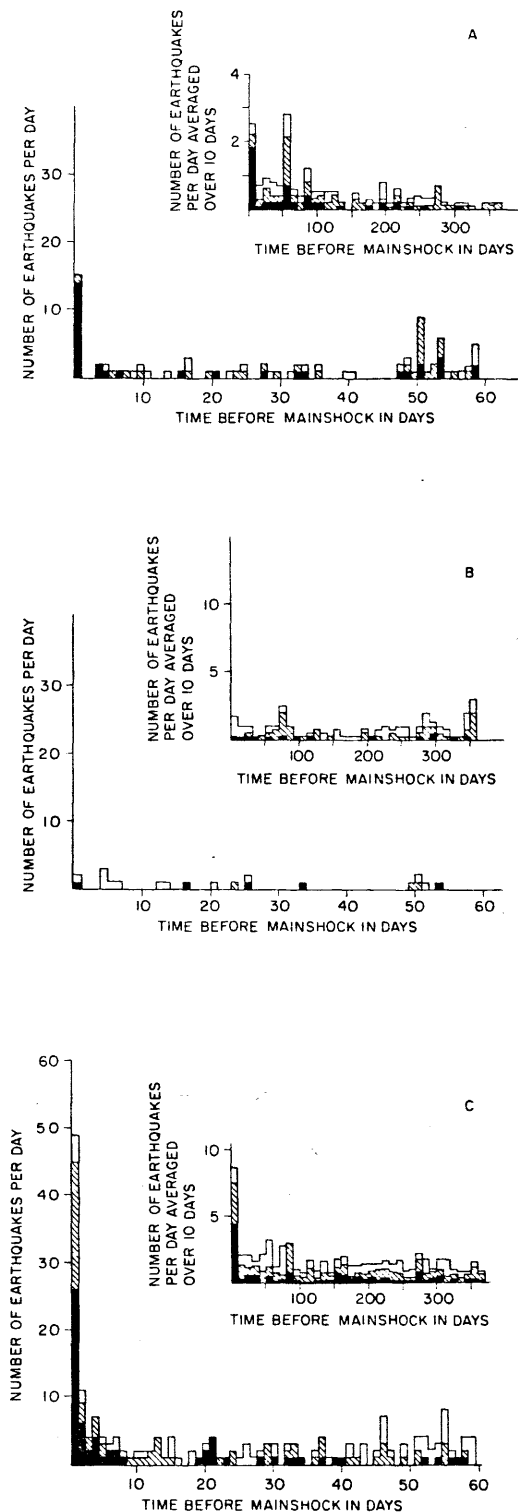


Fig. 5. Foreshock activity as a function of time before mainshocks in the New Hebrides, Solomon Islands, and the rest of the world between 1950 and 1973 (procedure as in Figure 2).

to be due to swarms of events preceding three main shocks and possibly not related to them (Figure 5). Therefore we do not think that the increase at 90 days is representative of foreshock sequences. The increase a few days

TABLE 1. Background Seismicity

Dis- tance	Time Interval, days	Main Shocks					
		All	Nonsubduction	Subduction			
				All	Without New Hebrides and Solomon Islands*	New Hebrides	Solomon Islands
		<u>40-Day Periods</u>					
30km	101-140 [†]	6	0	9	7	17	11
	118-220	7	0	10	10	11	11
	281-320	5	0	7	5	6	22
	average	6	0	8	7	11	15
60km	101-140	16	2	20	15	44	22
	181-220	16	2	21	21	22	22
	281-320	16	0	21	17	28	44
	average	16	2	21	18	31	30
100km	101-140	24	7	29	23	61	33
	181-220	27	5	34	33	44	33
	281-320	28	5	36	33	44	56
	average	26	6	33	29	50	41
		<u>10-Day Periods</u>					
30km	111-120	1	0	2	1	0	11
	201-210	2	0	3	3	0	11
	291-300	2	0	3	3	0	11
	average	2	0	3	3	0	11
60km	111-120	6	2	7	4	17	22
	201-210	6	2	7	7	6	11
	291-300	5	0	7	7	0	22
	average	6	2	7	6	7	19
100km	111-120	9	5	11	4	39	22
	201-110	8	2	10	10	11	11
	291-300	9	0	12	12	6	22
	average	9	2	11	9	19	19

Values are percentages of main-shocks with more than two aftershocks occurring between 1950 and 1973 preceded by earthquakes in arbitrary time intervals before the main-shocks and at different calculated distances from them.

*Main-shocks occurring on subduction zones except those in New Hebrides or the Solomon Islands.

[†]For example, 101-140 days before the main-shocks.

before the main shocks is more distinct and is especially clear for main shocks in non-subduction zones (Figure 6). There is no apparent dependence of these temporal patterns on the magnitudes of the main shocks or on the regional or tectonic settings of them.

Table 2 summarizes the frequency of occurrence of seismicity preceding mainshocks in different time intervals and at different computed distances from them. It is intended to summarize the range of possible definitions of foreshocks and background seismicity. Regardless of the definition, foreshocks are not a rare occurrence. Moreover, many events are preceded by foreshocks that are not located teleseismically and therefore not included in Figures 1-8. The 1966 Congo

[Lahr and Pomeroy, 1970], the 1915 Pleasant Valley (R. E. Wallace, personal communication, 1978), the 1952 Kern County and the 1954 Dixie Valley - Fairview Peak earthquakes [Richter, 1958] were all preceded by foreshocks not located with teleseismic data. There probably are many other major events with foreshocks too small to be located. It is noteworthy that none of the more than 500 foreshocks of the 1975 Haicheng earthquake [Wu et al., 1976] were located teleseismically. It is almost certain that there have been other foreshocks about which we could not find any information.

Relative Magnitudes of Foreshocks and Main Shocks

The time dependence of foreshock activity does not appear to be sensitive to the magnitude

Jones and Molnar: Some Characteristics of Foreshocks

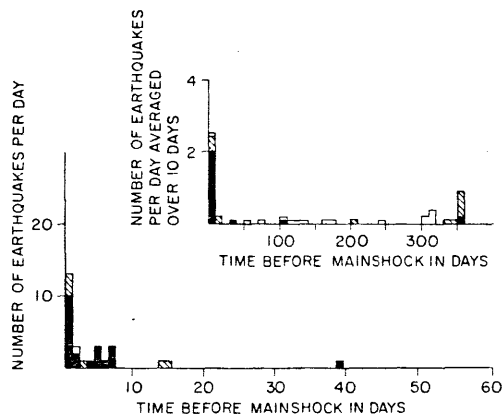


Fig. 6. Foreshock activity as a function of time before main shocks in nonsubduction zone regions between 1950-1975 (procedure as in Figure 2).

of the main shocks (Figure 7). If foreshocks are to be used for earthquake prediction, some other characteristic must be used to estimate the magnitude of the main shock. Papazachos [1974a, 1975b] and Wu et al., [1976] suggested that in spite of a great deal of scatter there is a linear relationship between the magnitudes of main shocks and those of their largest foreshocks. Figure 9 explores this possibility using all of the data available to us. Even allowing for an error of 0.5 units in magnitude, we can see no relationship between the magnitudes of main shock and largest foreshock. The only limits on the distribution of the magnitudes of the largest foreshocks appear to be that a foreshock be smaller than its main shock and large enough to be located. We suspect that the crude relations in the data of Papazachos and Wu et al. are the result only of the limited magnitude range of their data. We thus conclude that foreshocks cannot be used to predict reliably the magnitude of an

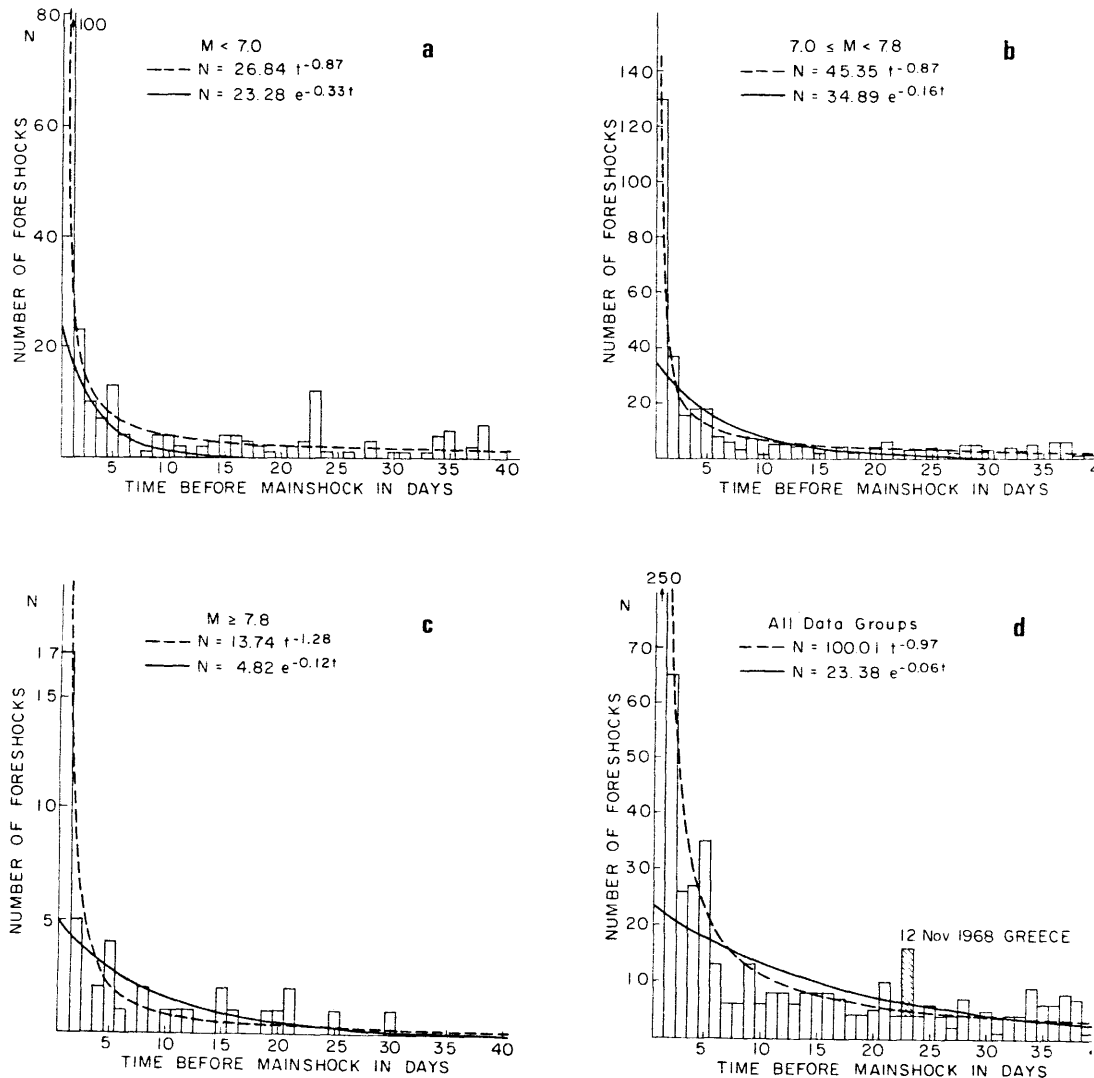


Fig. 7. Foreshock activity (a-c) as a function of time before main shocks of different magnitudes and (d) for all main shocks from all three data sets. Also shown are the exponential (solid line) and power law (dotted line) equations that best fit these data. Note that the temporal variation does not depend upon the magnitude of the main shock.

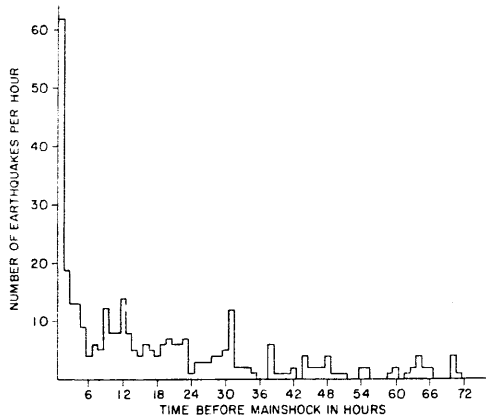


Fig. 8. Foreshock activity as a function of time before main shocks for the 3 days before the main shocks.

impending earthquake. This lack of correlation can be interpreted to mean that neither the area that slips nor the amount of slip during foreshocks is a constant fraction of the fault area or displacement caused by the main shock.

Amplitude Ratios of P and S Waves

From Foreshocks

Jin et al. [1976] suggested that the fault plane solutions of foreshocks are similar and that this aspect would be diagnostic of them. Because most foreshocks are too small for determination of a fault plane solution, they suggested that the similarity could be examined by comparing the amplitudes of P and S waves

recorded at one station. The ratio of these amplitudes depends upon three factors - the propagation path, the fault plane solution, and the position of the station with respect to the fault plane. If the amplitudes are measured at only one station and the foreshock hypocenters are very close to each other, the amplitude ratios will depend only on the fault plane solution. Jin et al. [1976] found that the foreshocks of the 1975 Haicheng earthquake did have very similar amplitude ratios. Lindh et al. [1978] observed essentially the same pattern for three foreshock sequences that they studied (see also Bolt et al. [1977]), but Engdahl and Kisslinger [1977] did not for foreshocks preceding an Aleutian event by a few weeks.

We studied three main shocks with many foreshocks, the only ones that have occurred since the World Wide Standardized Seismograph Network (WWSSN) was installed and that occurred sufficiently close to a WWSSN station to be well recorded. Records from the station at Baguio (BAG) were used for the August 1, 1968, earthquake in the Philippines [Su, 1969], and records from the station at Athens University (ATU) were used for the December 5, 1968, earthquake near Greece and the March 28, 1969, earthquake in western Turkey [Papazachos, 1975a]. In all cases the events preceding the main shocks are too small to be located reliably. They are brought to be foreshocks from their approximate locations determined from recordings at a single station. Their times of occurrence and P and S wave amplitudes are listed in Table 3. The maximum amplitudes of the P and S waves, plotted versus one another for the three sequences in Figures 10,

TABLE 2. Foreshock Activity

Dis- tance From Main Shock, km	Time Before Main Shock, days	1950-1973							
		Aftershocks > Magnitude 2							
		Non Subduc- tion				Subduction			
		1914- 1949		All		Without New Hebrides and Solomon Islands		Solomon New Hebrides Islands	
		(511)	(250)	(161)	(41)	(120)	(93)	(18)	(9)
100	40	11.3	42.2	50.3	36.6	55.0	48.4	77.8	77.8
60	15	9.6	21.2	29.9	34.1	26.7	24.7	44.4	11.1
30*	10	9.4	15.6	24.8	29.3	20.0	17.2	38.9	11.1
30†	10†			28.6	48.3	21.7	19.4	38.9	11.1

Values are percentages of main shocks in different regions preceded by premonitory seismicity within different time intervals and calculated distances of the main shocks. Numbers in parentheses after the headings are the number of main shocks.

*There are also two main shocks not appearing in these percentages that occurred before 1964 in non subduction regions and three others in subduction zones that are preceded by events occurring within 10 days of the main shocks but located between 30 and 60 km from them. As these earthquakes are in remote regions (such as Tibet and the South Pacific), it is likely that they are mislocated and are actually closer to their main shocks.

†Including written reports.

11, and 12, define straight lines passing through the origin. In fact, not only are the amplitude ratios the same, but in general the shapes of the signals are remarkably similar. The only points that deviate from the lines in Figures 10, 11, and 12 are those for a few foreshocks occurring more than 3 weeks before the earthquake in Greece. All of the other foreshocks occur within 4 days of the main shocks.

Although not proof, these data are consistent with identical fault plane solutions for the foreshocks occurring within about 4 days of their main shocks. The different amplitude ratios of the earlier foreshocks of the event in Greece could be due either to differing fault plane solutions or different locations, as Engdahl and Kisslinger [1977] report for the Aleutian event.

Discussion

One purpose of this study is to consider possible implications of foreshock activity for precursory deformation. We think that characteristics of foreshocks mentioned here are suggestive of accelerating precursory fault slip. Foreshocks, being earthquakes, definitely represent slip somewhere; the close proximity of the events to one another and identical amplitude ratios (for the few events that we could study) suggest that in general, the slip takes place on the same plane for each. We presume that this plane is the one that ruptures during the main shock, although the data of Bolt et al. [1977] and Engdahl and Kisslinger [1977] suggest that this may not always be the case. The temporal distribution implies that wherever the slip is, it is accelerating. The lack of a correlation between the magnitudes of the main shock and foreshocks suggests that the area that slips during the foreshocks is not a constant fraction of the rupture area of the main shock. The foreshocks probably involve slip only in the vicinity of the main shock hypocenters, where the main shocks are triggered. To illustrate how accelerating premonitory fault slip can explain these properties of foreshocks, we derive a simple expression for the development of an instability to compare with these data. Although the particular instability that we discuss was motivated by the observed characteristics of foreshocks, we do not claim that the data prove that it is an accurate description of what actually occurs.

Assume that the fault plane is held in place at a number of asperities. This could also represent a plane of inhomogeneous stress where the points of highest stress are modeled by asperities. During the short time period involved (a few months or less) the tectonic stress acting on the whole fault plane can be assumed to be constant. If A_0 is the rupture area, A_u is the portion of A_0 that has not yet slipped, σ_0 is the tectonic shear stress, and σ is the average shear stress acting on the unslipped portion, these assumptions can be expressed as

$$A_0 \sigma_0 = A_u \sigma \quad (1)$$

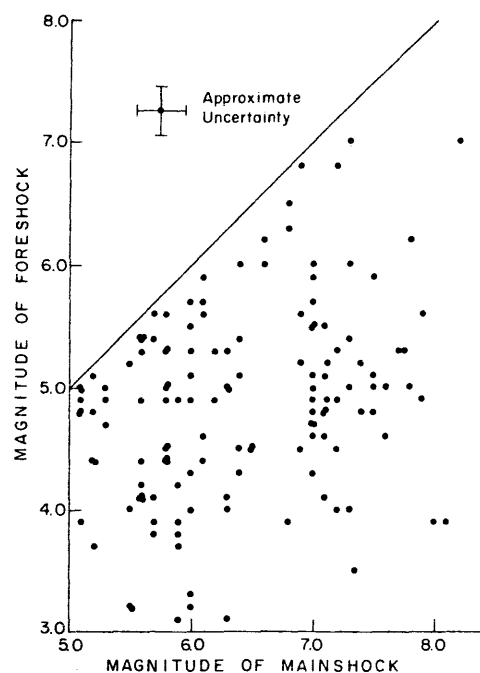


Fig. 9. The magnitudes of the largest foreshocks as a function of the magnitude of their main shocks. No pattern is obviously discernible. This is the only figure in which data from written reports of foreshock activity are used.

The number of asperities, N , can be related to A_u by

$$A_u = \bar{N} \bar{A} \quad (2)$$

where \bar{A} is the average area of an asperity. As slip occurs on some segments of the fault (rupture of some asperities), the stress on the remaining unslipped segments will increase, and the increased stress will increase the probability of further slip on the remaining asperities. Eventually, the rate of failure of asperities increases rapidly, causing an instability. With some additional, simple assumptions we can derive a differential equation relating the change in unslipped area to time.

Presumably, the lifetime of an asperity depends upon the stress acting on it. For instance, in the static fatigue of quartz in uniaxial compression, Scholz [1972] showed that such a dependence could be expressed in terms of the mean time before failure

$$\langle t \rangle = T \exp(-k\sigma) \quad (3)$$

where σ is the differential stress and T and k are constants that can be determined experimentally [see Scholz and Martin, 1971]. T is a time constant that depends upon the fluid pressure in the rock. Scholz [1972] did not evaluate T , and it is difficult to calculate it for conditions in the earth. Scholz did evaluate k , which is a measure of the rock strength. We assume that the lifetime of asperities on a fault obeys an equation like (3).

TABLE 3. Maximum Amplitudes of Events Preceding Major Earthquakes

Date	Time, UT	Vertical		North		East	
		P	S	P	S	P	S
<u>Earthquakes Preceding the August 1, 1968,</u> <u>Event in the Philippines</u>							
Aug. 1, 1968	2013	18	(70)	15	(70)
	2008	3	18	3	15	5	17
	2000	8	38	6	33	9	...
	1858	5	30	4.5	28	6	...
	1823	(25)	(70)	24
	1716	2	13	2	10	3	(15)
	1638	3	18	3	15	4	35
	1117	5	30	10	55
<u>Earthquakes Preceding the December 5, 1968,</u> <u>Event in Greece</u>							
Dec. 4, 1968	2048	2.5	6	2	7	2.5	6
	2030	6	24	6	22	7.5	18
	2011	5	16	5	20	6	15
	1937	40	(75)	(24)	(100)	(40)	(86)
	1852	20	(48)	(14)	(60)	20	50
	1842	7	22	6	25	10	22
Nov. 26, 1968	0430	15	(120)	13	...	21	53
Nov. 13, 1968	1748	12	40	10	38	20	70
Nov. 12, 1968	2309	(2)	15	2	10	5	10
	0652	(3)	30	(4)	36	28	52
	0609	(52)	(100)	(30)	(84)	(30)	(76)
	0401	8	50	8	(30)	10	38
	0342	15	42	9	(40)	19	(60)
	0120	2	11	2	8	4	9
	0117	2	20	2	16	3	18
Nov. 3, 1968	1408	4	20	2	10	3	10
<u>Earthquakes Preceding the March 28, 1969,</u> <u>Event in Turkey</u>							
March 27, 1969	1807	4	6			3	6
March 26, 1969	0900	2	3			2	4
	0331	7	12			7	14
March 25, 1969	1613	10	25			15	31
	1440	4	10			5	14
	1419	16	30			16	37
March 24, 1969	1213	6	13			7	16
	1135	6	24			6	14
	0813	9	21			8	20
	0259	3	6			3	7
March 23, 1969	0351	5	8			4	9
	0016	5	9			4	9

Amplitude recorded on short-period instruments are given in millimeters (accuracy, ±10%). Parentheses around a number indicate that the wave trace was too faint to allow accurate readings.

If static fatigue is a random process, then for a given stress we might expect that the number of asperities that break per unit time will be proportional to the number of unbroken asperities. Therefore

$$\frac{dN}{dt} = -\frac{N}{t_0}$$

where t_0 is the average lifetime of an asperity. If $t_0 = \langle t \rangle$ defined in (3), then

$$\frac{dN}{dt} = -\frac{N}{T \exp(-k\sigma)}$$

Combining this equation with (2) to express

this failure rate in terms of area, we have

$$\frac{dA_u}{dt} = -\frac{1}{T} A_u \exp(k\sigma) \quad (4)$$

Using (1) and introducing a dimensionless variable

$$x = \frac{A_0}{A_u} = \frac{\sigma}{\sigma_0}$$

(4) becomes

$$\frac{dx}{dt} = \frac{1}{T} \exp(k\sigma_0 x),$$

which can be integrated to give

$$\frac{t}{T} = \ln(k\sigma_0 x) + \sum_{n=1}^{\infty} \frac{(-k\sigma_0 x)^n}{n \cdot n!} - \frac{C}{T} \quad (5)$$

While the tectonic stress on the fault plane remains constant, as slip occurs on some asperities, the actual stress on the locked sections of the fault increases as shown in Figure 13.

This equation can also be expressed in terms of area. In Figure 14 a nondimensional area variable, $(\frac{1}{k\sigma_0 x})$ is plotted as a function of a nondimensional time, $(\frac{t+C}{T})$. The former is related to the unslipped area A_u by

$$\frac{1}{k\sigma_0 x} = \frac{1}{k\sigma_0} \frac{A_u}{A_0}$$

and to the area that has slipped, $A_s = A_0 - A_u$,

$$\text{by } \frac{1}{k\sigma_0 x} = 1 - \frac{A_s}{A_0}$$

The curve in Figure 14 is applicable only for a range of values of x : $1 \leq x < \infty$, corresponding to $A_0 \geq A_u \geq 0$. Notice that

$$\lim_{k\sigma_0 x \rightarrow \infty} \frac{\ln(k\sigma_0 x)}{\sum_{n=1}^{\infty} \frac{(-k\sigma_0 x)^n}{n \cdot n!}} = -1 \quad (6)$$

Therefore as x approaches ∞ and A_u approaches zero, t approaches $-C$. The choice of C arbitrarily sets the origin, or completion time of the process. The instability begins when $A_u = A_0$, or $x = 1$, for which

$$\frac{t}{T} = \ln(k\sigma_0) + \sum_{n=1}^{\infty} \frac{(-k\sigma_0)^n}{n \cdot n!} - \frac{C}{T} \quad (7)$$

Below we set $t = 0$ in (5) to correspond to the time of the main shocks, so that the absolute value of t in (7) gives the duration of the instability. Because the first and second terms in (5) approach one another in magnitude as $k\sigma_0 x$ approaches infinity but differ in sign, the duration of the instability is less

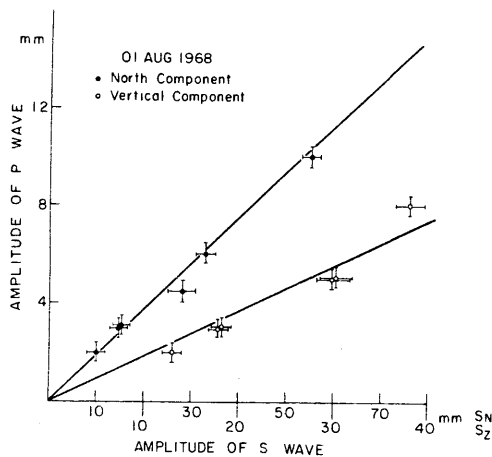


Fig. 10. The maximum amplitude of the P wave versus the maximum amplitude of the S wave of both the vertical and north-south records of the August 1, 1968, earthquake in the Philippines recorded at Baguio (BAG).

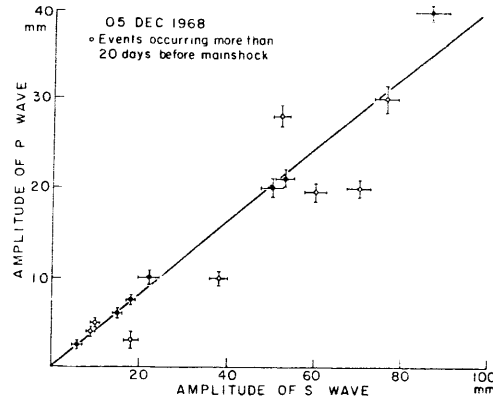


Fig. 11. The maximum amplitude of the P wave versus the maximum amplitude of the S wave of the December 5, 1968, earthquake near Greece recorded at Athens University (ATU). The solid circles are foreshocks that occurred within 4 days of the main shock, while the open circles are foreshocks occurring more than 20 days before it.

for larger values of σ_0 or k (higher tectonic stress or weaker asperities) than for smaller values.

If foreshocks are a manifestation of premonitory slip and the dependence on time of premonitory slip is approximately that of foreshock activity, then the time dependence of A_s/A_0 should match the cumulative plot of foreshock activity with time (Figure 14). These two curves are remarkably similar. Expressing the time scale in terms of days allows values of $T = 3000$ days and the constant of integration, $C = 1732$ days, to be assigned. This value of C corresponds with setting the time of the main shock at $t = 0$. Because of the dependence of T on fluid pressure, temperature, and pressure, it is probably futile to attempt to compare this estimate of T with estimates calculable from laboratory data.

One feature of the fit of (5) to the data in Figure 14 is that the main shock does not occur until almost 100% of the area has slipped. This need not mean that almost 100% of the total rupture area slips before the main shock. It appears that in a few days before the mainshock, foreshocks occur very close to the epicenter of the mainshock (Figures 2 and 7) [e.g., Kelleher and Savino, 1975; Wesson and Ellsworth, 1973; Wu et al., 1976]. Perhaps premonitory slip occurs only over a small fraction of the total area, which could be termed a triggering area. A rupture of the triggering area then propagates through to the rest of the fault plane [e.g., Brune, 1978].

The duration of the instability is related to the tectonic stress and the strength of the asperities. Using the fit of (5) to the foreshock data (Figure 14) for $k\sigma_0 = 4$, the instability would begin to develop 10 days before the mainshock, but for $k\sigma_0 = 1$ or 0.2 the instability would begin to develop 330 days or 2576 days (~ 7 years) before it. Scholz [1972] obtained a value of $k = 3.7 \text{ kbar}^{-1}$ for the a axis of uniaxially loaded single quartz

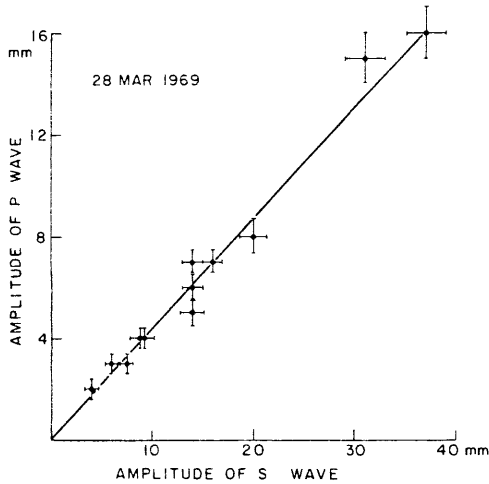


Fig. 12. The maximum amplitude of the P wave versus the maximum amplitude of the S wave of the March 28, 1969, earthquake in western Turkey recorded at Athens University (ATU).

crystals. This value of k is for the case where σ is differential stress: if σ represents shear stress as in (5), then the value of k should be doubled. Using $k = 7.4 \text{ kbar}^{-1}$ in (5), we obtain estimates of the tectonic stress of 1081, 270, and 54 bars for $k\sigma_0 = 4, 2, \text{ and } 1$, respectively. If the asperities were weaker than Scholz's single quartz crystals, such estimates of the tectonic stress would be lower.

Figure 14 and (5) describe a simplistic model strictly valid only for a static situation. If this sort of instability takes place, the assumptions of static fatigue and of setting $t_0 = \langle t \rangle$ in (3) are probably invalid as the ruptured area grows rapidly near the time of the main shock. Nevertheless, the remarkably good fit encourages us to pursue it further.

Conclusions

Although long sequences of foreshocks are not common, small numbers of foreshocks occur before a large fraction of major earthquakes (see Table 2). We combined these short sequences, often with only one event, into one average sequence by plotting all data as a function of the time before their corresponding main shocks. Activity increases only slightly until about 5-10 days before the main shocks, when it begins to increase rapidly, apparently near the main shock epicenters. This increase culminates with a peak in activity on the last day. On the last day the activity continues to increase until the time of the main event, except for a possible slight and apparently temporary drop in activity a few hours before it. Neither the magnitudes of foreshocks nor the time dependence of foreshock activity seem to depend significantly on the magnitudes of the mainshocks. The magnitude of the largest foreshock can range from being too small to locate to nearly the magnitude of the mainshock (20% of the world's major earthquakes occur in series with at least one other major event).

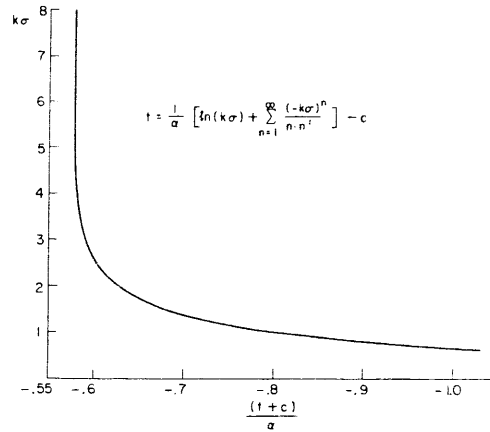


Fig. 13. A plot of (5) in terms of the nondimensional variables $k\sigma (= k\sigma_0 x)$ and $(t+C)/T$. This shows the increase of stress on the remaining area with unbroken asperities with increasing time to the left.

Judging by a few sequences studied, it seems likely that faulting mechanisms are usually the same for foreshocks within one sequence.

These findings suggest that foreshocks alone are insufficient for earthquake prediction. In many cases they will not occur at all. When they do occur, they might be recognized by their temporal distribution or, in some cases, by the similarity of their radiation patterns. Therefore they will in some cases be of use in predicting the location and time of the impending main shock, but they will not provide much information about the magnitude of the main shock.

The frequency of foreshock occurrence shows that precursory deformation does occur before many major earthquakes. Many characteristics of foreshock activity could be explained if the deformation occurs by accelerating premonitory fault slip.

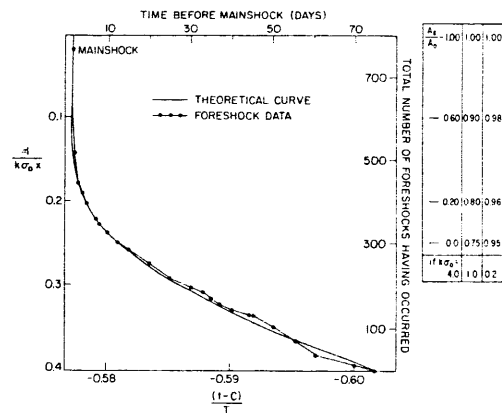


Fig. 14. A plot of (5) in terms of the non-dimensional variables $1/k\sigma_0 x$ and $(t+C)/T$. Smooth curve shows the decrease of unslipped area with time. The fraction of this area that has slipped is shown at the right for three values of $k\sigma_0$. Dots connected by line segments show the total integrated number of foreshocks that have occurred up to the given time (in days) before the main shock.

Jones and Molnar: Some Characteristics of Foreshocks

Acknowledgements. Some of the materials incorporated in this work were developed with support from the United States Geological Survey, Department of the Interior, contract 14-08-0001-16758, and the Alfred P. Sloan Foundation grant in Aid Research Fellowship, #7350. The views and conclusions contained in this paper are those of the authors and should not be interpreted as necessarily representing the official policies, either expressed or implied, of either the U.S. government or the Alfred P. Sloan Foundation. We would like to thank both Bernard Minster and Tom Heaton from the California Institute of Technology for valuable suggestions and J. Ebel, T. C. Hanks, and A. Lindh for constructive criticisms of the manuscript. In particular, Lindh pointed out several weaknesses in the data analysis and presentation that led to important revisions.

References

- Bolt, B. A., J. Stifler, and R. Uhrhammer, The Briones Hills earthquake swarm of January 8, 1977 Contra Costa County, California, Bull. Seismol. Soc. Amer., 67, 1555-1564, 1977.
- Brune, J. N., Implications of earthquake triggering and rupture propagation for earthquake prediction based on premonitory phenomena, in Proceedings of the Conference on Fault Mechanics and its Relation to Earthquake Prediction, U.S. Geological Survey, Menlo Park, CA, 1978.
- Duda, S., Secular seismic release in the circum-Pacific belt, Tectonophysics, 2, 409-452, 1965.
- Engdahl, E. R., and C. Kisslinger, Seismological precursors to a magnitude 5 earthquake in the central Aleutian Islands, J. Phys. Earth, 25, S243-S250, 1977.
- Evernden, J. F., Study of regional seismicity and associated problems, Bull. Seismol. Soc. Amer., 60, 393-446, 1970.
- Evernden, J. F., Location capability of various seismic networks, Bull. Seismol. Soc. Amer., 61, 241-256, 1971.
- Jin, Y., Y. Zhao, Y. Chen, J. Yan, and Y. Zhou, A characteristic feature of the dislocation model of foreshocks of the Haicheng earthquake, Lianoning Province, Acta Geophys. Sinica, 19, 156-164, 1976.
- Jones, L., and P. Molnar, Frequency of foreshocks, Nature, 262, 677-679, 1976.
- Kagan, Y., and L. Knopoff, Statistical study of the occurrence of shallow earthquakes, Geophys. J. Roy. Astron. Soc., 55, 67-86, 1978.
- Kelleher, J., and J. Savino, Distribution of seismicity before large strike slip and thrust-type earthquakes, J. Geophys. Res., 80, 260-271, 1975.
- Lahr, J., and P. W. Pomeroy, The foreshock-aftershock sequence of the March 20, 1966 earthquake in the Republic of Congo, Bull. Seismol. Soc. Amer., 60, 1245-1258, 1970.
- Lindh, A., G. Fuis, and C. Mantis, Foreshock amplitudes and fault plane changes: A new earthquake precursor? Science, 201, 56-59, 1978.
- Mogi, K., Some discussions on aftershocks, foreshocks, and earthquake swarms: The fracture of a semi-infinite body caused by an inner stress origin and its relation to earthquake phenomena (third paper), Bull. Earthquake Res. Inst. Tokyo Univ., 41, 615-658, 1963.
- Papazachos, B., On certain aftershock and foreshock parameters in the area of Greece, Ann. Geofis., 27, 497-515, 1974a.
- Papazachos, B., On the time distribution of aftershocks and foreshocks in the area of Greece, Pure Appl. Geophys., 112, 627-631, 1974b.
- Papazachos, B., Aftershock and foreshock sequences in the area of Greece during the period 1911-1973, Bull. Sci. Group Space Res., 3, 1-44, 1975a.
- Papazachos, B., Foreshocks and earthquake prediction, Tectonophysics, 28, 213-226, 1975b.
- Papazachos, B., M. Delibasis, N. Liapis, G. Mousoulidis, and G. Purcaru, Aftershock sequences of some large earthquakes in the region of Greece, Ann. Geofis., 20, 1-93, 1967.
- Pho, H.-T., G. Wittlinger, and H. Haessler, Enregistrement et distribution temporelle des repliques, 80h après le séisme destructeur du Frioul (Italie) du mai 1976, C. R. Acad. Sci., Ser. D, 283, 611-614, 1976.
- Raleigh, C. B., et al., Prediction of the Haicheng earthquake, EOS Trans. AGU, 58, 236-272, 1977.
- Richter, C. F., Elementary Seismology, W. H. Freeman, New York, 1958.
- Scholz, C. H., and R. J. Martin, Crack growth and static fatigue in quartz, J. Amer. Ceram. Soc., 54, 474, 1971.
- Scholz, C. H., Static fatigue of Quartz, J. Geophys. Res., 77, 2104-2114, 1972.
- Su, S. S., The Luzon earthquake of 7 August 1968: A preliminary report, Bull. Seismol. Soc. Amer., 59, 459-472, 1969.
- Sykes, L. R., Earthquakes swarms and sea-floor spreading, J. Geophys. Res., 75, 6598-6611, 1970.
- U.S. Government Printing Office, United States Earthquakes, 1965 to 1973, Washington, DC, 1967-1975.
- Wesson, R. L., and W. L. Ellsworth, Seismicity preceding moderate earthquakes in California, J. Geophys. Res., 78, 8527-8546, 1973.
- Wu, K., M. Yue, H. Wu, X. Cao, H. Chen, W. Huang, K. Tian, and S. Lu, Certain characteristics of Haicheng earthquake ($M = 7.3$) sequence, Acta Geophys. Sinica, 19, 109-117, 1976.
- Zhu, F., An outline of prediction and forecast of Haicheng earthquake of $M = 7.3$ in Proceedings of the Lectures of the Seismological Delegation of the People's Republic of China, Jet Propulsion Laboratory, Pasadena, CA, 1976.

(Received March 20, 1978;
revised January 16, 1979;
accepted February 1, 1979.)

CHAPTER II:

THE FORESHOCK SEQUENCE OF THE 4 FEBRUARY 1975
HAICHENG EARTHQUAKE (M = 7.3)

by

Lucile Jones

Department of Earth and Planetary Sciences
Massachusetts Institute of Technology
Cambridge, Mass. 02139Wang Biquan, Xu Shaoxie
Institute of Geophysics
State Seismology Bureau
Beijing, People's Republic of ChinaThomas J. Fitch
Applied Seismology Group
Lincoln Laboratory
Cambridge, Mass. 02139

Introduction

Understanding the characteristics of foreshock occurrence is important both for earthquake prediction and for the study of the mechanics of faulting. It is obvious that if foreshocks could be distinguished from other earthquakes before the mainshock occurred, they could be a powerful tool for earthquake prediction. In addition, foreshocks are the most obvious manifestation of crustal strain immediately preceding a mainshock so that a study of the location and mechanisms of a foreshock sequence could shed light on the pattern of ground deformation that leads to a mainshock.

Since the number of recorded foreshock sequences has been limited, they have often been studied by putting the foreshocks of many different mainshocks together, forming an average foreshock sequence (e.g., Mogi, 1963; Jones and Molnar, 1979; Kagan and Knopoff, 1978). This provides enough data that patterns can be seen but details are obscured (and apparent patterns may be created) by the variations among them. In addition to studies of average sequences, we need to have case studies of many individual sequences to compare with the average sequences and with each other to see what characteristics the different sequences have in common and how they differ. Some sequences have been studied (e.g., Lindh et al., 1978; Billington et al., 1981) but this research has been impeded by a lack of adequately recorded foreshock sequences.

The foreshock sequence of the 4 February 1975 Haicheng earthquake ($M = 7.3$) provides a unique opportunity to study this problem. The first major earthquake to be accurately predicted, the Haicheng event was preceded by over 500 foreshocks in the four days prior to and very near the epicenter of the mainshock. Although most of them were too small to be located, because six seismographs were in operation at the time within 170 kilometers of the foreshocks' epicenters, sixty of the events could be located. This is the largest foreshock sequence yet recorded and the purpose of this paper has been to study the events in this sequence from the local seismograms to further our understanding of foreshocks and precursory deformation. We have located the foreshocks relative to each other and to the mainshock and looked at the change in location with time. We also examined the mechanisms of the events by measuring the ratios of the amplitudes of the P and S waves. We compared these results with what has been predicted for foreshocks and examined the implications of the results for the pattern of precursory deformation.

Data

The Haicheng earthquake occurred in a geologically complex region that is dominated by northnortheast trending faults (Figure 1). However, the aftershock distribution showed that mainshock occurred on a west-northwest trending fault. This is consistent with the $N67^{\circ}W$ trending plane in

the fault plane solution determined for the mainshock from first motion data (Wu et al., 1976) and waveform modeling (Cipar, 1979). Before the mainshock occurred, no fault had been mapped in this area although a northwest trending fault, which experienced a small amount of slip during the earthquake, has been recognized at the eastern end of the aftershock zone (Raleigh et al., 1977).

While the foreshock sequence started four days before the mainshock, the rate of activity increased markedly 26 hours before the mainshock and all but seven of the foreshocks occurred after this time. All of the events located in this study were in this later period. The temporal distribution of the located events is shown in a magnitude-time plot in Figure 2. The largest foreshock occurred about half way through this time period, twelve hours before the mainshock. The magnitude distribution of the foreshocks is different before and after the largest event with all but two of the nine foreshocks with $M > 3$ occurring before it. We found that other characteristics of the foreshocks changed after the largest one as well.

The Haicheng foreshocks were recorded by a local network run by the Liaoning Provincial Seismology Bureau. The six stations that were used in this study are shown on the map in Figure 1. All of the stations had three-component, short period instruments with amplifications of about 10^5 . During the two days before the mainshock, the seismographs were operated at a speed of

12 cm/min so that arrival times could be read with an uncertainty of less than 0.1 second.

The largest source of error in the data is the clock corrections of the seismographs, which were made to the nearest tenth of a second using a stop watch. Since the corrections were made manually, there is a possibility of several tenths of a second of error. To reduce this error, for each station we plotted the clock corrections versus time for two weeks around the time of the foreshocks. An example is shown in Figure 3. We then drew a straight line that was the best fit to these points and used the value of the line at any time as the clock correction rather than the recorded value. This is equivalent to assuming that the clock varied at a constant rate and that any apparent sudden jump is due to human error. The correction is still accurate only to the nearest tenth of a second but larger errors are avoided with this method.

Technique

To define the spatial relationships among the foreshocks and between individual foreshocks and the mainshock, we computed locations relative to master events that were chosen from among the better recorded foreshocks. That the spatial relationships determined by these relative locations are more accurate than those determined by the usual absolute locations is suggested by the diminished dependence on the assumed earth model. The model

used in this study is a two layer crust over a half space with velocities and thicknesses shown in Table I.

The basic algorithm used to compute the locations is

$$T_{ij} - T_{im} = T_{oi} - [L_j \cos(S_{ij})/V] \quad (1)$$

where T is time and the subscripts i , j , m , and o refer to the i^{th} station, the j^{th} event, the master event and the origin time, respectively. L_j , S_{ij} and V are the scalar distance between the master and the j^{th} event, the angle between the relative location vector and the ray path to the i^{th} station, and the appropriate material velocity (e.g., the compressional velocity for the P arrival times) respectively. Equation (1) is valid when the source region is sufficiently small that the ray paths in the region have negligible curvatures, i.e. a Fraunhofer approximation is implied. This algorithm has been used to investigate shallow seismicity associated with reservoir faulting (Fitch and Muirhead, 1974) and more recently in a study of the depths of earthquakes in the Middle East generally and in particular the depths of thrusting beneath the Zagros mountain belt in Iran (Jackson and Fitch, 1979).

Both of these studies used arrival times from the bulletins of the International Seismological Centre (ISC), which are mostly teleseismic observations. In this study our data are observations made by us of the onset times of the direct P wave, the P wave refracted from the base of the

crust (Pn), and the corresponding S phases. The stations used (Figure 1) are from 100 to 170 kilometers from the epicenters of the foreshocks with the exception of YIN which is only 20 kilometers away. YIN is too close to ignore the geometry of the ray path beyond the source region. To accommodate the data from YIN data, the algorithm was rewritten into a form that is exact for the case of straight rays. (For details, see Fitch and Ryan, 1979.) The adjustments to the calculated differential arrival times (the difference between the arrival time of the j^{th} event and that of the master) caused by this modification are at the most one second.

Unlike data sets compiled from teleseismic observations, our data with the inclusion of the Pn and Sn arrival times can nearly perfectly resolve all of the relative location parameters from the differential arrival time. In particular, relative depth is resolved. This can be inferred from the normalized inner product matrix which has diagonal elements of almost equal magnitude. This inner product matrix is the one generated by the usual least squares algorithm. The individual equations are weighted by the inverse of the standard errors of the differential arrival times thereby yielding maximum likelihood estimates of the model parameters. In this study, the reduced chi square statistic has generally lain in the range of 0.5 to 1.5 which shows that the standard errors we assigned to the data are compatible with those computed for the model. Thus, separations between events that are greater than about one kilometer are significant. This can be asserted in spite of some of the obvious defects in this master

earthquake technique such as the propagation of the errors in the arrival times of the master event through the sets of time differences and the assumption of the ray parameters appropriate for rays from the master to each station.

The spatial relationships were calculated using several different earth models and master events. The assumed earth model appears in the calculations only as the seismic velocities at the locations of the events and the take-off angles of the waves refracted from the base of the crust. P wave velocities ranging from 6.0 km/sec to 6.3 km/sec and takeoff angles for Pn waves from 15° to 45° were used in various attempts. Changes in locations caused by these modifications were all less than one kilometer. The locations were also computed relative to three different master events with less than one kilometer variation in locations of all the events. All of the characteristics of the zone of activity mentioned below were unaffected by these modifications. The model used for the results presented in this paper was determined by the Liaoning Provincial Seismology Bureau (Table I).

Results

The relative locations determined for the Haicheng foreshocks are listed in Table II and shown in Figures 4a,b,c and 5. Since the pattern of activity changed with time, the epicenters have been plotted in three groups. Since the changes in locations occur at the times of the two largest foreshocks, these times have been used as the dividing points of the three groups.

The most notable feature of these locations is the large distance from all of the foreshocks to the mainshock in a direction perpendicular to the strike of the mainshock's fault. Because we considered this unusual, we recomputed the location of the mainshock four different ways. The location shown in Figures 4c and 5 was computed in the same manner as the foreshocks, using local P and Pn arrival times relative to foreshock #21. The location of the mainshock was also computed using local data relative to #21 and #3 with depths held constant, and using both local and teleseismic data reported in the ISC bulletins relative to the largest foreshock (#36). These four locations are listed in Table III. All of these methods resulted in the mainshock being located between six and seven kilometers south of the foreshocks (therefore nearly perpendicular to the trend of the mainshock's fault) and (if depth was allowed to vary) four to five kilometers shallower than the foreshocks. This is also consistent with the absolute location computed for the foreshocks and mainshocks. Also the difference in the arrival times of the largest foreshock and the mainshock was larger at stations north of the epicenters (COL (WWSSN) and FUX (Liaoning)) than those at stations to the south (SHL (WWSSN) and ZHU (Liaoning)) by almost two seconds which is consistent with the six kilometers southerly offset. Thus we are confident that the foreshock did not include and indeed was not on the same fault plane as the point of nucleation of the mainshock.

Another interesting feature of the locations is the expansion of the area of the foreshock cluster with time.

Before the occurrence of the largest foreshock (Figure 4a), the foreshocks are clustered in a very small volume with dimensions on the order of two kilometers. After the largest foreshock, the activity expanded a few kilometers to the northwest although the largest events (#42 $M = 3.3$ and #55 $M = 4.3$) are still within the originally active area (Figure 4b). After the second largest foreshock (#55), there is a further expansion of activity both to the northwest and especially to the southeast (Figure 4c). There is no similar expansion in the depths of the events (Figure 5). Thus the character of the seismically active zone changes sharply with continued activity. Before the largest event, the foreshocks occurred in a small, approximately equidimensional volume. Moreover, all of the foreshocks with magnitude greater than three, even including those that occurred after the largest event, were in this small volume. But, if all of the events are considered, the activity is distributed along a plane that is approximately parallel to but not coincident with the mainshock rupture.

Ratios of the P and S Wave Amplitudes

We also examined the ratios of the amplitudes of the P and S waves. It has often been assumed that all of the events within a foreshock sequence would have the same faulting mechanisms, which, if the foreshocks occurred in the same place, would produce identical amplitude ratios for the different events at a given station. Several researchers

have examined whether or not the amplitude ratios are the same within a foreshock sequence with conflicting results (e.g., Jin et al., 1976; Lindh et al., 1978; Jones and Molnar, 1979; Bolt et al., 1977; Engdahl and Kisslinger, 1977; Chen et al., 1978). The Haicheng sequence, because of the large number of events and stations, provides a good opportunity to study this question.

We found that the amplitude ratios of the foreshocks were definitely not the same. Two definitely different waveforms were recorded at YIN (the nearest station, $\Delta = 20$ km) throughout the sequence. One had a relatively sharp P arrival while the other had a much smaller one (Figure 6). Within these two groups, the amplitude ratios remained quite constant throughout the foreshock sequence (Figure 7). It was impossible to correlate the waveforms at Yingkou with events at other stations. In general, if an event was large enough to be recorded at other stations, the arrivals at YIN were too large and the waveforms were clipped. Six events with recognizable large or small P phases at YIN were located but only two or three of these events had clear amplitude ratios at each of the other stations.

The other stations did not have two clearly different waveforms as YIN did. The waveforms and amplitude ratios of all the foreshocks were similar. However, there were slightly larger variations in the ratios at these stations, especially after the largest foreshock occurred, than existed within either of the two groups of ratios at YIN. The mean amplitude ratios and their standard deviations for all of the stations are listed in Table IV.

Since the purpose of examining the amplitude ratios is to learn more about the focal mechanisms of the foreshocks, we compared the recorded amplitude ratios with those expected from the fault plane solutions determined for the largest foreshocks. We calculated the expected amplitude ratios with the double-couple formula of Ben-Menahem et al. (1965), including the effect of the angle of incidence at the surface and the instrument response. Since the fault plane solution of the foreshock is not very well constrained, we calculated the amplitude ratios for three slightly different solutions at two different locations. The results are listed in Table V. Because of the range in amplitude ratios possible from these variations, the calculated ratios cannot produce a definitive answer. However, a comparison of Tables IV and V shows that the recorded amplitude ratios are consistent with the determined fault plane solution. Moreover, it can be seen that amplitude ratios at YIN are sensitive to changes in focal mechanism but not to changes in locations. Thus it seems likely that the different waveforms at YIN result from two different focal mechanisms occurring during the foreshock sequence.

There seems to be some correlation between the two mechanisms and location within the zone of foreshock activity. The three located foreshocks with large P phases at YIN (#9, 10, and 12 in Table II) were all located within the small central volume where all of the largest foreshocks occurred. The three events with a small P arrival (#38, 50

and 74), however, all occurred outside of this volume, both to the northwest and the southeast. This of course does not prove that all of the events with large P phases occurred within this volume and all of the events with small P phases outside of it, but the S-P times recorded at YIN suggest that this might indeed be the case. Since the foreshocks were distributed along a northwest-southeast direction and YIN was situated northwest of the events, events in and out of the volume should have different S-P times at YIN. Looking at these times, we found that all of the events with large P phases had S-P times of 2.5 or 2.6 seconds - the S-P times for events in the central cluster. On the other hand, the events with small P phase had S-P times ranging from 2.2 seconds (corresponding to the northwest end of the cluster like #38) to 2.8 seconds (corresponding to the southeast end like events #50 and 74). Thus we consider it possible that the foreshocks in the central area which includes all of the largest events may have had a different mechanism than those outside of it. This could explain why the amplitude ratios at more distant stations began to vary more after the largest foreshock - that was the time when events large enough to be located began to occur outside of the cluster.

Discussion

The three notable features of the Haicheng foreshock sequence are (1) the large distance between all the foreshocks and the mainshock in a direction perpendicular to both the aftershock and foreshock zone, implying that they did not occur on the same fault, (2) the occurrence of two different radiation patterns during the foreshock sequence that might be correlated with location of events within the cluster, and (3) the expansion of the area of foreshock activity with time. The first two features contradict common assumptions about foreshock sequences. Because of the small temporal and spatial separation between foreshocks and mainshocks, it has often been assumed that foreshocks result from premonitory slip on the mainshock fault at the mainshock epicenter that then accelerates into an instability resulting in the mainshock. This is obviously an untenable simplification in this case since at least two faults, and maybe three were involved. (The different radiation patterns in the foreshock sequence allow for the possibility that two faults were active during that sequence.) Although we cannot determine exactly what happened during the foreshock sequence, there is enough data that considering the local tectonic structure, we can draw some conclusions about what must have occurred.

The earthquakes occurred in a geologically complex region. Because of the lack of identifiable features of the Proterozoic schists and gneisses in the area, the main strand

of the mainshock's fault has not been recognized. The fault plane solution, aftershock zone and isoseismal lines of the mainshock, however, do delineate the approximate location of the fault (Figure 1). At the eastern end of the aftershock zone is a geologically recognizable fault, the Dayanghe fault, that has a slightly different strike ($N45^{\circ}W$) than that of the mainshock's fault as determined by the fault plane solution ($N67^{\circ}W$). The Dayanghe fault slipped left-laterally (the same sense as the mainshock) during the mainshock or early aftershocks because surface ruptures were found on it (Raleigh et al., 1977). The absolute locations of the foreshocks place them at the western end of this fault where it intersects a small north-northeast trending fault, the Ximuhe fault. Since the Dayanghe fault has a slightly different strike than that of the mainshock plane and the mainshock location is six kilometers south of the foreshocks, our supposition is that the junction between the Dayanghe fault and the unmapped strand is an en echelon step. Although this cannot be proved by the geology, this seems the most probable explanation of the observed spatial configuration.

First, we will consider the characteristics of the foreshock sequence itself. Although other explanations are possible, all of the features of the foreshock sequence can be explained by assuming that some aseismic slip or concentration of strain propagated to the northwest along the Dayanghe fault but was stopped by the barrier formed by the

end of the fault. The foreshocks reflect the energy expended trying to break through the barrier. Thus the first half of the foreshock sequence occurred in a very small volume, the eastern edge of the barrier. The two largest foreshocks broke part of the barrier, enough to allow some slip on the Dayanghe fault as shown by the final distribution of foreshocks (Figure 4c) but not enough to allow continued propagation of the strain through unfaulted rock. The two different mechanisms of the foreshocks could be the result of a slightly different fault strike for slip on the Dayanghe fault and for the plane of least resistance through the barrier.

Alternatively, the two mechanisms could reflect the fact that the barrier was sufficiently strong to resist rupture and the foreshocks in the central volume were actually on the north-northeast trending Ximuhe fault. The locations and errors in location of the foreshocks with $M > 3$ (Fig. 4a) are such that they could as easily be aligned on a north-northeast trending plane as a northwest trending plane. The redistribution of stress after the largest foreshock could then have allowed slip on the Dayanghe fault to occur. Since the Dayanghe and the Ximuhe faults are almost perpendicular, both alternatives are consistent with the fault plane solution determined by Wu et al. (1976) for the largest foreshock. The first alternative seems preferable since the later foreshocks could then be considered direct aftershocks of the largest foreshocks but both alternatives are possible.

One supporting observation for the idea that strain propagated up the Dayanghe fault comes from reports of changes in ground water in the area before the earthquake. Although the foreshocks did not begin until 1 February 1975, changes in ground water were reported as early as December 1974. If we assume that these changes (primarily rising, falling and muddying of the water) reflect some sort of deformation of the crust, the spatial distribution of the changes can give us an idea of where strain was accumulating. Weekly maps of the reports of changes in Deng et al. (1981) show that they began about six weeks before the earthquake, 150 kilometers southeast of the epicenter in the Dandong region (Figure 1) and then migrated northwest, parallel to the Dayanghe fault, towards the epicenter. Thus there may have been an accumulation of strain on the Dayanghe fault that propagated to the northwest.

Even though we cannot be certain on which fault the foreshocks occurred on, we do know that they were not on the same fault as the mainshock. Specifically, they cannot have triggered the mainshock by rupturing some of the asperities that were inhibiting slip on the mainshock fault as has been suggested (i.e., Jones and Molnar, 1979). They could have triggered the mainshock only by changing the local stress field of slip on another fault. This change in stress at the mainshock epicenter is relatively easy to calculate. Since we are only interested in the change in stress and not the total stress state, we need only calculate the stress due to

slip on one crack (the foreshock plane) at the epicenter of the mainshock.

We have calculated this stress using the methods of Segall and Pollard (1980). To do this, several assumptions have to be made. The most important is the location, length and orientation of the crack representing the foreshock plane. As this is also the least well determined parameter, we have made the calculations for four different cracks, two northwest and two northeast trending to cover the range of possibilities. These four are shown in Figure 8 with the locations of the events. As there is a relatively large east-west error in the mainshock locations, three possible locations of it are used in each calculation. We must also assume a total stress drop for the foreshocks. Using Kanamori and Anderson's (1975) moment-magnitude relation we calculated a cumulative moment for the ten largest foreshocks and from it a stress drop of 8 bars. This is naturally only accurate to an order of magnitude but the resultant stress drop at the epicenter of the mainshock is directly proportional to the stress drop, so those who wish the stress drop higher or lower may scale the results as they wish.

Another factor to consider in these calculations is the change in pore pressure due to the change in stress state. Since the foreshocks occurred within one day of the mainshock, the stress gradients are small and the local rocks are relatively impermeable, it is reasonable to assume that any induced pore pressure change would not dissipate before

the mainshock occurred. The induced pore pressure will be

$$\Delta Pp = B \cdot \Delta(\text{mean stress})$$

where Pp is the pore pressure, and B is a constant that depends upon the rock type (Rice and Cleary, 1976). Since the local rocks are rigid schists and gneisses, we used the value Rice and Cleary determined for granite, .85.

The calculated stresses are listed in Table VI.

Positive stresses indicate tension for the normal stresses and right-lateral for the shear stresses. For each case, we have calculated the effective change in the shear stress needed for frictional sliding. We assume that Byerlee's Law,

$$\tau = .6(\sigma_n - Pp),$$

where τ is the shear stress and σ_n is the normal stress on the fault, holds for slip on the faults. Thus, either an increase in $(\sigma_n - Pp)$ or decrease in τ will promote left lateral slip. To represent this, we have calculated an effective shear stress change,

$$\tau_f = \Delta\tau - .6(\Delta\sigma_n - \Delta Pp),$$

that is negative for inducing left-lateral slip.

There is considerable variation between the different models but all of them produce only small changes in stress. In all cases, the change in stress is more likely to induce

the mainshock when the mainshock's epicenter is as far west as possible. The case most conducive to slip is case B, a short northwest trending fault but even then, τ_f is only one third of a bar. The only way to generate a larger change in stress would be to have the whole Dayanghe fault slip (shown for comparison in Table VI) but this produces a large decrease in the pore pressure so that τ_f becomes positive. In fact, reports of changes in ground water on the day of the foreshocks (Fig. 9; Deng et al., 1981) show that the wells in the vicinity of the mainshock generally rose, thus it seems very unlikely that all of the Dayanghe fault slipped at that time. Although many of the reports mapped in Fig. 9 of Deng et al. [1981] did not include how much the well rose, those that did ranged from 1/3 to 2 1/3 meters which is consistent with most of the calculated pore pressure changes in Table VI.

The two conclusions we can draw from this exercise are that a short-term change in pore pressure might have been important in triggering the mainshock and that the net change in frictional shear stress at the mainshock epicenter induced by the foreshocks was no more than 4% of the stress drop on the foreshock's fault. The latter implies that the mainshock's fault was already loaded close to failure (though obviously not as close as the Dayanghe fault) and the finally triggering stress was less than 1% of the total stress drop of the mainshock. With sections of two, or perhaps three, faults active, and others quiescent, the stress field must

have been quite heterogeneous. This could be one reason why such a large foreshock sequence occurred.

Summary

In conclusion, we have examined the spatial distribution and radiation patterns of the foreshocks of the $M = 7.3$ Haicheng earthquake and found three notable features. First, the mainshock did not occur on the same plane as the foreshocks but rather was located six kilometers away from the foreshocks, perpendicular to the direction of faulting. Second, the spatial distribution of the foreshock cluster changed with time expanding from a very small approximately equidimensional volume with a radius of one kilometer to a six kilometer long fault. Third, two different faulting mechanisms were activated during the foreshock sequence which may correspond to the volume and plane mentioned above. We think these features may result from the process of transferring strain across an en echelon step in the fault. Because of the large distance between the foreshocks and the mainshock, compared with the dimensions of the rupture area of the foreshocks, the largest change in shear stress that could have been induced on the mainshock's fault by the foreshocks is 4% of the foreshock's stress drop.

Table I
Velocity Structure

Layer	Thickness	Velocity of P wave
1	16	6.0 km/sec
2	15	7.0 km/sec
3	∞	8.0 km/sec

Table III

Locations of the Mainshock With Respect to Foreshock #21

Method of Computation*	North	East	Depth
#21 with depth	-6.17	0.63	4.76
#21 without depth	-6.60	1.41	-
#3 without depth	-6.97	1.47	-
#36 with depth	-6.47	1.15	4.71
#36 without depth	-6.09	0.88	-

*The master event used in the computation and whether depth was allowed to vary.

Table II. Locations of the Foreshocks of the Haicheng Earthquake

No.	Date	Time	Mag.	Location			Error		
				North	East	Depth	North	East	Depth
1	03 FEB	18:39	2.4	0.63	0.59	1.24	0.65	0.46	0.93
2	03 FEB	18:51	1.5	0.44	0.18	0.93	0.34	0.89	0.65
3	03 FEB	19:13	1.3	0.92	0.34	-0.18	0.10	0.84	0.95
5	03 FEB	21:22	3.1	-0.74	0.57	1.53	0.48	0.57	0.99
9	03 FEB	23:50	1.6	-0.46	0.31	-0.17	0.13	0.74	1.21
10	03 FEB	23:55	1.5	-0.33	0.16	0.35	0.46	0.33	0.71
11	03 FEB	23:56	1.5	-1.30	0.88	-0.44	0.90	0.51	0.76
12	04 FEB	00:02	1.5	-0.48	1.16	0.37	0.58	0.45	1.17
13	04 FEB	00:58	3.0	0.37	1.36	0.41	0.69	0.22	0.99
14	04 FEB	02:18	1.6	-0.49	0.63	0.18	0.26	0.60	1.06
15	04 FEB	03:22	2.4	-1.28	-0.93	0.70	0.50	0.53	1.10
16	04 FEB	03:54	1.3	0.11	0.10	-0.46	1.03	0.75	1.03
18	04 FEB	04:24	3.8	-0.65	0.01	-0.44	0.07	1.30	0.87
20	04 FEB	04:31	3.2	-2.26	-0.32	-0.26	0.42	0.92	0.88
21	04 FEB	04:35	1.7	Master Event					
22	04 FEB	04:49	1.3	-0.34	-0.28	0.81	0.04	0.65	0.82
23	04 FEB	05:22	1.3	0.68	0.55	1.47	0.63	0.14	0.92
24	04 FEB	05:33	1.5	0.17	-2.07	0.31	0.77	0.12	0.90
25	04 FEB	06:11	2.8	-0.69	-1.24	-0.05	0.60	0.58	0.89
26	04 FEB	06:13	3.1	0.49	0.21	1.12	0.49	0.35	0.78
27	04 FEB	06:53	3.3	-1.24	0.80	0.32	0.46	0.54	1.11
28	04 FEB	04:58	3.7	-1.48	1.94	1.31	0.56	0.42	1.19
30	04 FEB	07:10	1.2	-1.19	1.40	0.83	0.21	0.58	1.60
32	04 FEB	04:14	1.2	-0.90	0.69	1.95	0.47	0.64	1.43
36	04 FEB	07:50	4.7	-0.14	1.55	0.43	0.66	0.39	1.44
38	04 FEB	08:11	1.3	0.21	-3.00	0.52	0.71	0.00	1.48
39	04 FEB	08:13	2.3	-0.46	0.74	-1.11	1.62	0.24	0.35
40	04 FEB	08:15	1.5	0.64	-0.53	-0.87	1.60	0.65	0.84
41	04 FEB	08:30	1.2	0.46	0.21	1.29	0.35	0.57	1.14
42	04 FEB	08:57	3.3	-0.21	0.58	0.86	0.42	0.62	1.16
43	04 FEB	08:59	2.0	0.21	-1.74	0.32	0.98	0.35	1.90
44	04 FEB	09:03	1.4	-0.56	-0.57	0.44	0.57	0.53	1.22
45	04 FEB	09:04	2.2	-1.06	-1.09	0.22	0.72	0.85	1.12
46	04 FEB	09:17	1.3	-0.58	0.53	0.15	0.18	0.56	1.34
47	04 FEB	09:22	1.3	-0.13	1.34	-0.64	1.00	0.39	0.64
49	04 FEB	09:23	1.4	-0.56	-0.40	3.75	0.56	0.47	0.99
50	04 FEB	09:36	1.4	-1.13	1.62	0.40	0.67	0.26	1.06
51	04 FEB	09:51	0.7	-0.73	0.50	1.89	0.75	0.50	1.64
53	04 FEB	10:28	2.6	0.08	-1.04	-0.71	1.31	0.27	0.58
54	04 FEB	10:33	1.8	1.33	-0.91	0.57	0.37	0.50	1.01
55	04 FEB	10:35	4.3	-1.56	0.89	-0.06	0.70	0.54	0.92
56	04 FEB	10:47	2.0	-0.23	-2.33	0.80	0.68	0.12	0.88
57	04 FEB	10:55	1.1	-0.42	0.15	-0.78	0.52	1.94	0.80
59	04 FEB	11:25	2.3	-2.45	0.45	0.93	0.30	0.64	1.01
62	04 FEB	11:27	1.3	-2.19	2.71	0.91	0.91	0.28	1.27
63	04 FEB	11:48	1.9	-2.74	2.72	0.73	0.90	0.21	1.15
64	04 FEB	11:59	1.6	1.60	0.00	0.09	0.06	0.89	1.75
65	04 FEB	12:00	0.9	-0.15	0.89	0.09	0.44	0.47	1.37

No.	Date	Time	Mag.	Location			Error		
				North	East	Depth	North	East	Depth
66	04 FEB	13:08	1.6	-1.76	0.11	0.40	0.24	0.61	0.95
68	04 FEB	13:54	0.9	-1.01	2.40	0.79	0.60	0.25	1.24
69	04 FEB	13:59	0.6	-1.51	1.49	2.37	0.22	0.63	1.33
71	04 FEB	14:56	1.1	1.30	1.82	1.91	0.67	0.22	1.17
73	04 FEB	16:20	1.4	-2.27	3.85	2.80	0.74	0.32	1.35
74	04 FEB	16:23	0.8	-1.47	1.63	0.59	0.56	0.36	1.19
75	04 FEB	16:24	2.6	0.15	0.74	-0.76	1.19	0.58	0.49
76	04 FEB	16:37	1.4	-1.22	1.70	-0.06	1.01	0.43	0.95
77	04 FEB	16:42	1.4	2.42	-2.07	0.51	0.97	0.44	1.30
78	04 FEB	17:39	1.7	-2.04	2.48	0.20	0.95	0.37	1.09
Mainshock									
	04 FEB	19:36	7.3	-6.17	0.63	4.76	0.11	1.08	1.38

Table IV
Average Recorded Amplitude Ratios and Their Standard Deviations

		YIN	FUX	ZHU	LUD	CAO	JIN	
		Big P	Small P					
Before the largest foreshock	Ratio	0.30	0.08	0.36	0.28	0.20	1.01	0.11
	Standard Deviation	0.10	0.04	0.12	0.14	0.10	0.17	0.07
After the largest foreshock	Ratio	0.35	0.06	0.35	0.31	0.26	1.03	0.12
	Standard Deviation	0.04	0.03	0.14	0.19	0.07	0.28	0.10

Table V
Calculated Amplitude Ratios

No.	Earthquake	Calculated Amplitude Ratio A_p/A_s at						Notes
		YIN	FUX	ZHU	LUD	CAO	JIN	
1	Mainshock	0.11	0.53	2.47	0.36	0.76	0.03	Using fault plane solution and location of Gu, 1976
2	Foreshock	0.47	0.24	0.92	0.38	0.75	1.14	Using fault plane solution and location of Wu, 1976 for composite of foreshock
3	Foreshock	0.17	0.50	0.35	0.22	1.22	0.19	Using fault plane solution and location of Gu, 1976 for largest foreshock
4	Foreshock	0.15	0.53	0.38	0.22	1.48	0.07	Same as No. 1 but location shifted 3 km to west, 2 km to north and 2 km deeper of the location used in No. 1

Table VI

Case	Fault Length	Location of Mainshock	Normal Stress	Shear Stress	Pore Pressure	Frictional Stress [$0.6(\sigma_n - P_p) - \tau$]
1	Dayanghe 8 km	W	-1.79	-0.43	-0.91	+0.10
		M	-2.41	-0.06	-1.24	+0.64
		E	-2.72	+0.69	-1.52	+1.31
2	Dayanghe 5 km	W	-0.58	-0.48	-0.32	-0.32
		M	-1.21	-0.14	-0.83	+0.09
		E	-1.58	+0.08	-0.74	+0.58
3	Ximuhe 4 km	W	+0.60	+0.20	+0.02	-0.15
		M	0.0	+0.59	-0.20	+0.47
		E	-0.73	+0.50	-0.49	+0.64
4	Ximuhe 4 km	W	-0.50	+0.55	-0.43	+0.59
		M	-0.93	+0.34	-0.47	+0.62
		E	-0.95	+0.01	-0.42	+0.33
5	Dayanghe 36 km	W	+1.60	-0.19	+4.04	+1.27
		M	+0.76	+0.06	+4.00	+2.00
		E	-0.31	+0.65	+3.75	+3.09

Acknowledgements: We thank the Liaoning Provincial Seismology Bureau for making their seismograms available and especially Jiang Xiouqing and Cao Tingqing for their assistance. One of us (L.M.J.) thanks the State Seismology Bureau and the Ministry of Education for their courtesy and hospitality extended during her two visits in Beijing. The first part of this work was conducted as part of the National Program for Advanced Study and Research in China administered by the Committee on Scholarly Communications with the People's Republic of China of the National Academy of Sciences. We acknowledge funding for the second part from U.S.G.S. contract # 14-08-0001-19250. One of us (L.M.J.) was supported in part by an NSF Graduate Student Fellowship. We would also like to thank Peter Molnar and David Pollard for their helpful advice.

- Ben-Menahem, A., S.W. Smith and T.L. Teng, A procedure for source studies from spectrums of long-period seismic body waves, *Bull. Seism. Soc. Am.*, 55, 203-235, 1965.
- Billington, S., E.R. Engdahl, and S. Price, Changes in the seismicity and focal mechanism of small earthquakes prior to an $M_S = 6.7$ earthquake in the Central Aleutian Island Arc, in press, in Earthquake Prediction, Maurice Ewing Series, Vol. 4, 1981.
- Bolt, B.A., J. Stifler, and R. Urhammer, The Briones Hills earthquake swarm of January 8, 1977 Contra Costa County, California, *BSSA*, 67, 1555-1564, 1977.
- Chen, Rong, Consistency of focal mechanism as a new parameter in describing seismic activity, *Acta Geophysica Sinica*, 27, no. 3, 142-159, in Chinese, 1978.
- Cipar, J., Source processes of the Haicheng, China earthquake from observations of P and S waves, *BSSA*, 69, 1903-1916, 1979.
- Deng, Q., P. Jiang, and L. Jones, and P. Molnar, A preliminary analysis of reported changes in ground water and anomalous animal behavior before the 4 February 1975 Haicheng earthquake, Maurice Ewing Series, Symposium on Earthquake Prediction, A.G.U., in press, 1981.
- Engdahl, E.R. and C. Kisslinger, Seismological precursors to a magnitude 5 earthquake in the Central Aleutian Islands, *J. Phys. Earth*, 25, 5243-5250, 1977.
- Fitch, T. and K.J. Muirhead, Depths to larger earthquake associated with crustal loading, *Geophys. J.R. astr. Soc.*, 37, 285-296, 1974.

- Fitch, T. and J.M.W. Ryan, Inversion for V_p/V_s in shallow source regions, *Geophys. J.R. astr. Soc.*, 44, 253-267, 1976.
- Gu, H.D., Y.T. Chen, X.L. Gao, and Y. Zhao, Focal Mechanism of Haicheng, Liaoning Province, of February 4, 1975, *Acta Geophysica Sinica*, 19, 285-293, 1976.
- Jackson, J. and T. Fitch, Seismotectonic implications of relocated aftershock sequences in Iran and Turkey: an application of the master event technique, *Geophys. J.R. astr. Soc.*, 57, 209-229, 1979.
- Jin, Y., Y. Zhao, Y. Chen, J. Yan, and Y. Zhou, A characteristic feature of the dislocation model of foreshocks of the Haicheng earthquake, Liaoning Province, *Acta Geophys. Sinica*, 19, 156-146, in Chinese, 1976.
- Jones, L.M., Q. Deng, and P. Jiang, The role of conjugate faults in the development and occurrence of earthquakes, *Seismology and Geology*, 2, 19-26, in Chinese, 1980.
- Jones, L.M. and P. Molnar, Some characteristics of foreshocks and their possible relationship to earthquake prediction and premonitory slip on faults, *J. Geophys. Res.*, 84, 3596-3608, 1979.
- Kagan, Y. and L. Knopoff, Statistical study of the occurrence of shallow earthquakes, *Geophys. J. Roy. astr. Soc.*, 55, 67-86, 1978.
- Kanamori, H. and D. Anderson, Theoretical basis of some empirical relations in seismology, *BSSA*, 65, 1073-1095, 1975.

- Lindh, A., G. Fuis, and C. Mantis, Foreshock amplitudes and fault plane changes: A new earthquake precursor?, *Science*, 201, 56-59, 1978.
- Mogi, K., Some discussions on aftershocks, foreshocks and earthquake swarms: The fracture of a semi-infinite caused by an inner stress origin and its relation to earthquake phenomena (third paper), *Bull. Earthquake Res. Inst. Tokyo Univ.*, 41, 615-658, 1963.
- Raleigh, C.B., et al., Prediction of the Haicheng earthquake, *EOS Trans. AGU*, 58, 236-272, 1977.
- Rice, J. and M. Cleary, Some basic stress diffusion solutions for fluid saturated elastic porous media with compressible constituents, *Rev. Geophys. and Space Phys.*, 14, no. 2, 227-242.
- Segall, P. and D. Pollard, Mechanics of discontinuous faults *J. Geophys. Res.*, 85, no. B8, 4337-4350, 1980.
- Wu, K., M. Yue, H. Wu, X. Cao, H. Chen, W. Huang, K. Tian, and S. Lu, Certain characteristics of Haicheng earthquake (M = 7.3) sequence, *Acta Geophys. Sinica*, 19, 109-117, in Chinese, 1976.

- Fig. 1. A map of the tectonics of Liaoning Province. The seismic stations used are shown by triangles.
- Fig. 2. A plot of magnitude versus time for the foreshocks to the Haicheng earthquake located in this study.
- Fig. 3. Recorded clock corrections versus time in days for Dandong station. The solid line is the best fit to the points and was used as the clock correction in this study rather than the individual points.
- Fig. 4. The epicenters of the foreshocks of the 1975 Haicheng earthquake relative to event No. 21. The numbers correspond to Table II.
- a) Epicenters of the foreshocks that occurred before the largest foreshock ($M = 4.6$, $T = 07^{\text{h}}50^{\text{m}}$ 04 February, No. 36).
 - b) Epicenters of the foreshocks that occurred between the largest foreshock (No. 36) and the second largest foreshock (No. 55, $M = 4.3$, $T = 10^{\text{h}}35^{\text{m}}$ 04 February). The epicenters from (a) are shown by open circles.
 - c) Epicenters of the foreshocks that occurred after the second largest foreshock (No. 55) and the mainshock. The epicenters from (a) and (b) are shown by open and hatched circles, respectively.
- Fig. 5. The depth distribution of the foreshocks to the 1975 Haicheng earthquake projected onto a plane trending $N30^{\circ}E$. Foreshocks that occurred before No. 36 are shown by closed circles, those between No. 36 and No. 55 by hatched circles and those after No. 55 by open circles. The errors in location are listed in Table II.

Fig. 6. The amplitudes of the P waves versus the amplitudes of the S waves of the foreshocks of the Haicheng earthquake recorded at YIN.

Fig. 7. SEismograms for two foreshocks (Feb. 04, 08:16 and 08:31) of the Haicheng earthquake recorded at YIN.

Fig. 8. Lengths and orientations with respect to the epicenters of foreshocks and mainshock of the cracks used to model the stress changes.

Fig. 9. A map of the locations of reported changes in ground water on 04 February 1975 prior to the occurrence of the mainshock. Important recently active faults are shown by solid lines if exposed and dashed if buried. Thicker lines indicate more important faults. From Deng et al. (1981).

Symbols for changes in ground water are the following:

- - rising ground water (in wells, springs or seepage from the ground)
- ▲ - rising surface water (in ponds, lakes or streams)
- - falling ground water
- △ - falling surface water
- + - other ground water changes

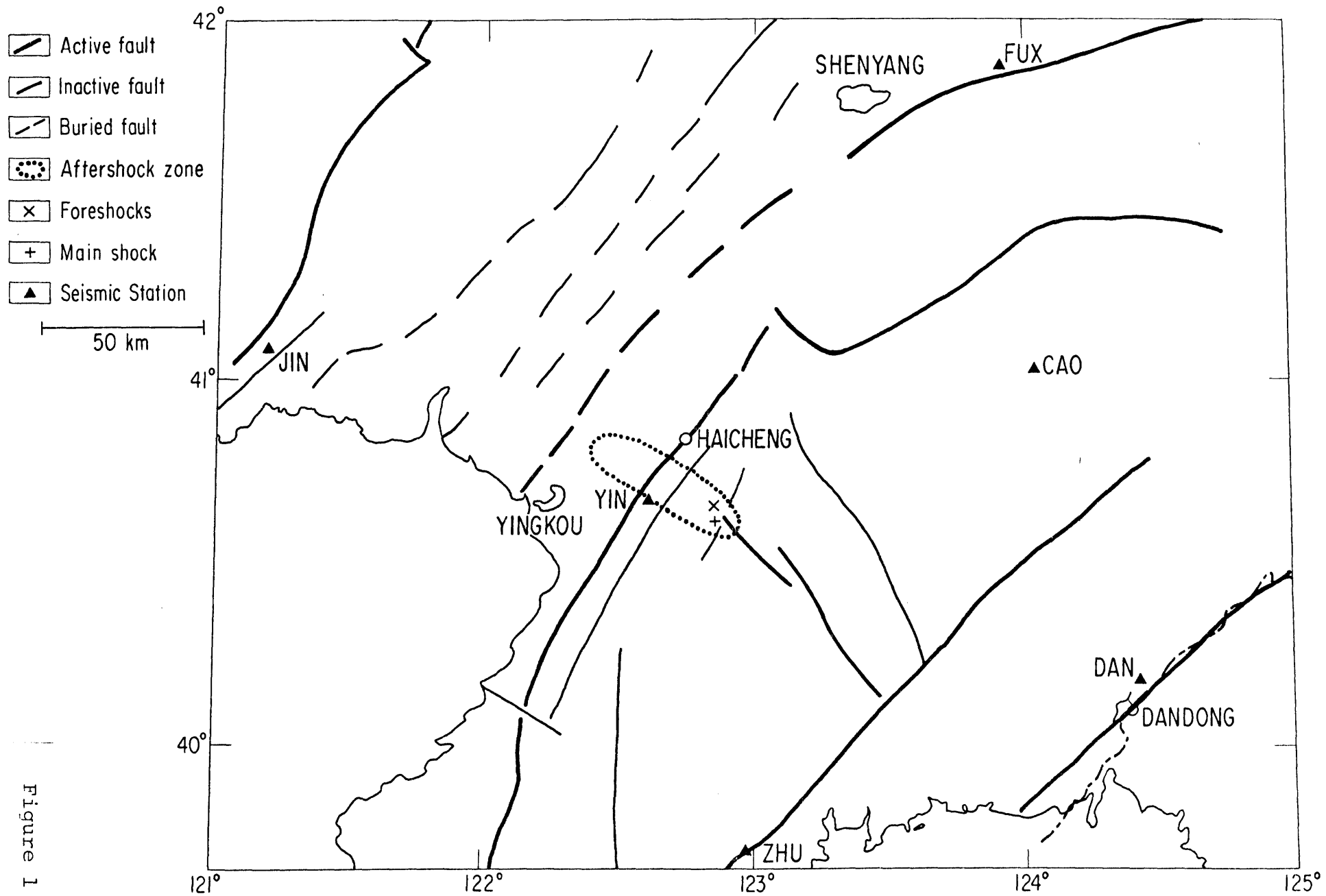
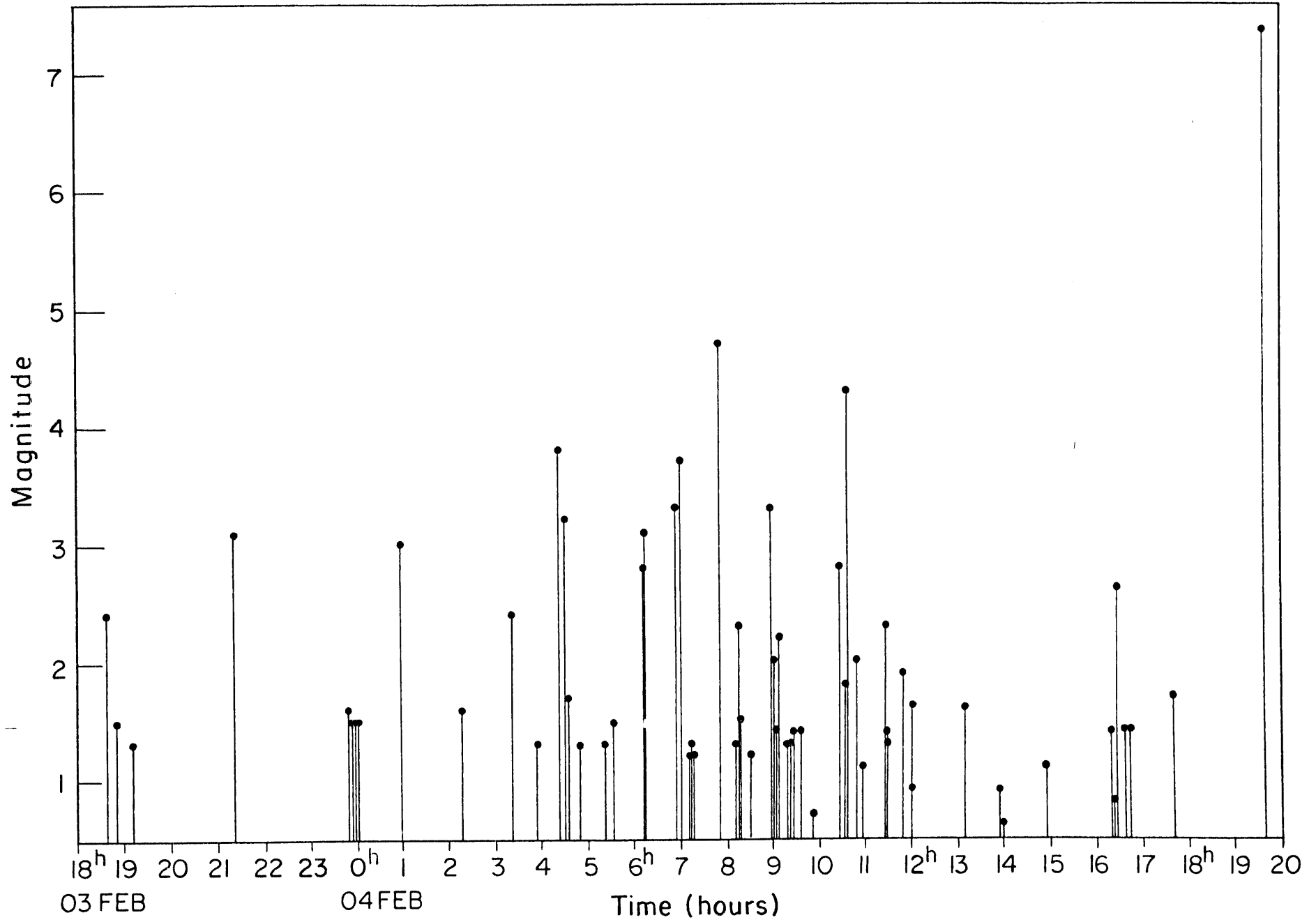


Figure 1

Figure 2



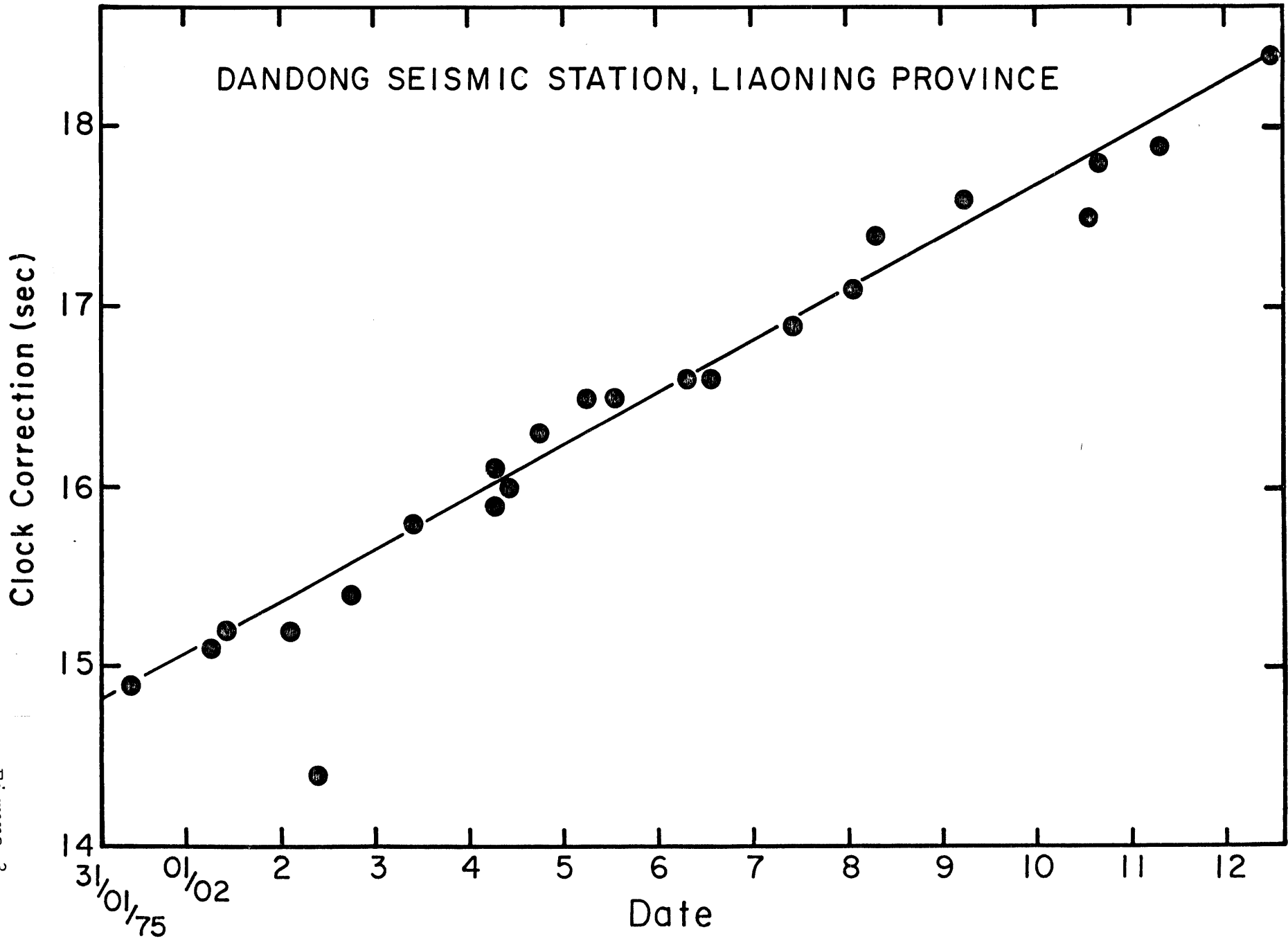
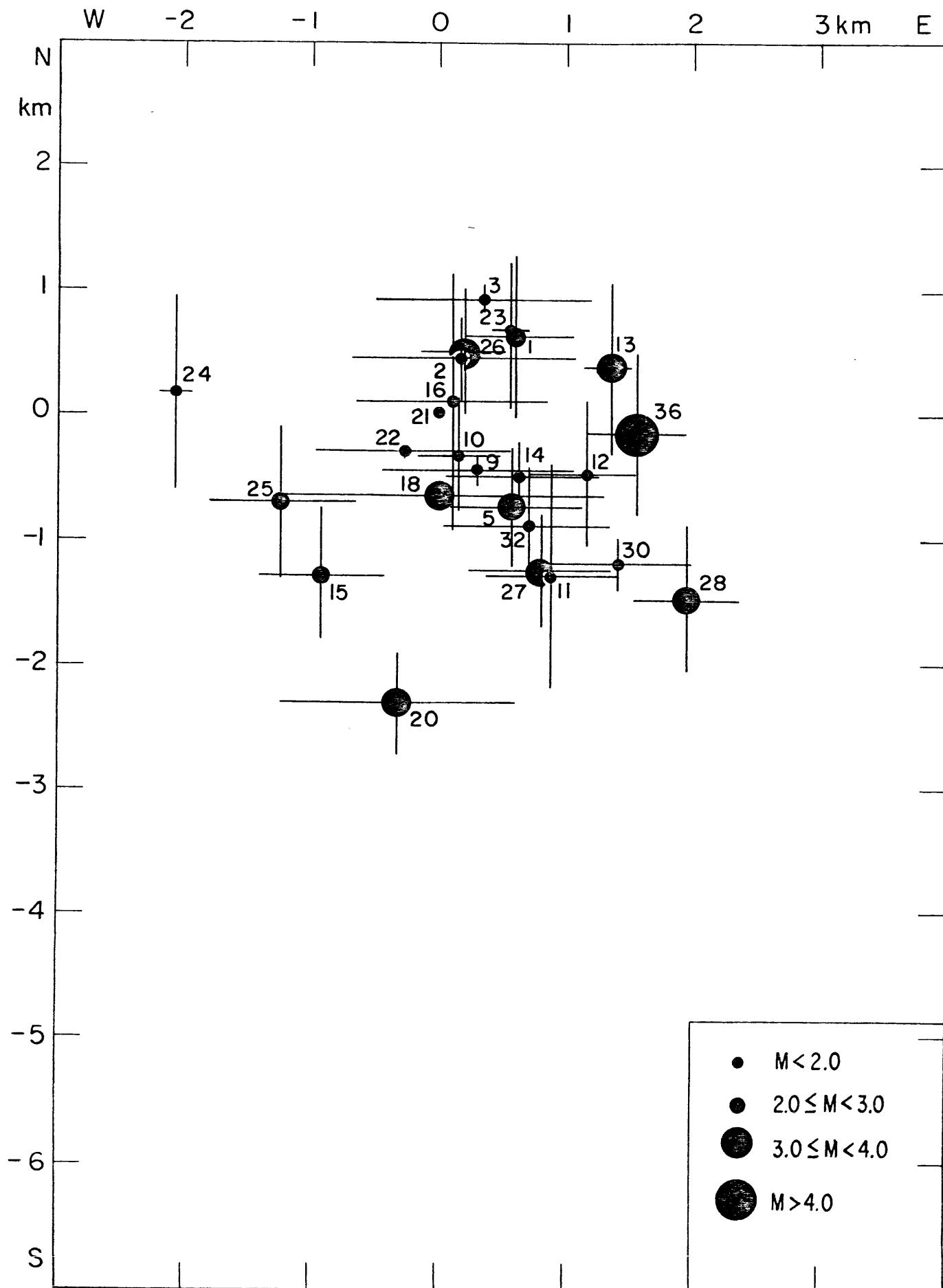


Figure 3



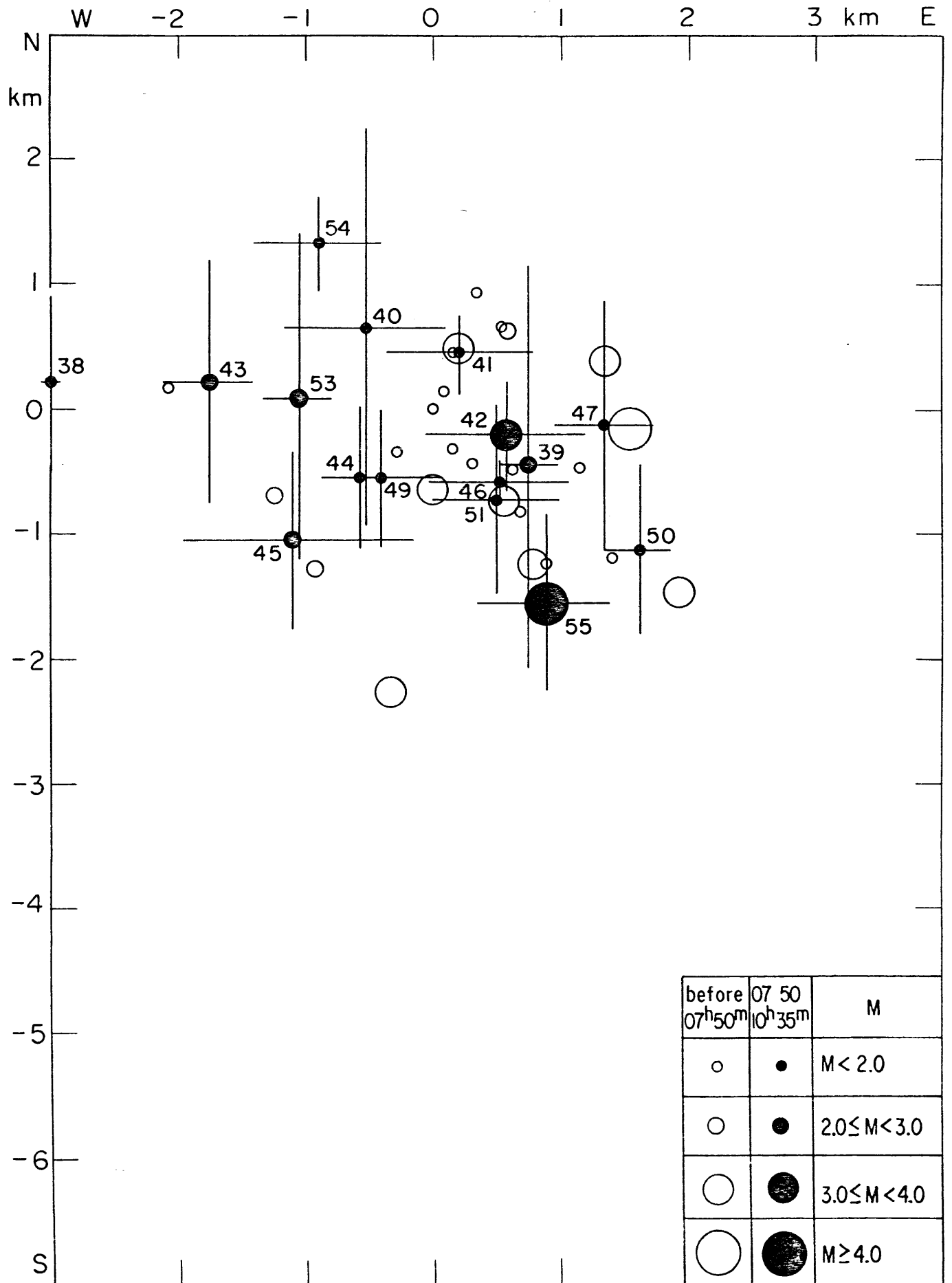


Figure 4b

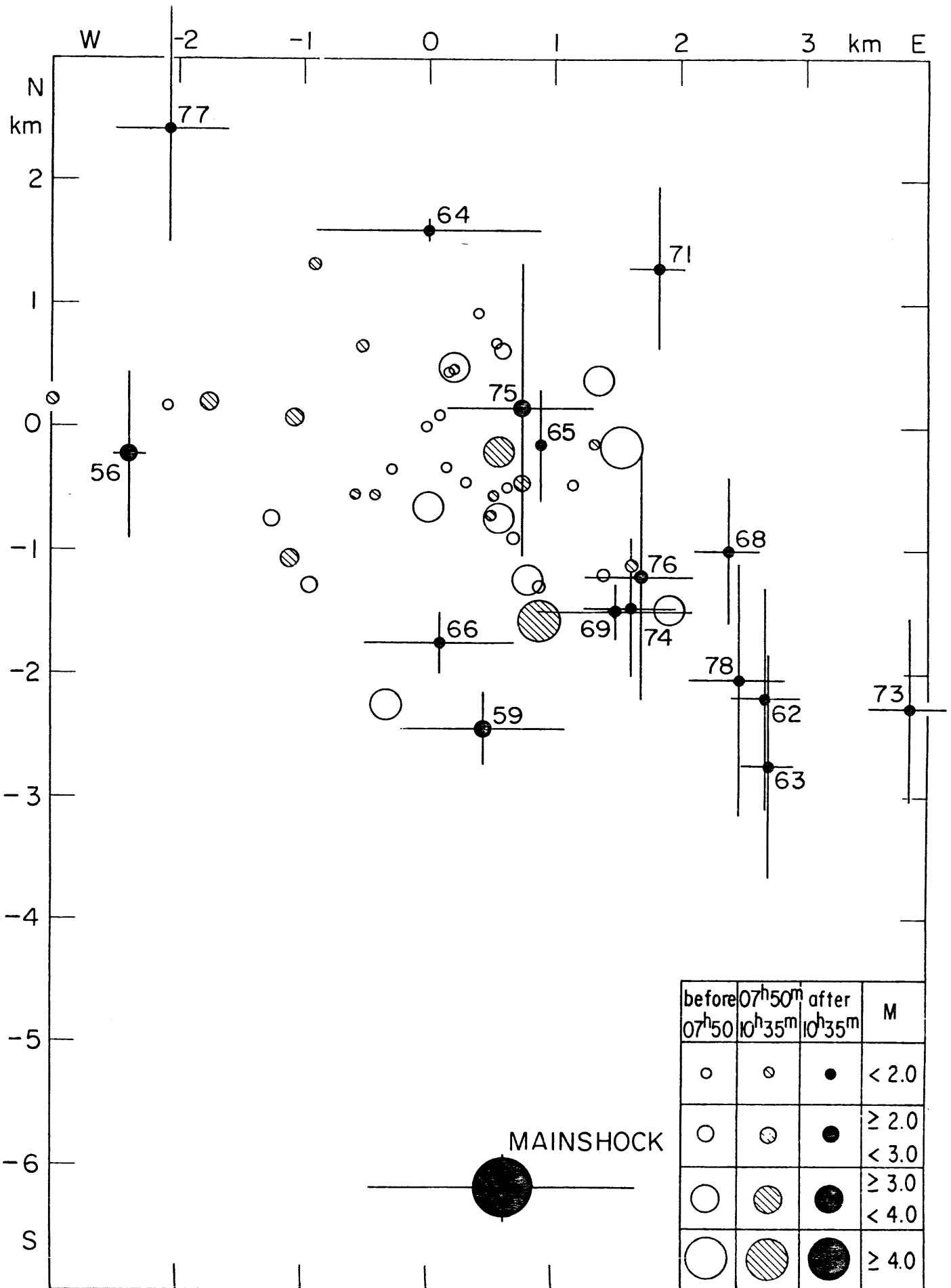
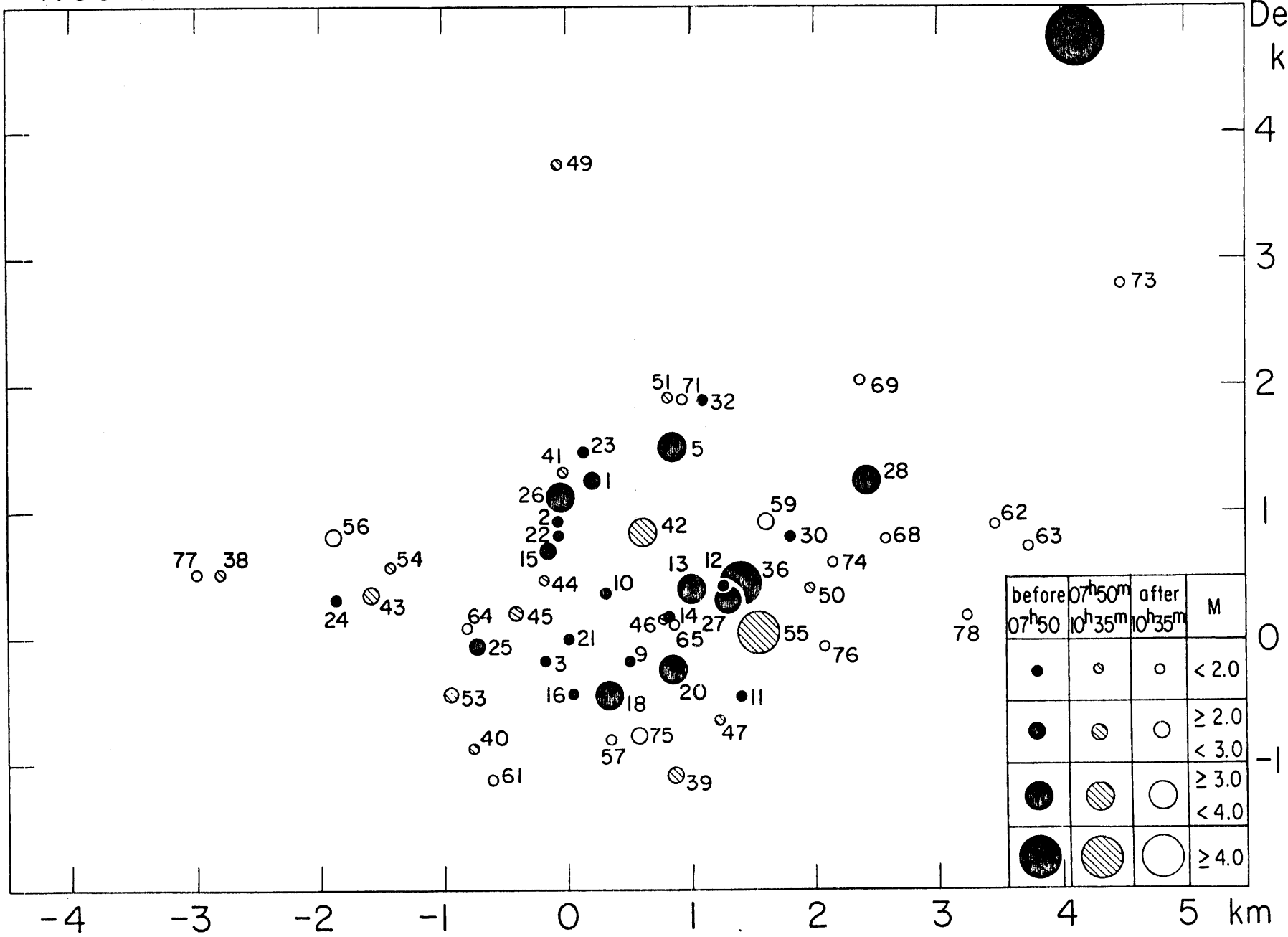


Figure 4c

N60°W

E 30°S

Depth
km



before 07 ^h 50	07 ^h 50 to 10 ^h 35 ^m	after 10 ^h 35 ^m	M
●	○	○	< 2.0
●	⊗	○	≥ 2.0 < 3.0
●	⊗	○	≥ 3.0 < 4.0
●	⊗	○	≥ 4.0

Figure 5

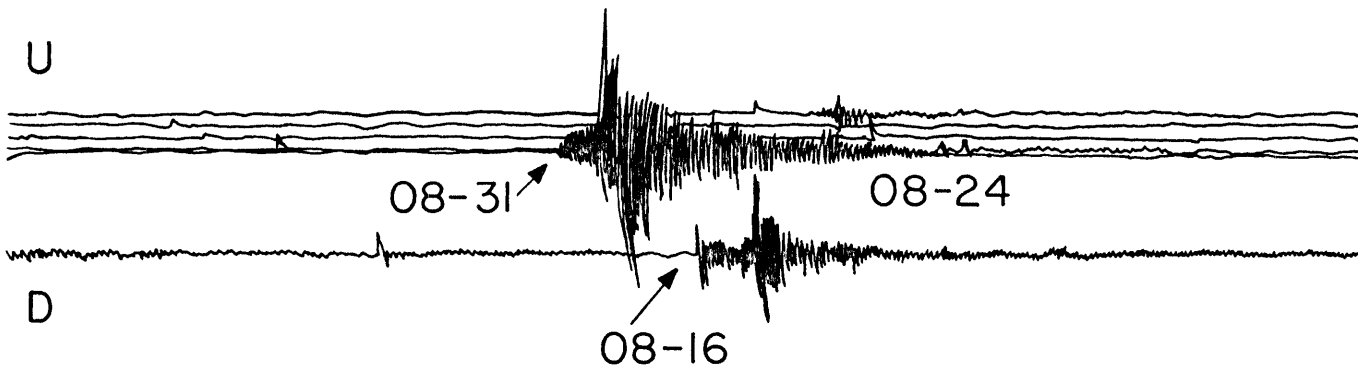


Figure 6

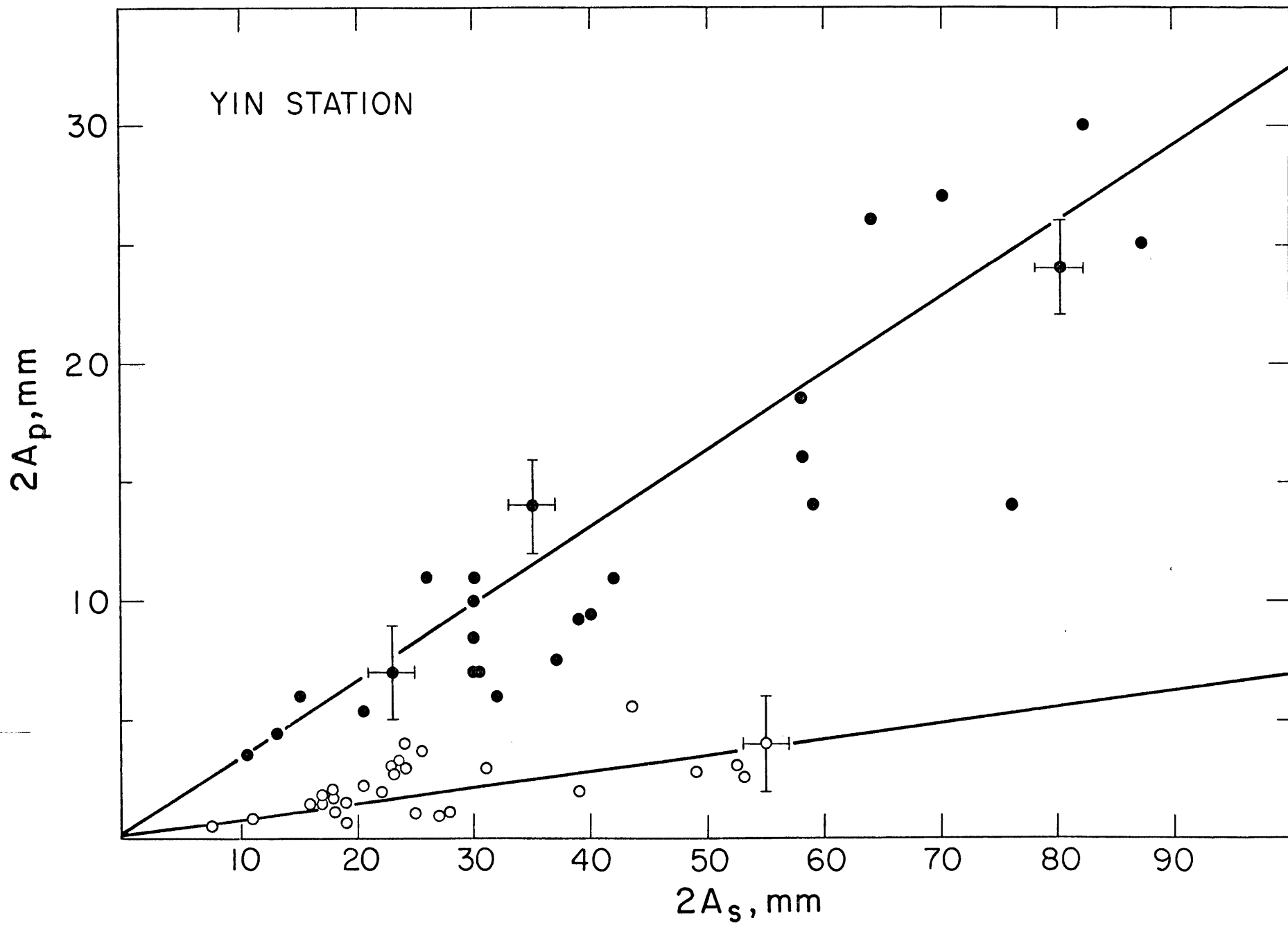


Figure 7

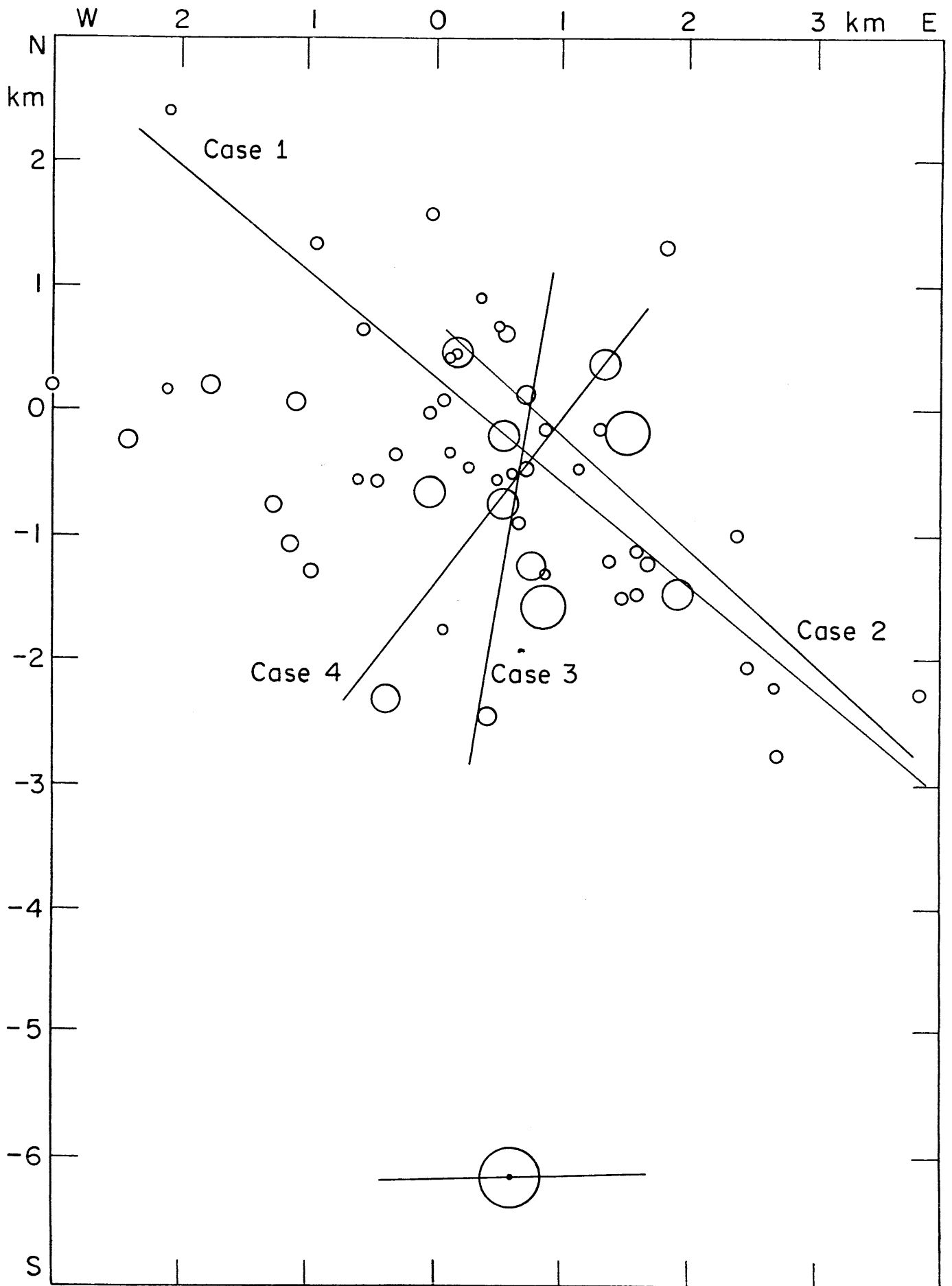


Figure 8

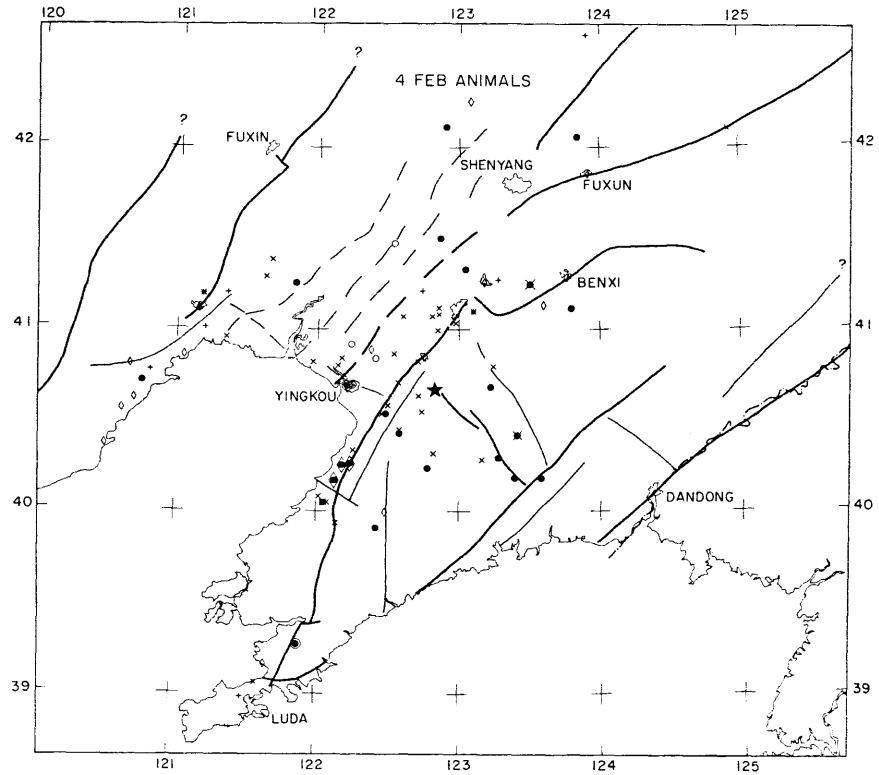
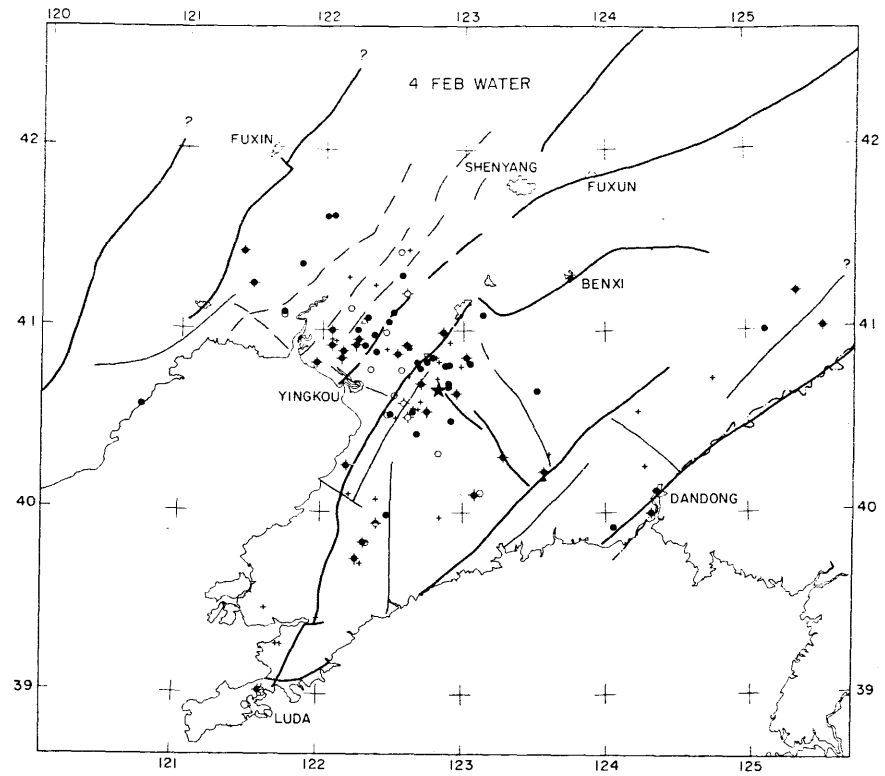


Figure 9

CHAPTER III :

CYCLIC LOADING OF SIMULATED FAULT GOUGE
TO LARGE STRAINS

CYCLIC LOADING OF SIMULATED FAULT GOUGE TO LARGE STRAINS

Lucile M. Jones

Department of Earth and Planetary Sciences,
 Massachusetts Institute of Technology
 Cambridge, Massachusetts 02139

Abstract. As part of a study of the mechanics of simulated fault gouge, deformation of Kayenta Sandstone (24% initial porosity) was observed in triaxial stress tests through several stress cycles. Between 50- and 300-MPa effective pressure the specimens deformed stably without stress drops and with deformation occurring throughout the sample. At 400-MPa effective pressure the specimens underwent strain softening with the deformation occurring along one plane. However, the difference in behavior seems to be due to the density variation at different pressures rather than to the difference in pressure. After peak stress was reached in each cycle, the samples dilated such that the volumetric strain and the linear strain maintained a constant ratio (approximately 0.1) at all pressures. The behavior was independent of the number of stress cycles to linear strains up to 90% and was in general agreement with laws of soil behavior derived from experiments conducted at low pressure (below 5 MPa).

Introduction

Much attention has recently been focused on the physical properties of fault zone materials because of potential relevance to earthquake mechanisms. Several investigators have examined the stress-strain relations of granular rock material deformed under various conditions. For instance, Byerlee and Summers [1976] and Engelder et al. [1975] examined the sliding characteristics at pressure of a layer of gouge on granite and sandstone faults, respectively. Engelder et al. [1975] also examined the behavior of a sample of quartz sand deformed through a few percent linear strain. Zoback and Byerlee [1976], using crushed granite, Shipman et al. [1974], and Gardiner et al. [1977], using a very porous sandstone (which becomes powder under small pressure), studied deformation to 20-30% linear strain.

All of these experiments have suggested the deformational behavior of these granular materials to be extremely dependent upon the strain history of the specimen. The fault gouge in a mature fault zone such as the San Andreas has experienced thousands of cycles of stress and large finite strains, a strain history very different from that of laboratory samples. How strongly does this difference affect deformational behavior? How far does the dependence on strain history extend? To examine these questions, we have in this experiment strained samples of simulated fault gouge to linear strains of 70-90% at pressures corresponding to the depths of California earthquakes. During these experimental runs, stress was cycled several times to try to gauge as far as

possible the effect on deformational characteristics.

Since actual specimens of fresh, unaltered gouge have not yet been recovered, its composition and physical state can only be surmised. Fault gouge presumably begins as rock powder formed by abrasion of the fault surfaces during frictional sliding [Byerlee, 1967]. Whether it then becomes clay or retains its original mineralogical composition is not known. Clay minerals are commonly found in surface outcrops of fault gouge and Wu et al. [1975] have suggested that some clay minerals are stable down to 10-km depth, lending credence to the idea that clay is an important part of fault gouge. It is possible, however, that the clay in outcrops is the result of surface weathering. Indeed, McGarr et al. [1979] examined newly exposed active faults in gold mines in South Africa and found that the gouge was rock powder with the same composition as the surrounding rock, supporting the contention that the mineralogy of fault gouge does not alter after original formation. It could be that both clay and crushed rock are present in fault zones such as can be seen at the Logan Rock Quarry, Gilroy, California, on the San Andreas fault. Until such time as fresh unaltered fault gouge from depth can be recovered and examined to resolve this question, we feel it is necessary to study the deformational behavior of both clay and crushed rock. This paper is the beginning of such a study in which we consider crushed rock.

Two methods have generally been used to study the deformational behavior of fault gouge. One uses as a sample a solid rock with a simulated fault zone (a sawcut filled with crushed rock) within the sample. This method has been used by Engelder et al. [1975], Logan [1978], Dieterich [1972], Byerlee and Summers [1976] and Scholz et al. [1972]. However, Logan et al. [1978] found that the behavior of this simulated fault not only is determined by the gouge layer but also strongly depends upon the solid rock used. Moreover, the size effects are not known. The second method in use is to determine the stress-strain relationships of fault gouge itself. This eliminates interference from the outer rock but does not supply a complete picture of the failure process [e.g., Weeks and Byerlee, 1978]. However, these data can be used in theoretical models such as those of Rice [1977], Rudnicki [1977], and Stuart [1979] which calculate the various contributions of the solid rock and the fault gouge to the failure mechanisms. This method has been used by Zoback and Byerlee [1976] and is what we used in this study.

Experimental Methods

To obtain crushed rock, we used a very porous sandstone, Kayenta sandstone from Grand Junction,

TABLE 1. Properties of Mixed Company Sandstone

Property	Value
Grain size	0.03-0.3 mm
Porosity	22.3-24.4%
Bulk density	2.00-2.03 g cm ⁻³
Composition	
Quartz	31-34%
Orthoclase	18-23%
Calcite	18-20%
Microcline, opaque, and lithic fragments	5-8%

Colorado. This rock is very weak and loses all cohesion under only a few hundred bars confining pressure. The composition and some physical properties of Kayenta sandstone are given in Table 1. Its porosity (~24%) is close to that for densest packing of perfect identical spheres.

The hydrostat for this rock is shown in Figure 1 (W.F. Brace, unpublished data, 1973). It was obtained by measuring the axial strain resulting from application of hydrostatic pressure. The volumetric strain was taken to be 3 times the linear strain. The most interesting feature of the hydrostat is the presence of an inflection point during loading. It is probably due to pore collapse resulting from failure of the calcite cement in the rock, and can also be seen in the first stress cycle of the triaxial compression experiments described below.

The sample configuration is shown in Figure 2. Cylinder samples, 1.90 cm in diameter and 5.08 cm long, were jacketed in 3-mm-thick polyurethane tubing which was clamped to steel pistons at the end of the sample with No. 14 steel wire. Pore fluid (tap water) was pumped into the sample through a tube in the plug at the bottom of the vessel. The inlet of this tube to the sample was shielded by a steel screen with holes 1/32" in diameter to prevent sand grains from entering and clogging the rest of the pore pressure system.

During an experiment the sample was subjected to constant external confining and internal pore pressure. The former was measured by a manganin coil, and the latter by a BLH pressure transducer. The volumetric strain was measured by determining the amount of fluid added to or taken from the pore fluid system to maintain constant pore pressure. Experiments were conducted with a pore pressure of 50 MPa and a confining pressure of 100, 250, 350, or 450 MPa, so that experiments were conducted at effective pressures of 50, 200, 300, and 400 MPa, respectively.

The sample was loaded by advancing the axial piston at a constant axial strain rate of approximately 10^{-4} /s in steps of approximately 2% axial strain. The axial strain was measured with a DC voltage differential transformer, and the axial force by a load cell (placed outside the pressure vessel), axially in line with the sample. The two pressures, axial strain and axial force, were monitored continuously. After each strain increment the system was allowed to equilibrate for 4 min, at the end of which time the volume change of the sample was recorded. To calculate the axial stress from the axial force, the

average cross-sectional area was used. This was determined from the average radial strain ϵ_r , which was calculated from the recorded volumetric strain $\Delta V/V$ and axial strain ϵ_z , since $\Delta V/V = \epsilon_z + 2\epsilon_r$.

Because the samples deformed stably, the end of a stress cycle had to be arbitrarily determined. In these experiments a cycle was ended when the loading piston had been fully advanced. To begin a new cycle, the piston had to be lengthened, which required lowering the confining and pore pressures (decreased simultaneously). The axial expansion of the sample was larger than the radial expansion during this process, most noticeably at the lower pressures. However, the three strains caused by representing the sample were approximately equal, so that the sample was longer at the beginning of a cycle than at the end of the previous cycle. We estimated the lengthening caused by this, but obviously this increases the uncertainty of the data. Therefore the absolute magnitude of the axial strain and stress (because the axial strain is used to determine the stress) is less accurate in later cycles than the changes in stress and strain within those cycles. Underestimation of the lengthening of the samples could be the cause of the lower stress at failure seen in the last cycle of most of the experiments.

There are large uncertainties in all the measurements. Although the accuracy of all the transducers was about $\pm 1\%$, all of the measurements are perforce average values. With such a large amount of deformation, the stress and strain could easily vary by a factor of 2 across the sample. The stress data are most susceptible to error, since the average cross-sectional areas were used to compute their values. The rock cylinders bulged noticeably during the experiments so that the diameter of the cylinder (and thus

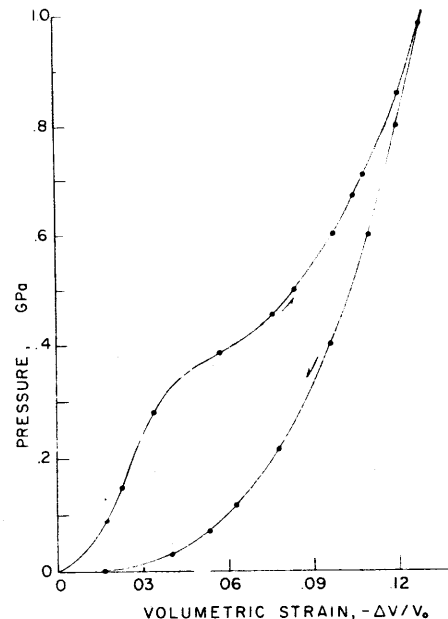


Fig. 1. Hydrostat for Kayenta sandstone. This sample was from Hole 1-1, Mixed Company site, near Grand Junction, Colorado (W.F. Brace, unpublished data, 1973).

the stress) varied by more than 50% at different points. Since the plotted stress was calculated using the average radius, the actual stress at various points in the sample is both lower and higher than the average plotted stress. It would seem that use of this average stress is justified. The stress-strain behavior during the first cycle (before significant bulging) closely resembles that of later cycles.

Experimental Results

Typical stress-strain behavior at various pressures is shown in Figures 3 and 4. All of the runs were duplicated except at 300-MPa, and the results were quite reproducible. The maximum stress, axial strain at failure, and volumetric strain rate (with respect to axial strain) varied only a few percent between samples—no more variation than existed between cycles of one sample. Typical reproducibility is shown in Figure 5. (There is less compaction in the first cycle for one sample because it had been pre-pressurized to 4 kbar.)

There were two markedly different styles of deformation. Below 300-MPa, deformation occurred throughout the sample with no essential change in the maximum stress once failure was reached. At 400-MPa, slip occurred on one plane accompanied by strain softening, and in one sample, small (<20-MPa) audible stress drops occurred. Intermediate behavior occurred at 300-MPa, as shown by a small decrease in stress with increasing strain (Figure 4) and a slight concentration of deformation on one plane. All slip planes were at $30^\circ \pm 2^\circ$ to the direction of maximum principal stress.

The volumetric strains were very consistent. All samples, after initial inelastic compaction, began to dilate at approximately 24% linear strain in the first cycle (Figures 3 and 4). Except for the 50-MPa run this was the point when maximum stress was reached. In later stress cycles, dilatancy always began with the achievement of peak stress. The rate of dilation was equally consistent. Except at the end of the 400-MPa cycles, when all deformation was occurring on one slip plane, the volumetric strain decrease was always one-tenth the linear strain regardless of pressure. This can be seen more clearly in Figure 6, where the volumetric

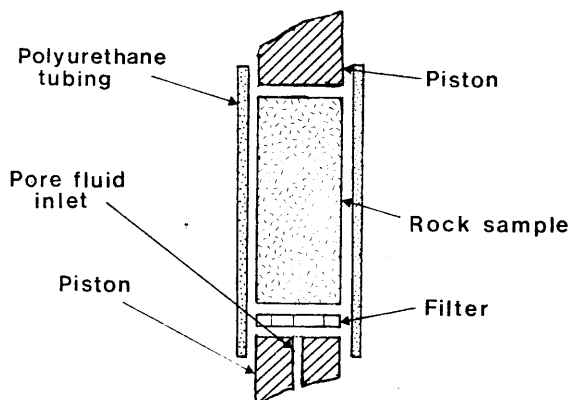


Fig. 2. Sample configuration used in these experiments. Schematic arrangement of sample. Except for filter, experimental details as given by Brace and Orange [1968].

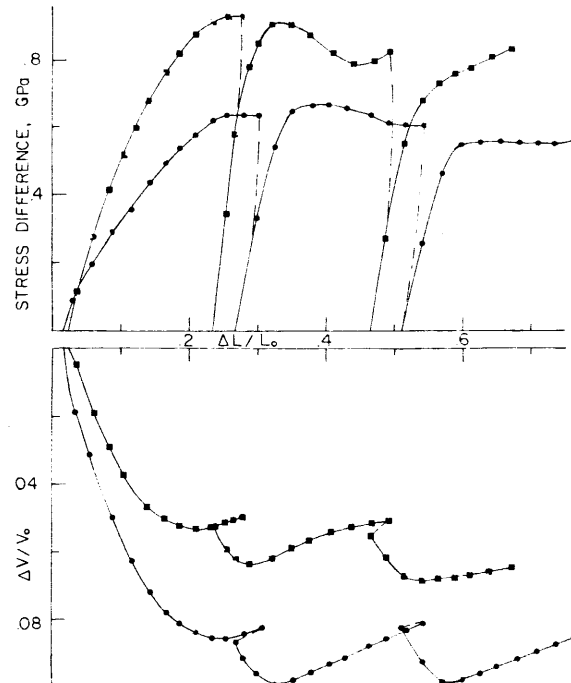


Fig. 3. Axial stress difference and volumetric strain versus axial strain. Data from experiments conducted at effective confining pressures of 300 MPa (circles) and 400 MPa (squares).

strain versus axial strain curves of all the later cycles are plotted together for comparison.

The stress rise at the end of the deformation at 400-MPa effective pressure may not be due to sample deformation. One experiment ended when the sample sheared through its jacket and split the steel pistons at both ends; and at some point near the end of the second experiment the sample ran into the pressure vessel wall. Both factors could have caused the stress increase, depending on when they occurred.

Discussion

Dilatancy

The dilatant behavior of this simulated fault gouge has several noteworthy features. First, a dependence on strain history only appeared during the first stress cycle. For example, the 50-MPa sample did not begin to dilate until well after peak stress, whereas the 200-MPa sample passed through an inflection point before reaching peak stress and dilation. For all of the samples, more linear strain occurred before attainment of peak stress in this cycle than in later cycles. These effects were probably due to breakdown of the original matrix of the sandstone. It is often assumed that compaction and dilatancy both occurred continuously during shear, and the volume change just showed which phenomenon predominated [Youd, 1972]. Thus one could say that more compaction occurred during the first stress cycle, when the original matrix of the rock was being destroyed, than in later cycles, resulting in a larger linear strain at failure. The unusual initial behavior of 50- and 200-MPa samples was probably due to the even greater

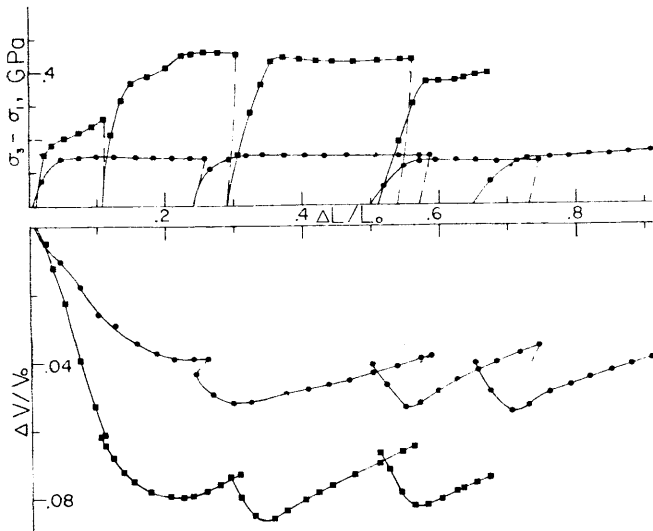


Fig. 4. Axial stress difference and volumetric strain versus axial strain. Data from experiments conducted at effective confining pressures of 50 MPa (circles) and 200 MPa (squares).

compaction that caused the inflection point on the hydrostat. This compaction occurred during the application of pressure for the 300- and 400-MPa samples, but during axial loading of the 200-MPa sample, causing an inflection point on the stress-strain curve. It occurred after peak stress for the 50-MPa sample, so that dilation could not supersede this increased compaction until well after achievement of peak stress. However, when the sample was prepressurized to 400-MPa so that the initial porosity was lower, dilatancy did begin with peak stress (Figure 5). During the later cycles, when the sample was consolidated sand rather than a rock, the strain history had no discernible effect upon the behavior.

Second, as has been commonly found for very porous materials [e.g., Shipman, 1974; Zoback and Byerlee, 1976; Weeks and Byerlee, 1978], dilatancy began at approximately peak stress. This occurred at the same strain regardless of pressure, 22-24% for the first cycle and 6-8% for later cycles (Figures 3 and 4).

Third, the rate of volume change was also constant, independent of pressure (Figure 6). Except when slip was concentrated along one fault plane (at the end of 400-MPa effective pressure experiments), the volume strain was one-tenth the linear strain. This is perhaps reasonable, since both strains resulted from the same shearing process. Obviously, the sample cannot dilate forever, but negative volume changes of several percent have been observed in shear of soils with a constant rate until near the end of dilation and predicted theoretically [Rowe, 1962].

Fourth, markedly different behavior was observed at low and high pressure. The samples deformed at 50- and 200-MPa showed constant yield stress behavior: no change in axial stress once peak stress was attained with deformation occurring uniformly throughout the sample. The samples deformed at 400-MPa showed strain-softening behavior: the axial stress decreased stably after achievement of peak stress, and the deformation of the sample became concentrated

along one fault plane. However, it appears that the difference in behavior is due to the difference in density between the samples rather than in pressure, as discussed below.

Comparison With Typical Soil Behavior

Cohesionless material, such as sand [Lambe and Whitman, 1969], deformed at low pressure often exhibits two contrasting types of behavior which are very similar to the constant yield stress and strain-softening deformation patterns that we have found for these materials at high pressure. However, it was found that the difference in behavior is a function of the density of the soil rather than the pressure at which the soil was deformed, so that the greater the density, the greater the strain-softening after peak stress. In fact, the reverse effect has often been reported, namely, that increased pressure will decrease the strain-softening effect [Lambe and Whitman, 1969, p. 137].

The samples deformed at 400-MPa effective pressure were significantly denser than the samples which were deformed at lower pressures because they had already passed through the inflection point in the hydrostat before deformation. To test if this density variation was the controlling factor, we prepressurized a sample to 650-MPa (well beyond the inflection point) and then sheared it at 200-MPa effective pressure in triaxial compression. Thus the porosity of this sample was approximately 16% at the beginning of loading, as compared to the 23% porosity of the normally consolidated samples that were also deformed at 200-MPa effective pressure. The deformational behavior of these two samples is shown in Figure 7. Although the

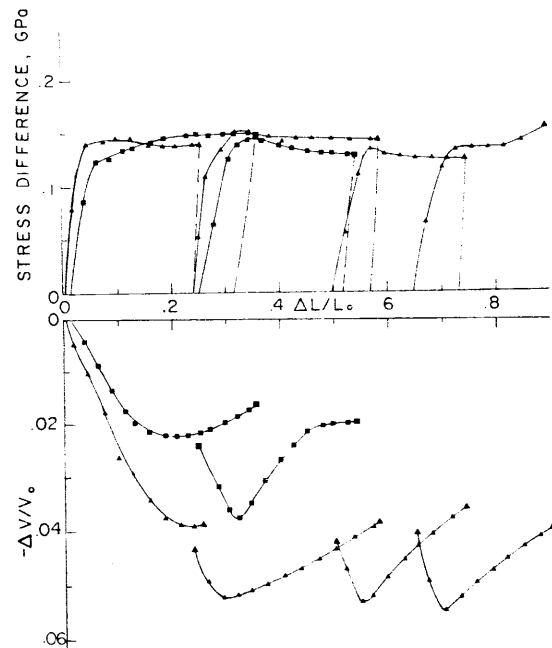


Fig. 5. Axial stress difference and volumetric strain versus axial strain for two samples, both deformed at 50-MPa effective confining pressure. One sample (shown by squares) was prepressurized to 400 MPa so that its maximum volumetric compaction is less.

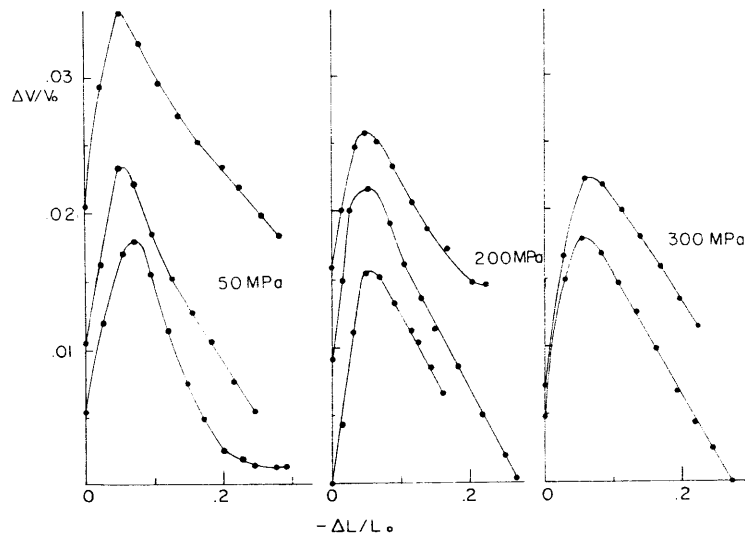


Fig. 6. Volumetric strain versus axial strain for stress cycles beyond the first. The beginning of each cycle has been put at zero linear strain, and the volumetric strains have been shifted arbitrarily for convenience. The numbers by each group of curves gives the confining pressure for that group.

looser sample compacted more during shear so that the difference in porosity at failure was only a few percent, there was still a significant change in behavior because of the increased density. The denser sample not only exhibited strain softening but also formed a single slip plane, whereas the loose sample had a constant yield stress and uniform deformation throughout the sample as previously described. Thus porosity, rather than pressure, seemed to control the behavior of cohesionless materials at high pressure.

The difference in behavior between dense and loose samples is probably due to the degree of interlocking between grains within the sample [Lambe and Whitman, 1969]. Energy in a sample under shear is expended in four ways: to overcome frictional resistance, to lift grains over others that lie in their path (thus causing dilatancy), to crush grains, and to resist external forces. The amount of energy needed to lift or crush grains is probably determined by the degree of interlocking of the grains. Thus in a loose sample, most of the energy is used to overcome friction which stays constant, so no stress drop is seen. In a dense sample, more energy must be put into a sample to bring it to failure, but once failure occurs and the sample begins to dilate, the extra energy expenditure will decrease until the maximum stress is equal to that of the loose sample.

The difference in density is also sometimes used to explain the presence or absence of a slip plane. A slip plane would normally form in shear failure. The shear-induced grain movement within a loose sample probably rearranges the grains sufficiently to break up a forming slip plane. In a dense sample, grain movement is more restricted and insufficient to destroy the plane.

Shear Strength

The Mohr envelope for peak stress at failure in these triaxial experiments is given by

$$\sigma_3 = 3.21\sigma_1 + 22 \text{ MPa}$$

or

$$\tau = \tan 31^\circ \sigma_n + 6 \text{ MPa}$$

where σ_3 is the maximum compressive stress. The good agreement of the angle of frictional sliding (31°) with the angle in Byerlee's law ($31^\circ \pm 4^\circ$) [Byerlee, 1978] supports the assumption that most of the energy is expended by frictional work.

Relevance to Earthquakes

In his theoretical model of earthquake occurrence, Rice [1977] concluded that fault zone materials must undergo strain weakening for an earthquake to occur. These data indicate that this is possible, but only if the fault gouge has a low porosity. However, this is likely, since repeated stress cycling significantly reduces porosity of cohesionless materials [Youd, 1972].

But what about the many other ways in which actual fault gouge may differ from crushed Kayenta sandstone? The largest variation in behavior would occur if clay were a significant component of fault gouge at depth. Clearly, a wide range of experiments must be done, but in the meantime, soil mechanics offers some guide as to how fault gouge might in general behave if clay were present.

Role of Clay

In drained conditions, clay behaves like sand [Lambe and Whitman, 1969, p. 306]. However, in clay the degree of overconsolidation (the ratio of the maximum past pressure to the present pressure) rather than the density controls the amount of strain softening. Clay in fault zones is probably heavily overconsolidated, so that in drained shear, strain softening would occur. However, in undrained shear (when the permeability is insufficient to allow equalization of

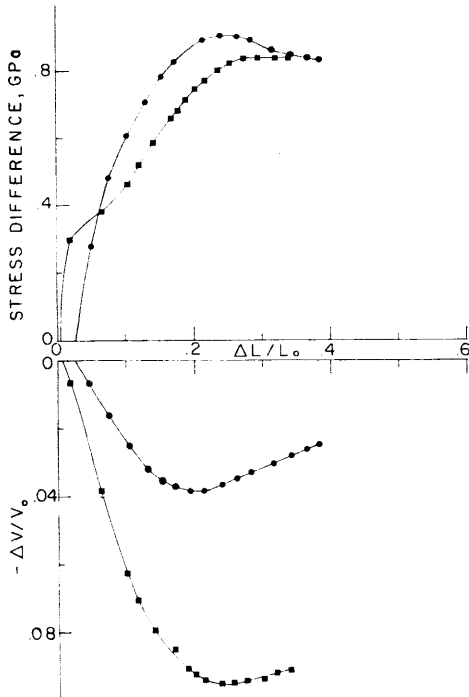


Fig. 7. Axial stress difference and volumetric strain versus axial strain for two samples of different density (circles for $\eta_0 = 16\%$ and squares for $\eta_0 = 23\%$), both deformed at 200-MPa effective confining pressure.

pore pressures throughout the system) the drop in pore pressure caused by the large amount of dilatancy accompanying shear of overconsolidated clay results in increased effective pressure and increased shear strength. Thus with undrained conditions, overconsolidated clay experiences strain hardening. Whether drained or undrained shear would occur in natural fault zones depends upon the amount of clay in the gouge. If the gouge is predominantly crushed rock with the clay occurring in veins through the rock (as can be seen in the nearly exposed section of the San Andreas fault at the Logan Rock Quarry), the zone would probably still be permeable enough to be drained. If, however, the gouge is mostly clay (like the surface exposure of the San Andreas fault at Fort Tejon Pass, California), undrained conditions might apply.

Strain Rate and Temperature

Because friction is only slightly dependent on strain rate [Stesky, 1975], the main concern of soil mechanics with strain rate is its effect upon drainage. In permeable crushed rock, drained conditions occur, and the effect of strain rate is not significant. When clays are present, a comparison of the strain rate and permeability of the total system of crushed rock and clay is necessary to determine the amount of excess pore pressure dissipation.

Soil mechanics obviously does not deal with temperature variation. Probably, temperature becomes important only when it is high enough that it alters the frictional process. For granite and gabbro this begins at 500°C or more [Stesky et al., 1974].

Conclusions

We have examined the deformational behavior of a simulated fault gouge and found that the strain history dependence only occurred in the initial compaction of the sample. Dilatancy occurred in the same manner in every cycle, beginning when peak stress was reached and continuing at a constant rate equal to one-tenth the linear strain independent of pressure. The linear strain at achievement of peak stress was also independent of pressure and approximately equal to 7% in later cycles. Finally, whether or not the sample undergoes strain weakening depends upon the density of the material. All of these observations are consistent with the behavior of typical cohesionless soils.

Acknowledgments. The author thanks W. F. Brace and H. H. Einstein for their advice and helpful suggestions. She was supported by a National Science Foundation graduate student fellowship while this work was being done. Laboratory expenses were covered by National Science Foundation grant EAR77-23158.

References

- Brace, W. F., and A. S. Orange, Electrical resistivity changes in saturated rocks during fracture and frictional sliding, *J. Geophys. Res.*, **73**(4), 1433-1445, 1968.
- Byerlee, J. D., Frictional characteristics of granite under high confining pressure, *J. Geophys. Res.*, **72**, 3639-3648, 1967.
- Byerlee, J. D., Friction of rocks, *Pure Appl. Geophys.*, **116**(4/5), 615-626, 1978.
- Byerlee, J. D., and R. Summers, A note on the effect of fault gouge thickness on fault stability, *Int. J. Rock Mech. Mining Sci.*, **13**, 35-36, 1976.
- Dieterich, J. H., Time-dependent friction in rocks, *J. Geophys. Res.*, **77**, 3690-3697, 1972.
- Engelder, J. T., J. M. Logan, and J. Handin, The sliding characteristics of sandstone on quartz fault gouge, *Pure Appl. Geophys.*, **113**(1/2), 69-86, 1975.
- Gardiner, D. S., S. W. Butters, D. O. Enniss, and A. H. Jones, Material properties of Nevada Test Site tuff and grout - With emphasis on the Diablo Hawk and Hybla Gold events, final report, contract 001-76-C-0351, Def. Nucl. Agency, Washington, D.C., 1977.
- Lambe, T. W., and R. V. Whitman, *Soil Mechanics*, John Wiley, New York, 1969.
- Logan, J. M., Laboratory and field investigations of fault gouge, in *Summaries of Technical Reports*, vol. VI, pp. 370-373, U.S. Geological Survey, Reston, Va., 1978.
- Logan, J. M., and L. W. Teufel, The influence of rock type on the sliding behavior of rock-gouge systems with quartz gouge (abstr.), *Trans. AGU*, **59**(12), 1208, 1978.
- McGarr, A., S. M. Spottiswoode, N. C. Gay, and W. D. Ortlepp, Observations relevant to seismic driving stress, stress drop, and efficiency, *J. Geophys. Res.*, **84**, 2251-2261, 1979.
- Rice, J. R., Theory of precursory processes in the inception of earthquake rupture, in *Proceedings of the Symposium on Physics of*

- Earthquake Sources, Academy of Science, German Republic, 1977.
- Rowe, P. W., The stress-dilatancy relation for static equilibrium of an assembly of particles in contact, Proc. Roy. Soc., Ser. A, 269(1339), 500-527, 1962.
- Rudnicki, J. W., The inception of faulting in a rock mass with a weakened zone, J. Geophys. Res., 82, 844-854, 1977.
- Scholz, C., P. Molnar, and T. Johnson, Detailed studies of frictional sliding of granite and implications for the earthquake mechanism. J. Geophys. Res., 77, 6392-6406, 1972.
- Shipman, F. H., J. N. Johnson, and S. J. Green, Mechanical properties of two highly porous geological materials, final report, contract DAAG 46-72-C-0169, Army Mater. and Mech. Res. Center, Watertown, Mass., 1974.
- Stesky, R. M., The mechanical behavior of faulted rock at high temperature and pressure, Ph.D. thesis, 197 pp., Mass. Inst. of Technol., Cambridge, July 1975.
- Stesky, R. M., W. F. Brace, D. K. Riley, and P.-Y. F. Robin, Friction in faulted rock at high temperature and pressure, Tectonophysics, 23, 177-203, 1974.
- Stuart, W. D., Strain softening prior to two-dimensional, strike-slip earthquakes, J. Geophys. Res., 84, 1063-1070, 1979.
- Weeks, J., and J. D. Byerlee, Preliminary investigation of volume changes in crushed granite preceding stick-slip failure, Geophys. Res. Lett., 5, 832-834, 1978.
- Wu, F. T., L. Blatter, and H. Roberson, Clay gouges in the San Andreas fault system and their possible implications, Pure Appl. Geophys., 113(1/2), 87-96, 1975.
- Youd, T. L., Compaction of sands by repeated shear straining, Proc. Amer. Soc. Civil Eng., 98, 709-725, 1972.
- Zoback, M., and J. D. Byerlee, A note on the deformational behavior and permeability of crushed granite, Int. J. Rock Mech. Mining Sci., 13, 291-294, 1976.

(Received April 23, 1979;
 revised October 29, 1979;
 accepted November 26, 1979.)

CHAPTER IV :

THE EFFECT OF POROSITY AND GRAIN-CRUSHING ON
THE DEFORMATION BEHAVIOR AND PERMEABILITY OF
CRUSHED WESTERLY GRANITE

Introduction

Extensive study of the stress-strain behavior of crushed rock at low pressures (<10 MPa) has shown that porosity is the most important factor in determining the behavior of the material [e.g. Lambe and Whitman, 1969, p.130]. The purpose of this study has been to determine if the porosity of crushed rock continues to control its mechanical behavior at high pressures (200 MPa). To do this, samples of crushed Westerly granite with different initial porosities were deformed under identical conditions in triaxial compression and their behavior was compared.

In the last few years there have been several studies of the behavior of crushed rock at high pressures (10-400 MPa) because of the common occurrence of crushed rock as a constituent of fault gouge. None of these studies has directly examined the effect of porosity on the stress-strain behavior. In experiments on samples consisting solely of crushed rock, pressure has been the primary variable considered [Zoback and Byerlee, 1976a, 1976b; Jones, 1980]. In all cases, the normalized strength (divided by pressure) and amount of decrease in stress with strain after peak stress (strain-softening) increased with pressure. This is incompatible with the results at low pressure, which show that strength and strain-softening increased with decreasing porosity but, if porosity was held constant, actually decreased with increasing pressure (though the effect is smaller than that of porosity) [e.g. Lambe and Whitman, 1969, p.137]. Jones [1980] noted that her specimens which were deformed at higher pressures

had much lower porosities than those at lower pressures. The samples of Zoback and Byerlee [1975; 1976] had similar variations in porosity. Thus it is possible that the low and high pressure results are not incompatible but that the apparent pressure dependency at high pressure is the result of porosity variations, and it was to resolve the point that this study was conducted.

The most significant difference between the mechanical processes causing deformation at low and high pressures is that the crushing of individual grains is much more important at high pressure. This could affect the strength because of the energy expended to create new surface during grain crushing. The grain crushing will also lower the permeability of the material by decreasing the size of the pore spaces. Thus it was desirable to know the amount of grain crushing that was occurring during deformation. Previous experiments have estimated the grain crushing by optical examination of the grains after deformation [e.g. Engelder et al., 1975]. In this study, to get a more direct determination of the amount of grain crushing, two measurements were used. First, the permeability of the samples was measured at several points during shear. Second, at the end of the experiment, the surface area of the deformed samples was determined by the BET technique, which measures the low temperature nitrogen adsorption isotherms of the surfaces. A comparison of the surface areas and the final permeabilities of the samples confirmed that an equation relating porosity and surface area to permeability which has been found to adequately explain data

from sands at low pressure, can also be applied to this material. With this equation, the measured permeabilities and porosities could be used to calculate the surface area at each point. Thus the rate of surface area increase with strain could be determined.

The motivation for studying the behavior of crushed rock at high pressures is its relevance to earthquake mechanics. In the center of many active fault zones there are extensive regions of fault gouge, of which crushed rock is a primary constituent [e.g. Anderson et al., 1981]. (Clay is also commonly found in fault gouge, but to limit the scope of this work only crushed rock is considered here.) It is generally assumed that the presence of gouge, with different mechanical properties than the surrounding rock, will be influential in determining the reaction of the fault system when loaded to failure. All three parameters measured in these experiments - the stress-strain behavior, the permeability, and the grain crushing - are important factors in this regard. In a theoretical analysis, Rice [1979] showed that the occurrence of an earthquake in a fault zone depended upon (1) the ratio of length to thickness of the gouge zone, (2) the relative strengths of the gouge and surrounding rock, and (3) the rate of strain-softening in the gouge. Strain-softening is a characteristic of the behavior strongly controlled by the porosity at low pressure and closely examined in this study. The permeability will control how fast dilatancy and/or compaction-induced changes in pore pressure will dissipate

and thus determine the effective pressure acting on the gouge. The rate of grain crushing shows how much of the total energy put into deforming the gouge is being expended to create new surface. This is important in considering what heat flow should be expected from a fault zone because the more energy that is used in creating new surface, the less is available for frictional heating.

Experimental Methods

The material used as fault gouge in these experiments was crushed Westerly granite with the grain size distribution shown in Figure 1. It was impossible to insure that each sample had exactly the same grain size distribution, but the whole distribution rather than one particular grain size was used because having a wide range of grain sizes seemed more likely to correspond with the situation in a fault zone. In addition, picking out one grain size would alter the mineral composition of the samples.

The sample configuration is shown in Figure 2. The details of the experimental procedure are described in Jones [1980]. As in that paper, the volumetric strain was measured by determining the amount of water added to or removed from the system to maintain a constant pore pressure. The average cross-sectional area of the sample (which was needed to determine the axial stress from the axial force and the permeabilities of the samples) was calculated from the recorded volumetric strain, ϵ_v , and axial strain, ϵ_z , using $\epsilon_v = \epsilon_z + 2\epsilon_\theta$.

The initial porosities of the samples was determined from the volumes of the solids and the voids. The volume of the solids, V_s , was determined from the weight of the solids put into the sample and the known density of Westerly granite. After packing, the sample was evacuated and the water admitted to the sample. From the amount of water drawn into the sample, the volume of the voids was determined. The decrease in volume during application of pressure was measured, as described above, to give the volume of the voids at pressure, V_v . The porosity of the sample η , was then calculated from

$$\eta = V_v / (V_v + V_s)$$

The permeability was determined using the pressure pulse decay method [Brace et al., 1968]. Two reservoirs with volumes of 17.75 cc and 15.0 cc were placed at the top and the bottom of the sample, respectively. The pressure was increased abruptly in the lower reservoir and the decay of pressure with time in the lower reservoir was measured. Neglecting storage in the sample, the pressure should decay as

$$p - p_f = (p_o - p_f) e^{-\alpha t}$$

where p is the pore pressure in the lower reservoir at a given time, p_f is the final equilibrated pore pressure, p_o is the pore pressure to which the lower reservoir was increased, and t is time. A plot of $\ln(p - p_f)$ versus time should produce a straight line, which it did in all of these experiments. The

slope of this line is α , from which the permeability, k , can be calculated by

$$\alpha = \frac{kA}{\mu\beta L} \left(\frac{1}{V_1} + \frac{1}{V_2} \right)$$

where A is the area of the sample, L is the length of the sample, μ is the viscosity of the fluid, β is the compressibility of the fluid, and V_1 and V_2 are the volumes of the two reservoirs [Brace et al., 1968].

Since the purpose of these experiments was to determine the effect of porosity upon the mechanical behavior, samples with different initial porosities were deformed at the same effective confining pressure of 190 MPa (pore pressure of 10 MPa). This pressure was used because it is the hydrostatic value at approximately 10 km depth where earthquakes are common. The different porosities were attained by different degrees of packing in the initial preparation of the samples and in the densest case ($\eta_0 = 9.8\%$) by overconsolidation to 360 MPa.

The initial porosity measurements are accurate within $\pm 1\%$. The permeabilities are probably accurate only within $\pm 25\%$. Because the decay curves were indeed exponential, α could be determined at least within $\pm 10\%$, and usually within $\pm 5\%$. This procedure for determining the permeability, however, assumes that the samples are cylindrical, which is only an approximation in the latter parts of the experiments when the deformation has caused the samples to bulge. The accuracy of the other measurements is also affected by the bulging of the sample, as discussed in Jones [1980].

Experimental Results

Stress-Strain Behavior

The stress-strain curves for various samples are shown in Figures 3 and 4, and peak differential stress and other parameters of these curves are listed in Table I. Because the porosity changes with strain and is different in different cycles, the value of the porosity at peak stress was listed in this table to represent the porosity range of the material. Since all of the samples were deformed at the same effective confining pressure, it can be seen that the behavior does indeed depend upon the porosity of the sample. The peak differential stress and the rate of strain-softening after peak stress (the stress drop after peak stress divided by the strain over which it occurred) both increase with decreasing porosity. To show this more clearly, these two parameters are plotted against the porosity at peak stress of the samples in Figure 5. The formation of slip planes in the samples also depended on the porosities. In the high porosity samples, the deformation was distributed throughout the sample, with many fault planes (oriented about 30° from the maximum stress) barely visible. As the porosity decreased and the strain-softening increased, the deformation became more concentrated onto one fault plane.

The linear strain at peak stress and the maximum amount of volumetric compaction that the sample undergoes before dilatancy do not depend upon the porosity. They do, however, seem to relate to each other. They are plotted against each

other in Figure 6, which shows that the maximum compaction is about one-third the linear strain to peak stress. What determines the amount of compaction is unclear, but it does seem to depend in part on the strain history of the sample. This is quite obvious in the difference between first and second cycles. On the whole, the amount of compaction increased with decreasing porosity, except for the least porous sample which had been overconsolidated to 360 MPa. At low pressures, the compaction in general decreases with decreasing porosity, so in this regard the low and high pressure results differ.

All of the samples underwent dilatancy starting at or just before peak stress. In most but not all cases, there was a slightly higher rate of dilatancy when there was strain-softening than when the stress was constant (e.g. sample #7, Figure 3). In the latter parts of the cycles, the rate of dilatancy were quite constant - the volumetric strain was about one-tenth the linear strain. This is the same rate of dilatancy seen by Jones [1980] for crushed sandstone at confining pressures from 50 MPa to 400 MPa.

These findings show that the peak stress and strain-softening of the specimens are controlled by porosity. A less porous specimen will be stronger and have a higher rate of stress decrease after peak stress than a more porous specimen. The linear and volumetric strains at peak stress do not depend on porosity but are proportional to each other and seem to relate to the strain history of the specimen. There is a slight dependence of the rate of dilatancy on porosity. The rate

increased slightly (<15%) when strain-softening, which is a function of porosity, occurred, and then returned to a constant level when the stress was constant. Therefore, although not all of the parameters of the behavior depend on porosity, those most important to earthquake mechanics, peak stress, strain-softening and, to some extent, dilatancy, are controlled by it.

Permeability

The change in permeability with axial strain of the samples is shown in Figure 7. The most notable feature of these permeabilities is the very large change with strain. In the looser samples, two orders of magnitude of change in permeabilities occurred in one stress cycle. Even the densest sample with only 2.3% volumetric compaction experienced a twenty times decrease in permeability. The permeabilities never increased even when the samples were dilating. This rate of decrease is the same seen by Zoback and Byerlee [1976] for looser samples of crushed granites.

The final values of the permeabilities were in the microdarcy range, much lower than has previously been reported for granular material. Because of this, it was considered possible that the low values were the result of clogged screens or tubing in the pore pressure system. Therefore, a rock sample of known permeability (Chelmsford granite, $k = 700$ nanodarcies) was tested with the entire system unchanged from a previous experiment with sands. The results were within 10% of the values determined elsewhere [Coyner et al., 1979]. However, one sample (#3) had a large decrease in permeability

between cycles. Since there was no deformation between cycles but the sample was left under pressure for two days, this one point may be the result of clogged tubing. Thus the author is confident the drop in permeability with strain is real. In spite of the low values, there is no indication that the permeabilities are levelling off with strain.

Permeability and Surface Area

The permeability of a granular fault gouge depends upon (a) the interconnected porosity and (b) the size and shape of the pores through which the fluids must flow. To express this dependency, a theoretical equation, the Kozeny-Carman equation, was derived [Carman, 1937]. It is

$$k = \frac{1}{FS^2} \frac{\eta^3}{(1-\eta)^2}$$

where k is the permeability, S is the specific surface area (the surface area divided by the volume of the solids), η is the porosity, and F is the shape factor. It has been found to fit data for cohesionless materials very well at both low pressures with $2 < F < 5$ [e.g. Sullivan and Hertel, 1942] and high pressures [Wylie and Rose, 1950], with $7 < F < 30$.

In this equation, the permeability depends strongly on the specific surface area. Because the samples in this study have undergone a large amount of grain crushing during deformation, this surface area dependence could explain the large decreases seen in the permeability. To test the applicability of this equation, the specific surface areas of the original material and the samples after deformation

were measured. This was done by the BET technique that measures the low temperature nitrogen adsorption isotherms of the surfaces (for a complete description of this technique, see Emmet [1942]). This technique does not measure the total surface of the material since it can only detect spaces large enough to admit the nitrogen molecules. However, the nitrogen and water molecules are of similar size (3\AA and 5\AA , respectively), so the measured area should be comparable to that which affects the flow of the water.

The measured specific surface areas, as well as the porosity and permeability at the end of deformation, for each sample, are listed in Table II. Using the shape factor ($F = 17$) determined for sands at high pressure by Wylie and Rose [1950], a permeability was calculated using the Kozeny-Carman equation, also listed in Table II. The measured and calculated permeabilities are plotted against each other in Figure 8. As can be seen, the calculated values are within the limits of experimental error of the experimental values, except for sample #3. For this sample, the calculated permeability is too high. However, this sample had an anomalous drop in the measured permeability when no deformation was occurring. Thus it seems likely that in this sample the measured permeability was that of clogged tubing rather than that of the sample.

With this relation between permeability and surface area, the permeability measurements made during the experiments can be used to examine the grain crushing during deformation. The calculated specific surface areas are plotted against axial

strain in Figure 9. In each sample, the surface area increased at an approximately constant rate throughout the deformation. In no case is there any indication that the rate of increase tapers off. Since specific surface area roughly correlates inversely with mean grain size, if there is a minimum grain size for this material at this pressure, as has been previously suggested [Engelder et al., 1974], it is smaller than those achieved in this experiment. Thus one would expect that in a natural fault zone that has experienced even larger amounts of strain, the permeability of the gouge could be even lower than the microdarcy permeability recorded here.

Discussion

Physical Mechanisms of Deformation

The dependence on porosity of the stress-strain behavior is probably the results of differing degrees of interlocking between grains within the samples [Lambe and Whitman, 1969, p. 130]. Energy in a sample under shear is expended in four ways - to overcome sliding friction, to lift grains over others that lie in their path (thus causing dilatancy), to crush grains and to resist external forces. The amount of energy needed to lift or crush grains is probably determined by the degree of interlocking of the grains. Thus, in a loose sample, most of the energy is used to overcome sliding friction which stays constant, so no stress drop is seen. In a dense sample, more energy must be put into a sample to bring it to failure, but

once failure occurs and the sample begins to dilate, the extra energy expenditure will decrease until the maximum stress is equal to that of the loose sample. This is approximately what I have observed here (Figures 3 and 4).

The difference in density could also be used to explain the presence or absence of a slip plane. A slip plane would normally form in shear failure. The shear-induced grain movement within a loose sample probably rearranges the grains sufficiently to break up a forming slip plane. In a dense sample, grain movement is more restricted and insufficient to destroy the plane. This explanation is supported by the appearance of the grains in low and high porosity samples under a scanning electron microscope (Figure 10). The grains in the high porosity sample are well rounded, suggesting that they have been extensively rolled, breaking off rough corners. The grains in the low porosity are much more angular, which would indicate that their movement has been restricted.

It should be noted that the grain size does not affect the behavior of the material. The maximum stresses in the first and second cycles are comparable in all cases, even though the permeability shows that the grain sizes in the second cycle are one fifth or less of the grain sizes in the first.

Implications for Earthquakes

For an earthquake to occur in fault gouge, strain-softening must occur. If it did not, there would be no method

for releasing stored energy. Exactly how much strain-softening is needed to generate an earthquake is a complicated problem, depending on other characteristics of the fault zone such as shape of the fault zone and the contribution of the country rock, which have not been considered here. Models [e.g. Rice, 1979; Stuart, 1979] have been developed to estimate the contributions of the various factors, and the results from these experiments can be compared with them to approximate the conditions needed in a fault zone to produce an earthquake. For instance, using the model of Rice [1979], a fault zone 10 km long (a $M \approx 5$ earthquake) with a 20 m thick gouge zone would need gouge with a porosity less than approximately 16%, according to the results of this study. A longer or thinner zone could produce an earthquake with higher porosities. If this model is a reasonable approximation of the earthquake process, this would indicate that with geologically reasonable porosities (5% to 25%) both stable and unstable sliding would be possible, depending on the aspect ratio of the fault zone.

The low permeabilities allow for the possibility that anomalous pore pressures could be maintained in a fault zone long enough to affect the earthquake process. High pore pressures have been considered as a possible mechanism for lowering the stress needed to cause an earthquake but seemed only possible in clays. The microdarcy permeabilities measured here are as low as those in many clays, so that it is not necessary to invoke clay minerals at depth to have restricted fluid flow.

The direct surface measurements of these samples show that more new surface area is created during deformation than had previously been supposed. This is important in considering the energy expenditure in fault zones, because the more energy that is expended creating new surfaces, the less energy is available for frictional heating. Previous calculations of the energy used to create new surface have assumed a mean grain diameter (25 μ m [Engelder et al., 1975] and 1 μ m [Lachenbruch and Sass, 1980] and then calculated the surface area of spheres or cubes of that size. This underestimates the surface area in two ways. First, spheres and cubes have very low specific surface areas compared to other grains shapes, and the area of irregular grains can be many times larger [Herden, 1960, Chap. 11]. Second, as the grain size distribution of the samples before and after deformation (Figure 1) shows, deformation increases the range of diameters. Since the specific surface area is inversely proportional to the diameter of the grains, the very small grains contribute a large proportion of the area. This is not seen when average diameters are used. Even the direct surface measurements may underestimate the actual surface area, since surfaces in cracks with less than two nitrogen molecule diameters (6 \AA) will not be completely measured. However, a comparison of the energy needed to create these surfaces and the total energy expended will provide a maximum value for the energy expended in frictional heating.

This comparison has been made for the two samples with the maximum and minimum final specific surface areas (#6 and #7). The energy per unit volume used to create new surface is

$$W_S = S \cdot \gamma$$

where γ is the surface energy of the material. A range of 500 erg/cm² to 2000 erg/cm² for γ has been determined [Brace and Walsh, 1962], so 1000 erg/cm² was used here. For sample #6, W_S is 2.3×10^8 erg/cm³ and for sample #7, W_S is 7×10^7 erg/cm³, using ΔS (Table II) of 2.3×10^5 cm⁻¹ and 7×10^4 cm⁻¹ respectively. The total energy per unit volume, W_T , expended is the area under the stress-axial strain curves (Figure 3; because of end effects, sample #6 experienced strain-hardening in a third cycle that is not shown in Figure 3. See Appendix 1). For sample #6, W_T is 3×10^9 erg/cm³, and for sample #7, W_T is 1.7×10^9 erg/cm³. Thus, at least 8% and 4%, respectively, of the energy was used to create new surface. This is much higher than the percentage, 0.1%, calculated by Engelder et al. [1975].

Conclusions

These experiments have shown that in granular material at high pressure (= 190 MPa), porosity is an important factor in determining the stress-strain behavior. Both peak stress and the amount of strain-softening after peak stress increase with decreasing porosity. The axial and volumetric strains of peak stress, however, do not depend upon porosity, but rather seem to depend on the strain history of the material.

Permeability of granular material decreases dramatically with strain, so that after 30-50% linear strain microdarcy permeabilities are common. The permeability decreases even when the porosity is increasing. This is attributed to the increased surface area of the particles in contact with the fluid, caused by the crushing of grains during deformation. In fact, direct surface measurements of the material showed that the specific surface area increased by more than ten times over two to three cycles of stress and that the permeability, k , is related to the specific surface area, S , by $k \propto \frac{1}{S^2}$. This means that the permeability of highly-strained granular fault gouge can be as low as that of clay gouge. Moreover, larger amounts of energy (at least 4% of the total energy) are being consumed by surface area production than had previously been supposed.

Acknowledgments: The author wishes to thank William Brace and Herbert Einstein for their advice and help. She also thanks Robert Coble for help and instruction in the use of the BET apparatus. The work was supported by the U.S. Geological Survey under Contract # 14-08-0001-09789.

TABLE I

Cycle	Sample	η_{initial} %	η_{failure} %	$\frac{\bar{\sigma}_1 - \bar{\sigma}_3}{\bar{\sigma}_3 \text{ max}}$	ϵ_f %	$\frac{\Delta V}{V_T} \text{ max}$	$\Delta \left(\frac{\bar{\sigma}_1 - \bar{\sigma}_3}{\text{MPa}^3} \right) / \epsilon_z^*$
1	2	9.8	8.1	3.13	9.5	2.31	2.00
	9	15.9	11.6	2.81	14.5	4.80	2.39
	1	17.6	11.7	2.69	17.2	6.69	1.77
	7	18.7	14.0	2.74	15.4	5.42	1.27
	6	21.5	17.7	2.64	14.1	4.69	0.97
	3	21.6	18.4	2.17	10.0	3.88	0.88
2	1		10.5	3.00			3.20
	7		12.8	2.75			1.22
	6		17.0	2.63			0.18
	3		18.3	2.52			0.62

*Stress drop after peak stress divided by the axial strain over which it occurred.

TABLE II

Sample	$\eta_{\text{final}}\%$	$S \times 10^4 \text{ cm}^{-1}$ measured	$k_{\text{measured}}^{\mu\text{d}}$	$k_{\text{calculated}}^{\mu\text{d}}$
1	13.2	10.0	1.5	1.8
2	10.0	13.8	0.35	0.38
3	18.9	6.6	2.7	13.9
6	18.2	25.3	0.87	0.83
7	14.6	7.3	6.4	4.7

References

- Anderson, J.L., R. Osborne, and D.L. Palmer, Petrogenesis of cataclastic rocks within the San Andreas Fault Zone of Southern California, U.S.A., Tectonophysics, in press, 1981.
- Brace, W.F., and J.B. Walsh, Some direct measurements of the surface energy of quartz and orthoclase, Amer. Mineralog., 47, 1111-1122, 1962.
- Brace, W.F., J.B. Walsh, and W.T. Frangos, Permeability of granite under high pressure, J. Geophys. Res., 73(6), 2225-2236, 1968.
- Carman, P.C., Trans. Inst. Chem. Engrs., London, 15, p. 150, 1937.
- Coyner, K., W.F. Brace, and J.B. Walsh, New laboratory measurements of permeability and electrical resistivity of crystalline rocks (abstract), Trans. AGU, 60, 943, 1979.
- Emmet, P.H., Measurement of the surface areas of solids, in Advances in Colloid Science, Vol. I, E.O. Kraemer (ed.), Interscience Publishers, Inc., N.Y., pp. 1-36, 1942.
- Engelder, T., Cataclasis and the generation of fault gouge, Geol. Soc. Amer. Bull., 85, 1515-1521, 1974.

- Engelder, T., J. Logan, and J. Handin, The sliding characteristics of sandstone on quartz fault gouge, PAGEOPH, 113(1/2), 69-86, 1975.
- Herdon, G., Small Particle Statistics, Butterworth & Co., London, 418 pp.
- Jones, L.M., Cyclic loading of simulated fault gouge to large strains, J. Geophys. Res., 85(B4), 1826-1832, 1980.
- Lachenbruch, A.H., and J.H. Sass, Heat flow and energetics of San Andreas Fault Zone, J. Geophys. Res., 85, 6185-6222, 1980.
- Lambe, T.W., and R.V. Whitman, Soil Mechanics, John Wiley & Sons, N.Y., 553 pp., 1969.
- Rice, J.R., Theory of precursory processes in the inception of earthquake rupture, Gerlands Beitr. Geophysik, 88, 91, 1979.
- Stuart, W., Strain-softening, prior to two-dimensional, strike-slip earthquakes, J. Geophys. Res., 84, 1063-1070, 1979.
- Sullivan, R.R., and K.L. Hertel, The permeability method for determining specific surface of fibers and powders, in Advances in Colloid Science, Vol. I, E.O. Kraemer (ed.), Intersciences Publishers, Inc., N.Y., pp. 37-80, 1942.

Wylie, M.R.T., and W.D. Rose, Application of the Kozeny equation to consolidated porous media, Nature, 165, 972, 1950.

Zoback, M., and J.D. Byerlee, Effect of high pressure deformation on permeability of Ottawa Sand, Bull. Amer. Assoc. of Petrol. Geol., 60(9), 1531-1542, 1976a.

Zoback, M., and J.D. Byerlee, A note on the deformational and fluid flow behavior of crushed granite, Int. J. Rock Mech. Min. Sci., 13, 291-294, 1976b.

Figure Captions

- Figure 1 Grain size distribution of crushed Westerly granite, initially (solid line) and after deformation (sample #7 - dotted line).
- Figure 2 Sample configuration used in these experiments.
- Figure 3 Axial stress difference divided by effective pressure and volumetric strain versus axial strain for samples #2 ($\eta_o = 9.8\%$), #6 ($\eta_o = 21.5\%$) and #7 ($\eta_o = 18.7\%$).
- Figure 4 Axial stress difference divided by effective pressure and volumetric strain versus axial strain for samples #1 ($\eta_o = 17.8\%$), #3 ($\eta_o = 21.7\%$) and #9 ($\eta_o = 15.4\%$).
- Figure 5 (a) Peak stress versus porosity at peak stress for both first (closed circles) and second (open circles) stress cycles. Numbers refer to Table I.
(b) Rate of strain-softening (the decrease in stress after peak stress divided by the axial strain over which the decrease occurred) versus porosity of peak stress for both first (closed circles) and second (open circles) stress cycles. Numbers refer to Table I.
- Figure 6 The axial strain at peak stress versus the volumetric compaction before dilation begins for all samples, both first (closed circles) and second (open circles) stress cycles. Numbers refer to Table I.

Figure 7 Permeability versus axial strain for all of the samples. In some of the experiments, the initial porosity was too high to be measured. In these cases, the curves begin with a dotted line.

Figure 8 The measured permeability at the end of each experiment versus the permeability calculated from the surface area measurements and final porosity, using the Kozeny-Carman equation.

Figure 9 Specific surface area calculated from the permeability and porosity measurements, using the Kozeny-Carman equation versus axial strain.

Figure 10 Scanning electron microscope photographs of samples #2 and #7 (see Figure 3).

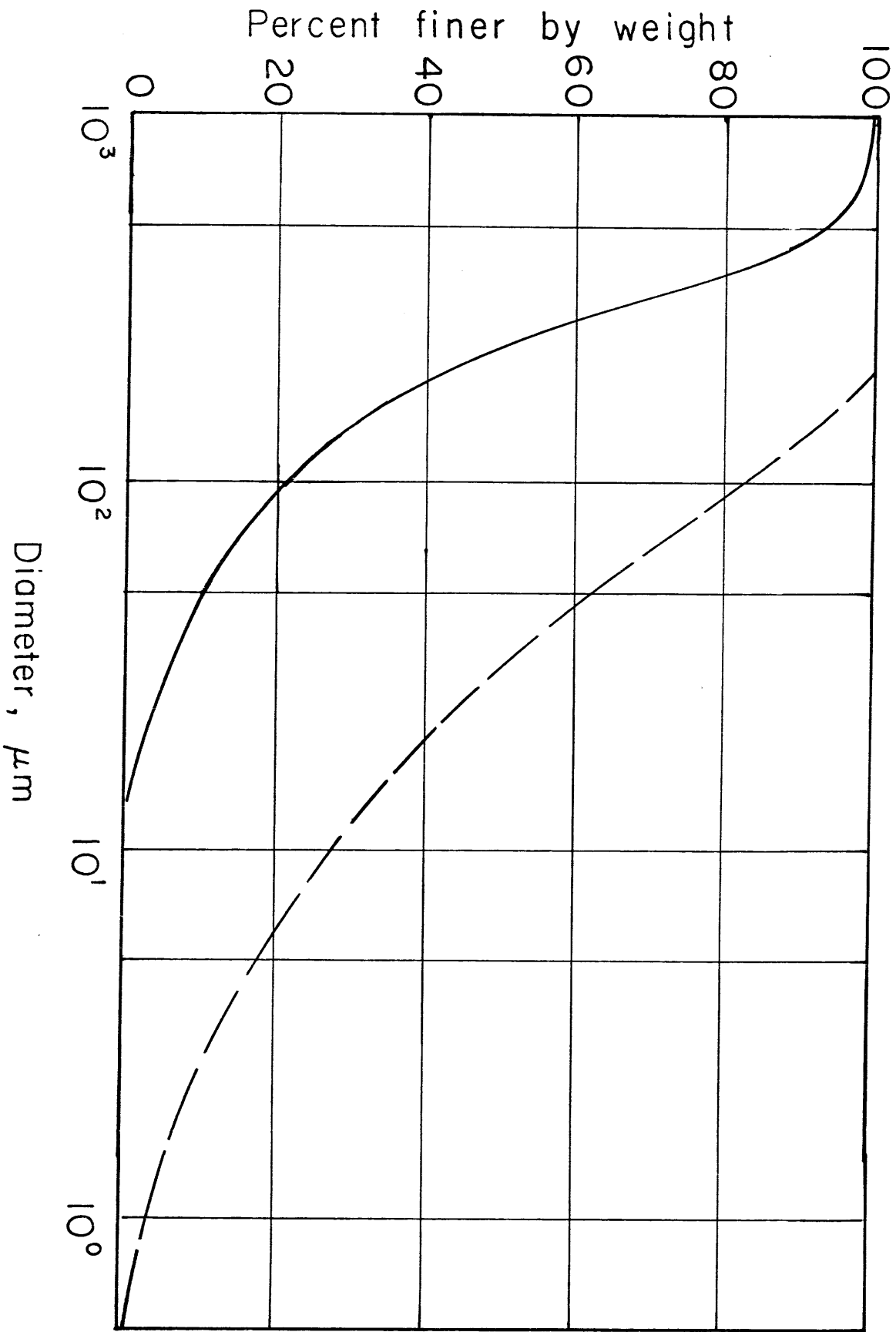


Figure 1

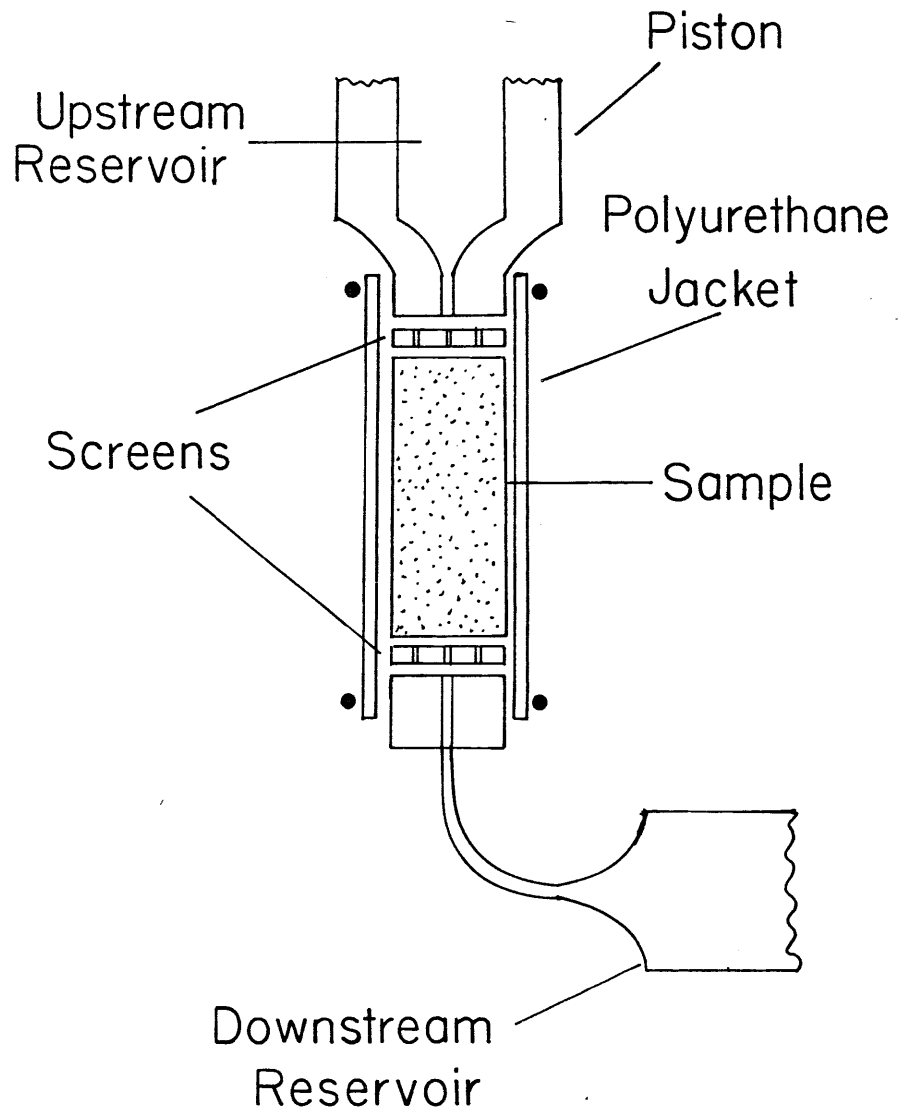


Figure 2

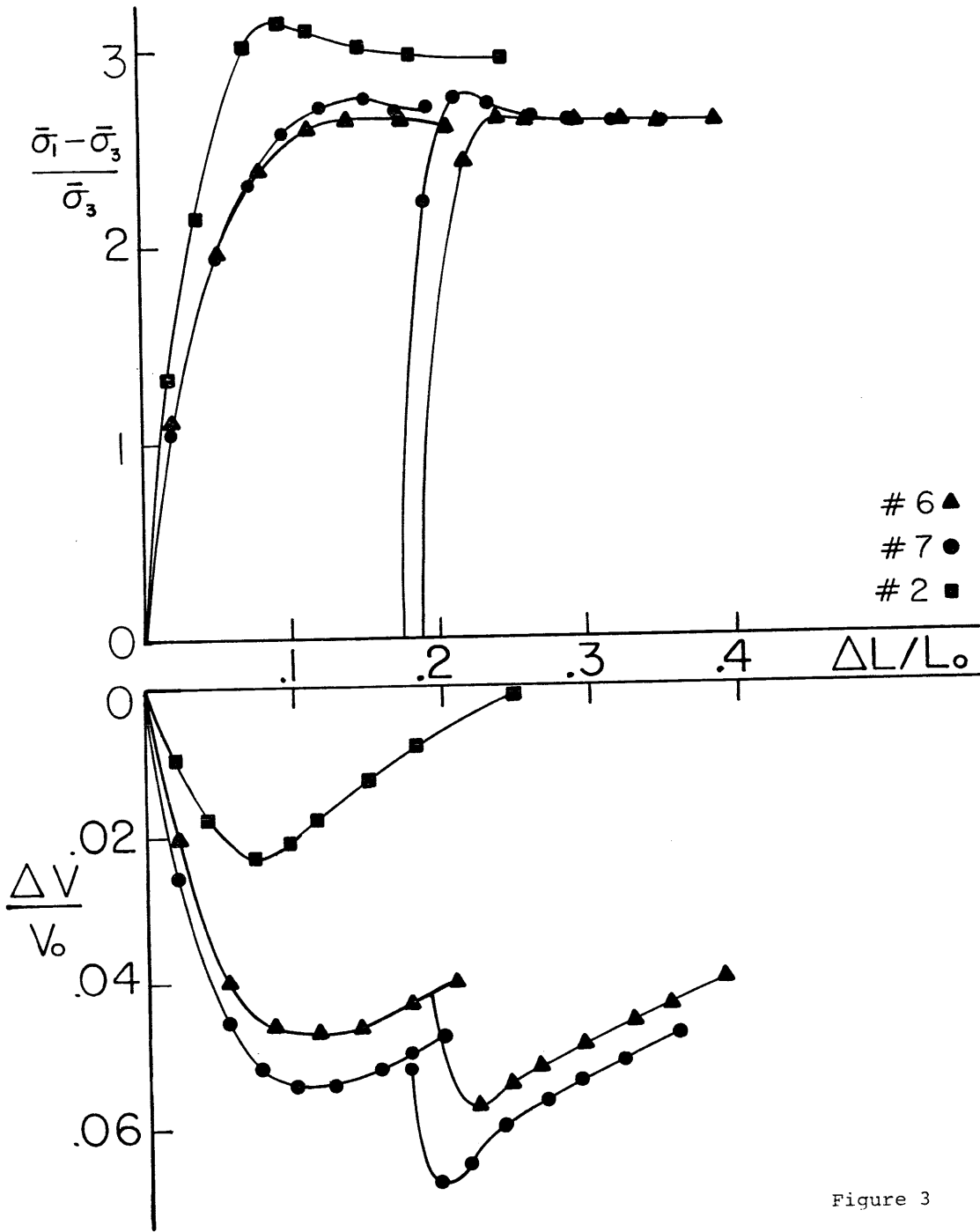


Figure 3

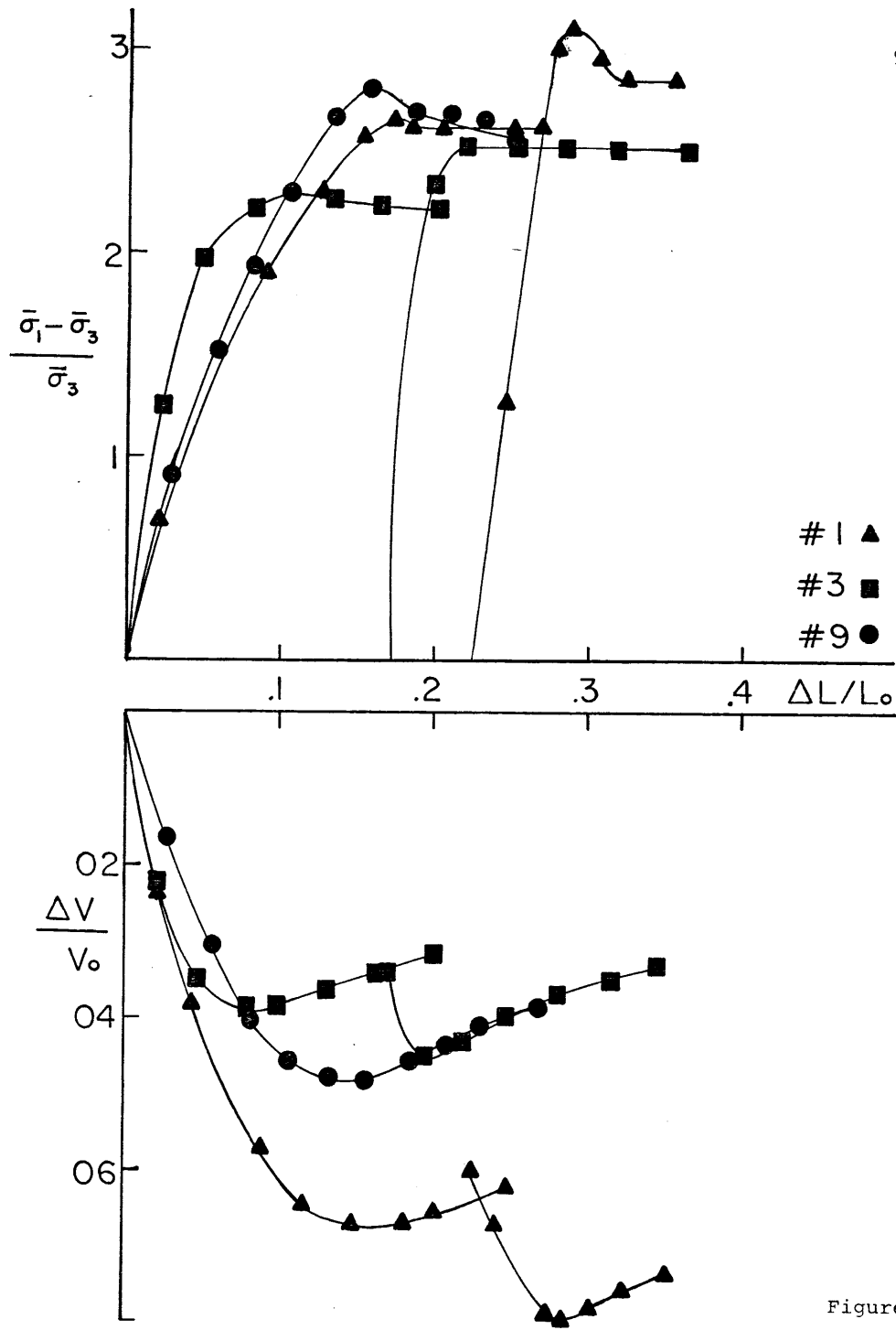


Figure 4

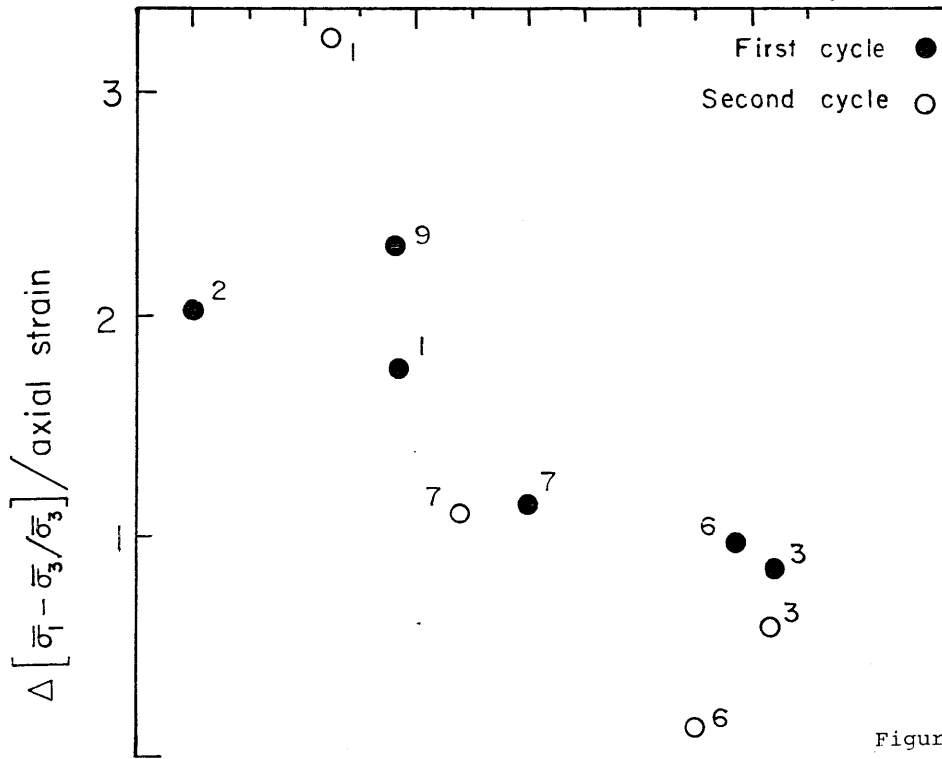
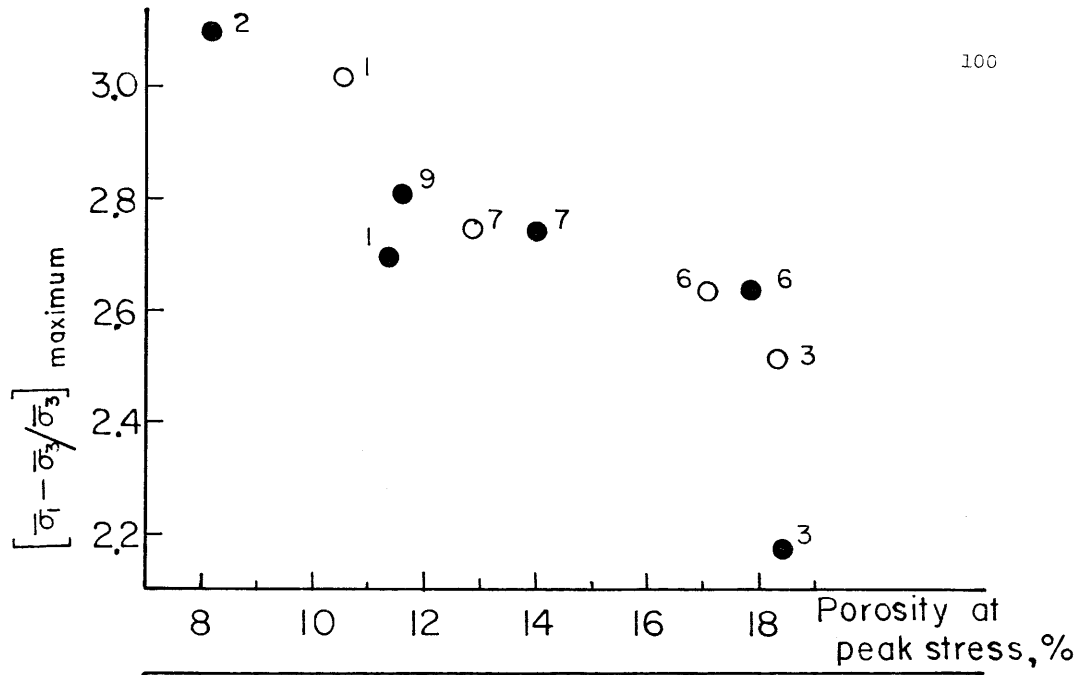


Figure 5

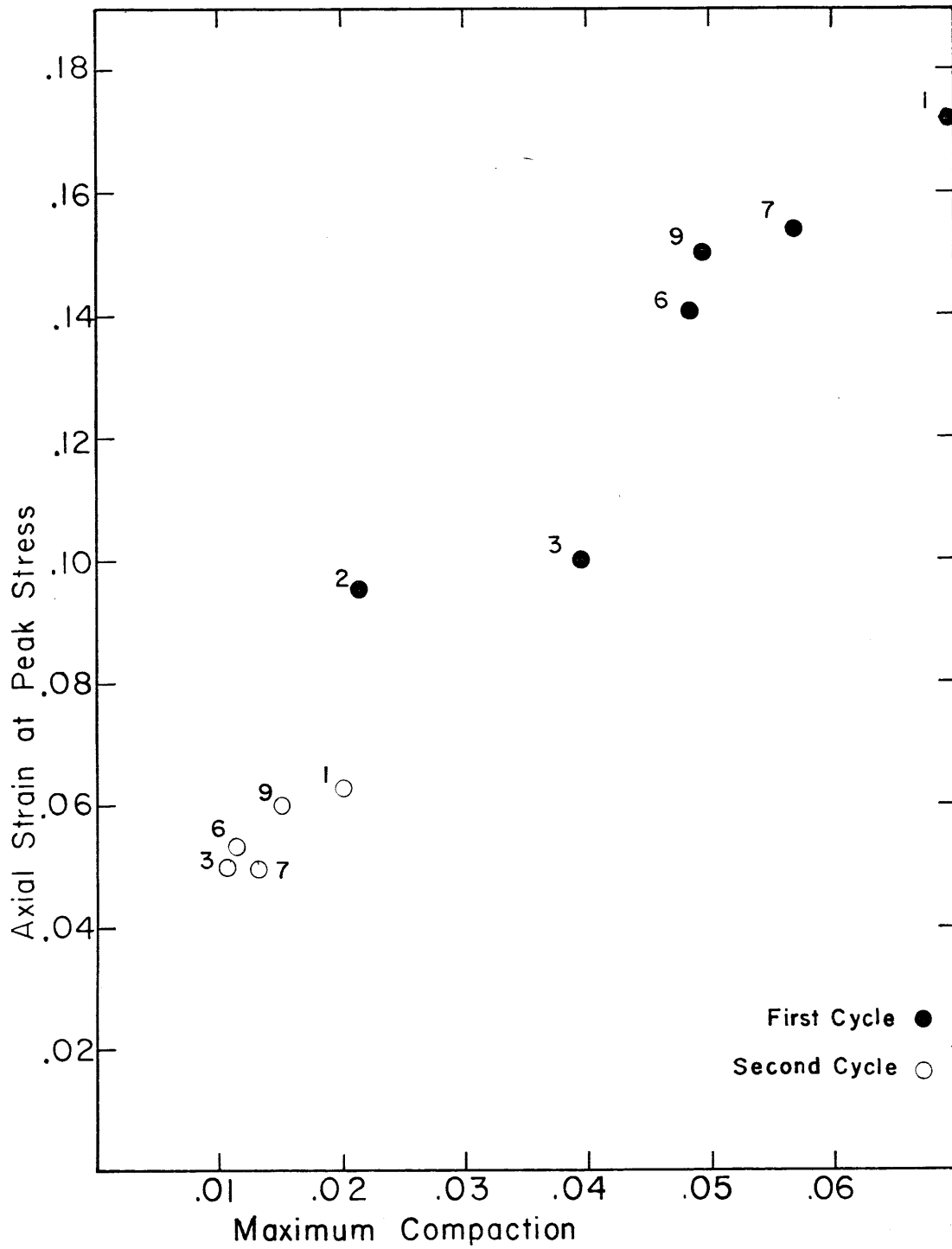


Figure 6

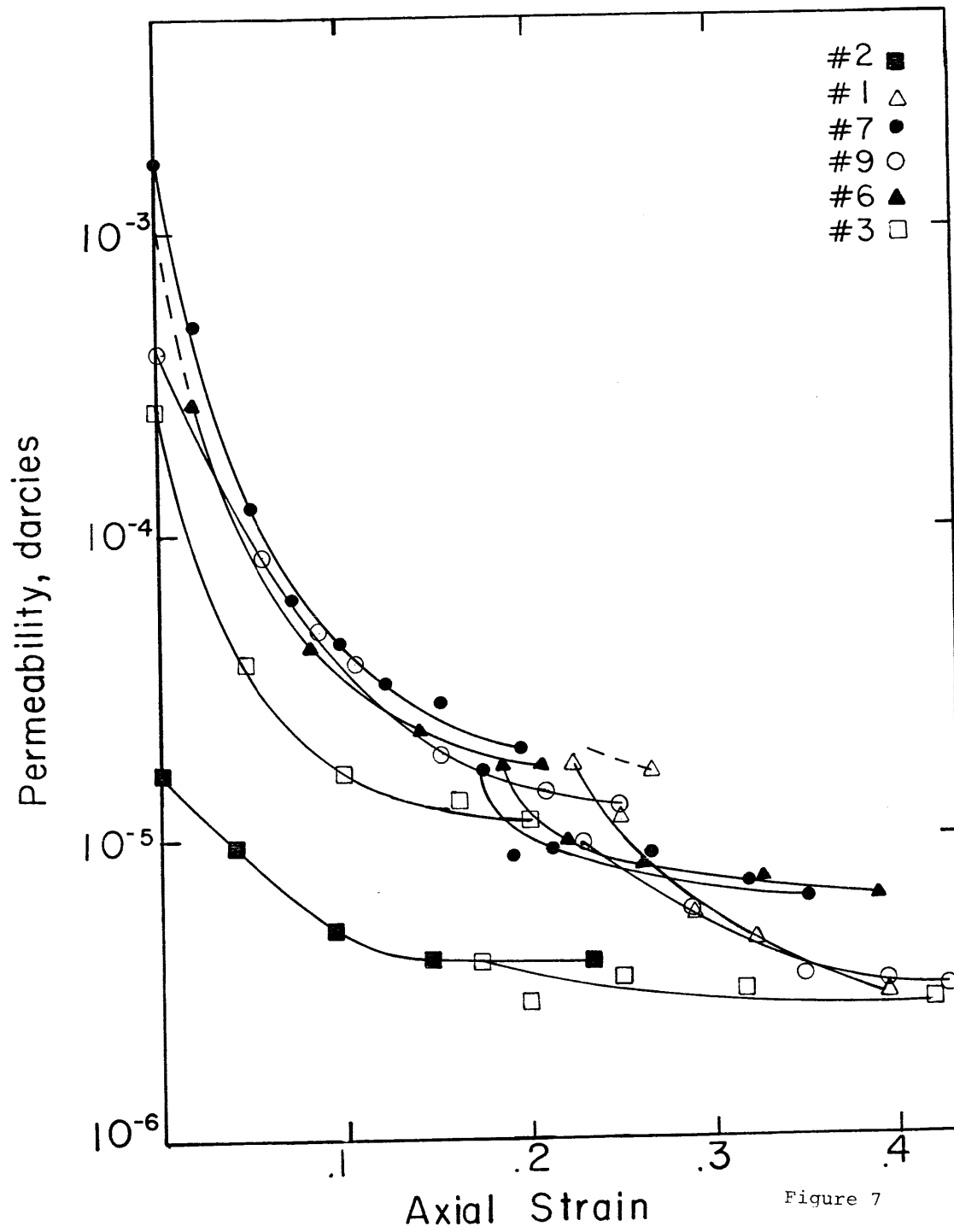


Figure 7

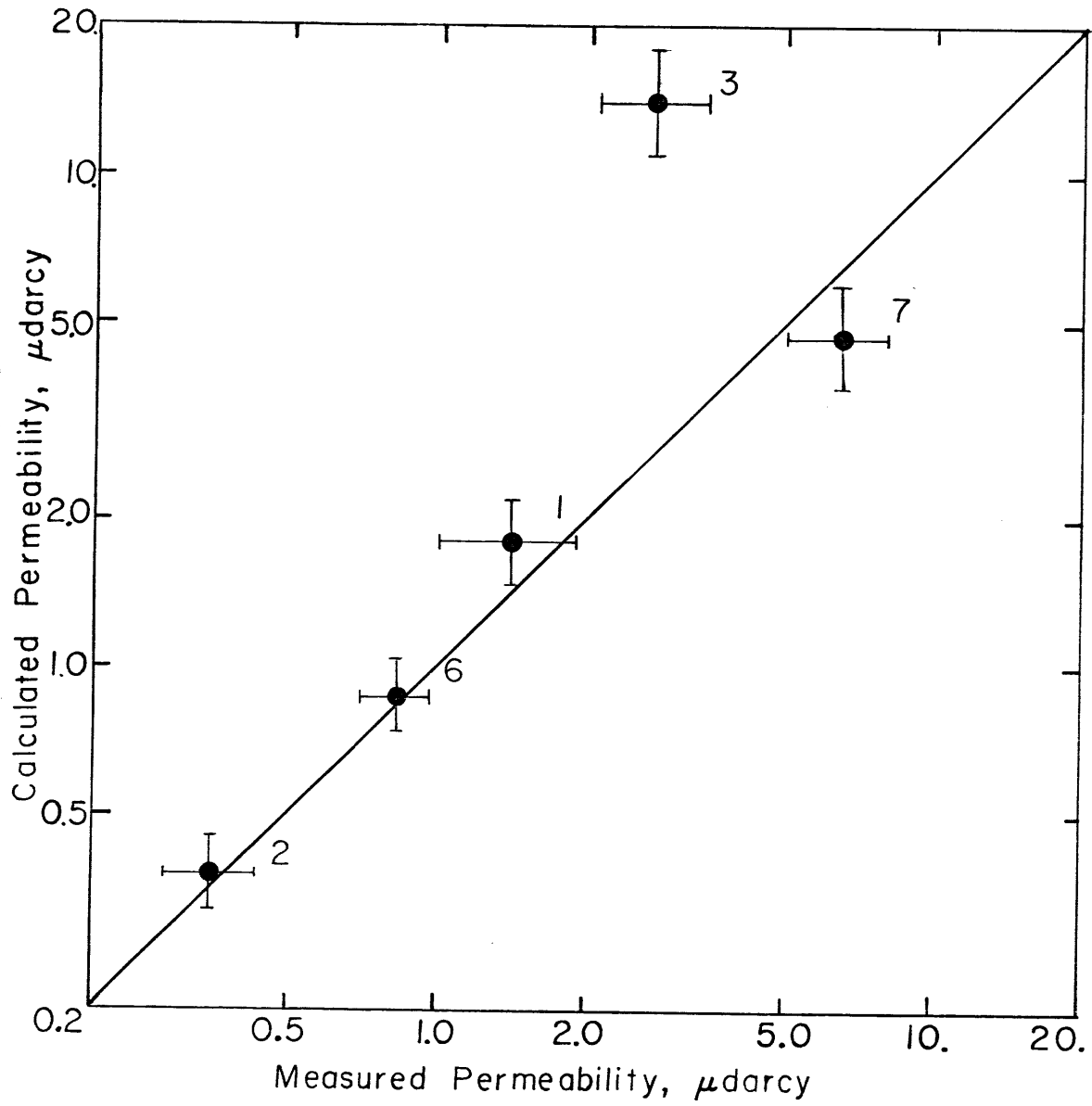


Figure 8

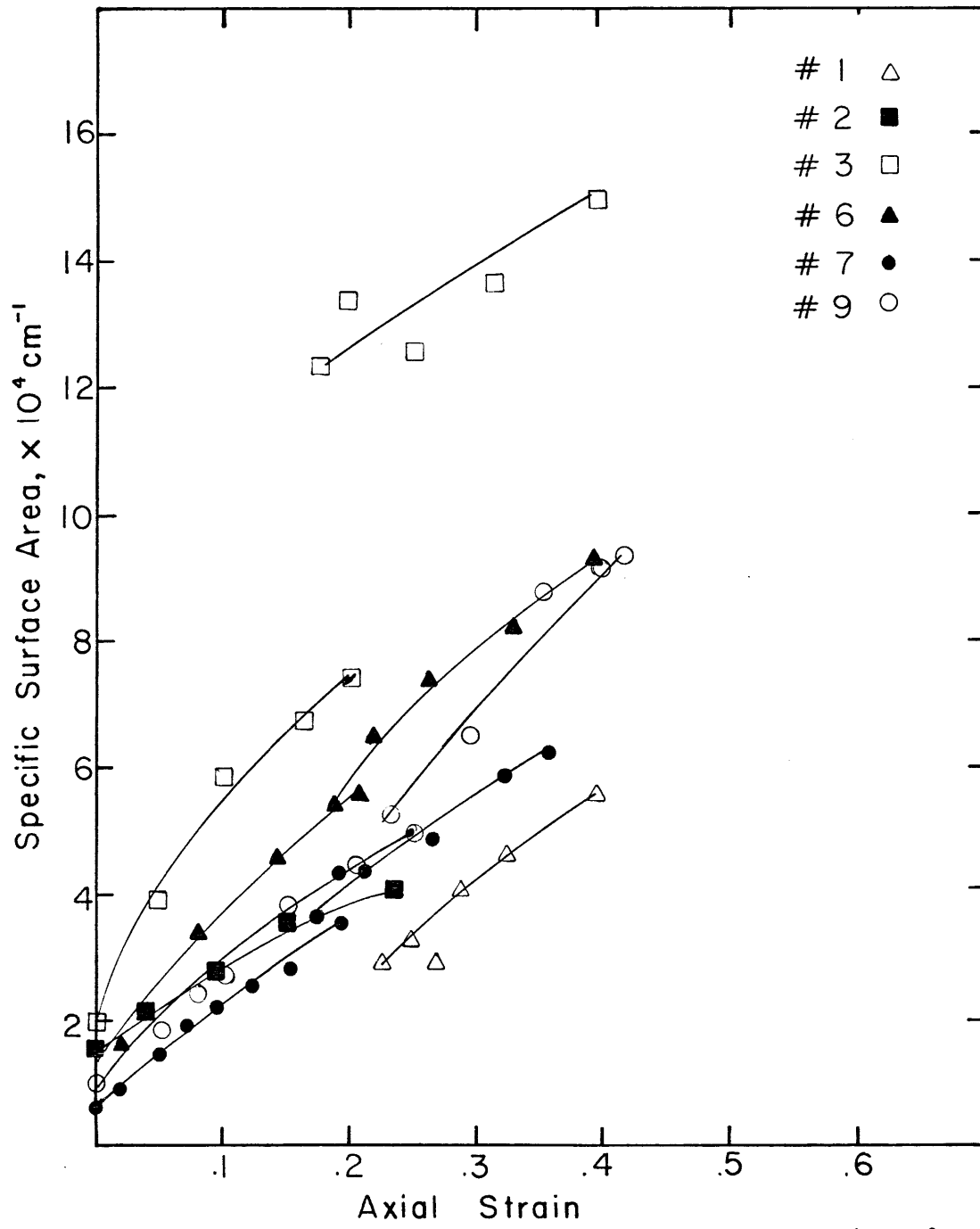


Figure 9

Biographical Note

I was born to Donald and Patricia Jones on February 13, 1955, in Santa Monica, California. I attended primary and secondary school in Los Angeles for ten years and then Taipei American School in Taipei, Taiwan, from which I graduated in 1971. I studied physics and Chinese at Brown University in Providence, Rhode Island, from 1972 to 1976. My junior year was spent at the Inter-University Program for Chinese Language Studies administered by Stanford University in Taipei, Taiwan. I graduated Magna Cum Laude and Phi Beta Kappa from Brown University in 1976 with a Bachelor of Arts degree in Chinese Language and Literature. I have been a graduate student and research assistant at the Massachusetts Institute of Technology from 1976 to 1981. In 1977, I received a National Science Foundation Graduate Student Fellowship. In 1979, I was selected to participate in the National Program for Advanced Study and Research in China administered by the Committee on Scholarly Communication with the People's Republic of China of the National Academy of Sciences. Supported as a Fulbright Fellow under this program, I worked at the State Seismological Bureau in Beijing, China, from March to July, 1979.